ISSN: 2164-5388 Volume 8, Number 3, July 2018

Scientific Research Publishing

Open Journal of Biophysics

ISSN: 2164-5388

www.scirp.org/journal/ojbiphy

Journal Editorial Board

ISSN Print: 2164-5388 ISSN Online: 2164-5396
http://www.scirp.org/journal/ojbiphy

Associate Editors

Editorial Board

Scientific Research Publishing

Open Journal of Biophysics, 2018, 8, 95-183
http://www.scirp.org/journal/ojbiphy
ISSN Online: 2164-5396
ISSN Print: 2164-5388

Table of Contents

Volume 8 Number 3 July 2018

Open Journal of Biophysics (OJBIPHY)
Journal Information

SUBSCRIPTIONS

The *Open Journal of Biophysics* (Online at Scientific Research Publishing, www.SciRP.org) is published quarterly by Scientific Research Publishing, Inc., USA.

Subscription rates:
Print: $79 per issue.
To subscribe, please contact Journals Subscriptions Department, E-mail: sub@scirp.org

SERVICES

Advertisements
Advertisement Sales Department, E-mail: service@scirp.org

Reprints (minimum quantity 100 copies)
Reprints Co-ordinator, Scientific Research Publishing, Inc., USA.
E-mail: sub@scirp.org

COPYRIGHT

PRODUCTION INFORMATION

For manuscripts that have been accepted for publication, please contact:
E-mail: ojbiphy@scirp.org

Scientific Research Publishing

Open Journal of Biophysics, 2018, 8, 95-103
http://www.scirp.org/journal/ojbiphy
ISSN Online: 2164-5396
ISSN Print: 2164-5388

Similarities of Modulation by Temperature and by Electric Field

Gyula Vincze, Andras Szasz

Department of Biotechnics, Szent István University, Godollo, Hungary
Email: biotech@gek.szie.hu

How to cite this paper: Vincze, G. and Szasz, A. (2018) Similarities of Modulation by Temperature and by Electric Field. *Open Journal of Biophysics*, **8**, 95-103.
https://doi.org/10.4236/ojbiphy.2018.83008

Received: March 29, 2018
Accepted: May 26, 2018
Published: May 29, 2018

Abstract

Glycolytic oscillation is one of the first observed and described nonlinear phenomena in living objects. Our recent paper points out the similarity of the temperature and outer electric field to influence this oscillation. The electric field is absorbed and changes the molecules. Similarly to the effect of heating, molecules have various structural, dynamical and chemical changes promoted by electric field. The changes sometimes happen without increasing the temperature. Temperature, as the average energy of the included particles, has various kinds of "waste" energy used to heat up the particles which do not participate in the desired changes. The inaccuracy of the effects of temperature growth in local molecular changes could be remarkably high and could be corrected by the well-applied electric field absorption.

Keywords

Glycolytic Oscillation, Modulation, Electric Field, Temperature, Electric-Polarization

1. Introduction

Glycolytic oscillation was observed first in yeast suspension by pulsing-addition of glucose to the system [1], registering the transient oscillation of concentration of NAD (Nicotinamide-Adenine Dinucleotide [reduced form]). Cells were studied under anaerobic conditions and oxygen addition terminated the transient oscillation phenomenon. Soon, many biochemical oscillations were measured, [2] [3] pushing the process into the front of the non-linear reaction-kinetics described by ordinary differential equations [4]. This activity accelerated when the first glycolytic oscillation was explained strictly on a mathematical basis called Selkov's model [5]. This bifurcation-based phenomenon soon reached its direct biomedical applications too [6], mainly centered on the pancreatic activity [7].

Mathematical models (like [8]) had great support by the more and more precise experiments [9] [10]. Presently, precise metabolic activity in cells is measured by showing entrainment of heterogeneous glycolytic oscillations in single cells [11] [12], in which work was one of the vast news of the year. Interaction of glycolysis with external electric field stimulation has been known for a long time [13] [14] [15]. Our objective is to clear the following question in detail: are there any similarities between the temperature stimuli and electric stimuli in transient glycolytic oscillation?

2. Method

Temperature is a trivial driving parameter of glycolysis [16] [17]. It was widely investigated experimentally [18] and explained theoretically too [19] as further-developed Selkov's model. Two factors were introduced for this study: a constant α for positive feedback catalytic effect and a $\beta(T)$ for temperature dependence.

$$\begin{aligned} \frac{\mathrm{d}x}{\mathrm{d}t} &= \nu - \alpha x - \beta(T) xy^2, \\ \frac{\mathrm{d}y}{\mathrm{d}t} &= -wy + \alpha x + \beta(T) xy^2 \end{aligned} \tag{1}$$

where ν, α and w are constants, while $\beta(T)$ satisfies the Arrhenius-dependence of temperature.

$$\beta(T) = \beta_0 \mathrm{e}^{-\frac{E}{kT}} \tag{2}$$

Solving these equations, the results were as follows:

1) The average concentration of the reagents decreases by time.

2) The frequency of oscillation depends on the temperature by Arrhenius function.

3) The form of oscillation changes by the temperature.

4) Oscillation can be modulated by the periodic changing of the temperature.

Let us suppose that the activation energy in Arrhenius law depends on the electric field which can have strong synergy with the temperature [20].

Giving the perturbation of the temperature

$$T(t) = T_0 + \Delta T(t), \quad \max|\Delta T| \ll T_0 \tag{3}$$

after a Taylor-expansion and stop at the linear term:

$$\beta(\Delta T(t)) = \beta_0 \mathrm{e}^{-\frac{E}{kT_0}} \mathrm{e}^{\frac{E}{kT_0^2}\Delta(t)} \cong \beta_0 \mathrm{e}^{-\frac{E}{kT_0}} \left(1 + \frac{E}{kT_0^2}\Delta T(t)\right) \tag{4}$$

When the $\Delta E(t)$ changes have periodic part, then:

$$\beta(\Delta E) = \beta_0 \mathrm{e}^{-\frac{E_0 + \Delta E(t)}{kT}} = \beta_0 \mathrm{e}^{-\frac{E_0}{kT}} \mathrm{e}^{-\frac{\Delta E(t)}{kT}} \cong \beta_0 \mathrm{e}^{-\frac{E_0}{kT}} \left(1 - \frac{1}{kT}\Delta E(t)\right) \tag{5}$$

If P is the polarization and $\Delta\mathcal{F}(t)$ is the electric field strength, then $\Delta E(t) = -P\Delta E(t)$ and consequently

$$\beta\left(\Delta E\left(t\right)\right)=\beta_0 \mathrm{e}^{-\frac{E_0+\Delta E(t)}{kT}}=\beta_0 \mathrm{e}^{-\frac{E_0}{kT}} \mathrm{e}^{-\frac{\Delta E(t)}{kT}} \cong \beta_0 \mathrm{e}^{-\frac{E_0}{kT}}\left(1+\frac{P}{kT}\Delta\mathcal{F}\left(t\right)\right) \quad (6)$$

Comparing (4) and (6), the effects which we promote by temperature could be constructed on the same way by electric field, making substitution.

$$E\Delta T \leftrightarrow P\Delta\mathcal{F}\left(t\right)$$

3. Discussion

Comparing (4) and (6), electric field has a formally similar effect on the modulation of glycolytic oscillations to the temperature. Driving force is the change of the field strength $\Delta\mathcal{F}\left(t\right)$ (instead of the $\frac{\Delta T\left(t\right)}{T_0}$ relative temperature change), and chemical activation energy is replaced simply by the polarization of the material. The abovementioned similarity is based on the Arrhenius equation which is a general expression for the temperature dependence of chemical reaction rates, so in the simple empirical comparison of the reaction kinetics it allows the interchange of the temperature and electric field effects. So, the effect is formally similar, but their real action is different, the electric field needs polarizability of the materials which is not the condition for temperature. The glycolysis is a special effect involving the membranes (cytoplasmic and mitochondrial) which have a definite and well distinguishable polarization vector. This means that this similarity makes high parallel effects nearby the membrane of the cells. In the other chemical mechanisms of the living material the difference between the temperature effect and the electric fields is simply the mechanism which these effects induce in the process.

The electric field in this meaning makes equivalent changes in the chemical effects of glycolytic oscillations like temperature does when the heat-exchange is concentrated on a certain chemical reaction and not spread all over the target.

Heat spreads in the target by various convection and conduction effects. Therefore temperature rise in this case cannot be equal to the precisely concentrated electric filed for chemical changes. This is indispensable for making hyperthermia treatment precise, where the accurate approximation of the chemical changes is blocked by the spreading of the heat energy. According to the Pennes Equation [21] [22]:

$$\rho c\frac{\partial T}{\partial T}=div\left(\kappa gradT\right)+h_m+h_b+Q_s\left(x,t\right)+Q_D\left(x,t\right)$$

where

$$\begin{aligned}\rho c\frac{\partial T}{\partial t}&=div\left(\lambda gradT\right)+\rho_b c_b w\left(T-T_b\right)+p_e\\&=T\left(c_1-c_{11}\zeta_1\right)\frac{\partial\zeta_1}{\partial t}+Tc_2\frac{\partial\zeta_2}{\partial t}=-h_m-Q_s\left(x,t\right)\end{aligned} \quad (7)$$

The electric energy source has modified the Pennes Equation, and the changes are realized in reactions (introduced reaction coordinates $\zeta_i\,(i=1,2)$.

$$\rho c\frac{\partial T}{\partial t}+T\left(c_1-c_{11}\zeta_1\right)\frac{\partial \zeta_1}{\partial t}+Tc_2\frac{\partial \zeta_2}{\partial t}-div\left(\lambda gradT\right)$$
$$-\rho_b c_b w\left(T-T_b\right)=p_e \tag{8}$$

Moreover, two extra reaction-equations made the description valid for the system, where reactions could occur.

$$\frac{\mathrm{d}\zeta_1}{\mathrm{d}t}=-\frac{1}{\tau}\left(\zeta_1-\zeta_{1e}\right),$$
$$\frac{\mathrm{d}\zeta_2}{\mathrm{d}t}=L_{22}c_2, \tag{9}$$

This interconnected (coupled) equation-system must be solved for describing the system. A more straightforward form of the conventional system is:

$$\rho c\frac{\partial T}{\partial t}+T\left(c_1-c_{11}\zeta_1\right)\frac{\partial \zeta_1}{\partial t}+TL_{22}c_2^2-div\left(\lambda gradT\right)+\rho_b c_b w\left(T-T_b\right)=p_e,$$
$$\frac{\mathrm{d}\zeta_1}{\mathrm{d}t}=-\frac{1}{\tau}\left(\zeta_1-\zeta_{1e}\right) \tag{10}$$

If the initial condition was zero product (best assumption) then the solution of the second equation is:

$$\zeta_1=\zeta_{1e}\left(1-\mathrm{e}^{-\frac{t}{\tau}}\right) \tag{11}$$

where the saturated (equilibrium) value and the time-constant could be temperature dependent functions. The generalized Pennes Equation with these mathematical treatments:

$$\frac{\partial T}{\partial t}-\frac{\lambda}{\rho c}\Delta T+\frac{\rho_b c_b w}{\rho c}T=\frac{p_e+\rho_b c_b w}{\rho c}T_b-\frac{TL_{11}c_1^2}{\rho c}\mathrm{e}^{\frac{-2t}{\tau}}-\frac{TL_{22}c_2^2}{\rho c}$$
$$\rightarrow\frac{\partial T}{\partial t}-\frac{\lambda}{\rho c}\Delta T+\alpha T=g-N\left(T\right),$$
$$g=\frac{p_e+\rho_b c_b w}{\rho c}T_b,$$
$$N\left(T\right)=\frac{TL_{11}c_1^2}{\rho c}\mathrm{e}^{\frac{-2t}{\tau}}+\frac{TL_{22}c_2^2}{\rho c}, \tag{12}$$
$$\alpha=\frac{\rho_b c_b w}{\rho c},\ L_{11}=\frac{\Lambda_1\mathrm{e}^{\frac{\mu}{RT}}}{R},\ L_{22}=\frac{\Lambda_2\mathrm{e}^{\frac{\mu}{RT}}}{R}$$

The Pennes Equation formally could be rewritten as follows;

$$L\left(T\right)=g \tag{13}$$

where L is a linear differential-operator and g the inhomogeneity term, constructed from the blood-perfusion and the introduced electric-power. If chemical reactions (cellular disruptions) additionally happen, that makes non-linearity to the equation, and the original Equation (13) will be modified:

$$L\left(T\right)+N\left(T\right)=g \tag{14}$$

where $N(.)$ term contains the non-linearities. In a general form Equation (14)

could be:

$$L(T)+\lambda N(T)=g \tag{15}$$

where λ is an arbitrary parameter. (Naturally (14) and (15) are identical if $\lambda=1$).

The solution of (15) could be approached by perturbation approximation having a power-series of λ:

$$T=T_0+\lambda T_1+\lambda^2 T_2+\cdots \tag{16}$$

Because $L(.)$ is linear than:

$$L(T)=\sum_{i=0}^{\infty}\lambda^i L(T_i) \tag{17}$$

However, $N(.)$ is an analytical function of T; consequently, it could be presented as a series of λ powers.

$$N\left(T_0+\lambda T_1+\lambda^2 T_2+\cdots\right)=N(T_0)+\lambda N_1(T_0,T_1)+\lambda^2 N_2(T_0,T_1,T_2)+\cdots \tag{18}$$

Moreover, using these series in the Equation (15) grouping the terms by the power of λ as well as using the arbitrariness of λ, we get:

$$L(T_0)=g,\ L(T_1)=-N(T_0),\ L(T_2)=-N_1(T_1) \tag{19}$$

Solved and substituted to Equation (16) we have the solution of Equation (14) at $\lambda=1$:

$$T=T_0+T_1+T_2+\cdots \tag{20}$$

The T_0 is the ordinary solution of the usual Pennes Equation, and the further terms are the consequences of the non-linear extension, so these are the essentials in our approach.

Let us study the one-dimensional case at first. The one-dimensional Pennes Equation with neglecting of the thermal conduction, using Equation (12):

$$\begin{aligned} &L(T)=\frac{\mathrm{d}T}{\mathrm{d}t}+\alpha T=\frac{p+\rho_b w_b c_b T_b}{\rho c}=g,\\ &\alpha=\frac{\rho_b w_b c_b}{\rho c} \end{aligned} \tag{21}$$

which has a solution:

$$\begin{aligned} &T_0=T_{00}\mathrm{e}^{-\alpha t}+\int_0^t \mathrm{e}^{-\alpha t}\mathrm{e}^{\alpha t^1} g(t')\mathrm{d}t\\ &T_{00}=36.5+273^{\circ}\mathrm{C} \end{aligned} \tag{22}$$

If the electromagnetic power is constant (not time-dependent), then:

$$\begin{aligned} &T_0=T_{0\infty}-(T_{0\infty}-T_{00})\mathrm{e}^{-\alpha t},\\ &T_{0\infty}=\frac{g}{\alpha},\\ &T_{00}=36.5+273^{\circ}\mathrm{C} \end{aligned} \tag{23}$$

Naturally, g could depend on the space-vector so T_0 as well.

The first term of the perturbation solution by (19) is the solution of the fol-

lowing equation:

$$L(T_1)=\frac{\mathrm{d}T_1}{\mathrm{d}t}+\alpha T_1=-N(T_0) \tag{24}$$

Its solution (because the initial condition has been satisfied before) is:

$$T_1=-\int_0^t \mathrm{e}^{-\alpha t}\mathrm{e}^{\alpha t'}N\left[T_0(t'),t'\right]\mathrm{d}t', \tag{25}$$

Substitute N(.) from Equation (12) we have:

$$\begin{aligned}T_1=-\int_0^t \mathrm{e}^{-\alpha t}\mathrm{e}^{\alpha t'}\Bigg[&\frac{T_0(t')L_{11}\left(T_0(t')\right)c\left(T_0(t')\right)_1^2}{\rho c}\mathrm{e}^{\frac{-2t'}{\tau(T_0(t'))}}\\&+\frac{T_0(t')L_{22}\left(T_0(t')\right)c\left(T_0(t')\right)_2^2}{\rho c}\Bigg]\mathrm{d}t',\end{aligned} \tag{26}$$

We only have numerical possibility to solve this, although it has no great importance. We must have the stationery solution, which is enough for hyperthermia conditions.

In stationery cases, T_0 is constant in time, and the first term of the integrands is zero, so:

$$T_1=-\int_0^t \mathrm{e}^{-\alpha t}\mathrm{e}^{\alpha t'}\frac{T_0L_{22}(T_0)c(T_0)_2^2}{\rho c}\mathrm{d}t'=-\frac{T_0L_{22}(T_0)c(T_0)_2^2}{\alpha\rho c}\left(1-\mathrm{e}^{-\alpha t}\right), \tag{27}$$

where the only stationer solution is:

$$T_1=-\frac{T_0L_{22}(T_0)c(T_0)_2^2}{\alpha\rho c} \tag{28}$$

What did we get for the value of the temperature correction?

Nothing on the absolute value, because no experimental data exists. However, the relative change could be guessed by the experimental dose-function.

The correction at 43˚C for arbitrary T temperature, based on the Equation (28), is:

$$\frac{T_{1T}}{T_{143}}=\frac{T_{0T}}{T_{043}}\frac{L_{22}(T)c(T)_2^2}{L_{22}(T_{43})c(T_{43})_2^2}\frac{\rho cw_{b43}}{\rho cw_{bT}} \tag{29}$$

Using the results from the dose-idea:

$$t_{eq}=\frac{L_{22}c_2^2\big|_{T=T_{43}}}{L_{22}c_2^2\big|_T}t:=R^{(T_{43}-T)}t \tag{30}$$

where according to Sapareto and Dewey [23]:

$$R=\begin{cases}0, & \text{if } T<3^{\circ}\mathrm{C}\\ 0,25, & \text{if } 39^{\circ}\mathrm{C}\le T<43^{\circ}\mathrm{C}\\ 0,5, & \text{if } T\ge 43^{\circ}\mathrm{C}\end{cases} \tag{31}$$

Based on these equations:

$$\frac{T_{1T}}{T_{143}} = \frac{T_{0T}}{T_{043}} \frac{\rho c w_{b43}}{\rho c w_{bT}} \frac{1}{R^{(T_{43}-T)}} \tag{32}$$

For example, when we compare two temperature points: $T_{41} = 273 + 41 = 314$ K, and $T_{45} = 273 + 45 = 318$ K. In the first interval (41˚C - 43˚C) $R_{41} = 0.25$ and the second: (43˚C - 45˚C) $R_{45} = 0.5$. The blood-perfusion rate at T_{41} $w_{b41} = 20$ ml/min/100g, and at T_{45} is w_{b45} 5 ml/min/100g [24].

Then the ratio of corrections according to Equation (32) is

$$\begin{aligned} \frac{T_{141}}{T_{143}} &= \frac{T_{041}}{T_{043}} \frac{w_{b43}}{w_{b41}} \frac{1}{R_1^{(T_{43}-T_{41})}}, \\ \frac{T_{145}}{T_{143}} &= \frac{T_{044}}{T_{043}} \frac{w_{b43}}{w_{b45}} \frac{1}{R_2^{(T_{43}-T_{45})}} \end{aligned} \tag{33}$$

where

$$\frac{T_{141}}{T_{145}} = \frac{T_{041}}{T_{045}} \frac{w_{b45}}{w_{b41}} \frac{R_2^{(T_{43}-T_{41})}}{R_1^{(T_{43}-T_{45})}} == \frac{314}{318} \frac{5}{20} \frac{0.5^{-2}}{0.25^2} \cong 16 \tag{34}$$

This means if at temperature 45˚C we have an inaccuracy $\Delta T_{45C} = 0.2$˚C due to the chemical reactions, then the correction on $T = 41$˚C became $\Delta T_{41C} = 3.2$˚C. Due to the general hyperthermia practice, the temperature does not exceed the 41˚C in average, so the inaccuracy in these practical temperatures is large. The application of electric field enhances the accuracy to target the chemical bonds directly. Consequently, this energy-absorption has better efficacy at the same temperature when applied according to the targeted bonds. General electromagnetic radiation or capacitive heating affects all dipoles, not only the concentration for those which are devoted for cellular destruction. This is the reason why certain cell-destruction can occur at a lower temperature [25] [26], when precise impedance-matched electric field action is applied, [27].

4. Conclusion

Modulation of the glycolysis both by temperature and external field is feasible. The values of the reaction change depend on the temperature and field changes by activation energy multiplied by change of temperature, and by the polarization multiplied by the change of the field. The electric field has a similar dynamic change to heating. Temperature, as the average energy of the included particles has various "waste" energy used to heat up the particles which do not participate in the desired changes. The various molecular changes in their spatiotemporal structure and the dynamical, geometrical, chemical changes could be promoted by electric field without increasing the temperature. The inaccuracy of the temperature effect could be high and must be corrected by the well-applied, electric field application.

Acknowledgements

This work was supported by the Hungarian Competitiveness and Excellence Program grant (NVKP_16-1-2016-0042).

References

[1] Winfru, A.T. (1972) Oscillatory Glycolisis in Yeast: The Pattern of Phase Resetting by Oxygen. *Archives of Biochemistry and Biophysics*, **149**, 388-401. https://doi.org/10.1016/0003-9861(72)90337-2

[2] Goldbeter, A. (1996) Biochenmical Oscillations and Cellular Rythms. Cambridge University Press, Cambridge. https://doi.org/10.1017/CBO9780511608193

[3] Novak, B. and Tyson, J.J. (2008) Design Principles of Biochemical Oscillators. *Nature Reviews Molecular Cell Biology*, **9**, 981-991. https://doi.org/10.1038/nrm2530

[4] Place, C.M. and Arrowsmith, D.K. (1990) An Introduction to Dynamical Systems. Cambridge University Press, Cambridge.

[5] Selkov, E.E. (1968) Self-Oscillations in Glycolysis. *European Journal of Biochemistry*, **4**, 79-86. https://doi.org/10.1111/j.1432-1033.1968.tb00175.x

[6] Gilon, P., Ravier, M.A., Jonas, J.C. and Henguin, J.C. (2002) Control Mechanisms of the Oscillations of Insulin Secretion *in Vitro* and *in Vivo*. *Diabetes*, **51**, S144-S151. https://doi.org/10.2337/diabetes.51.2007.S144

[7] Westermark, P.O. and Lansner, A. (2003) A Model of Phosphofructokinase and Glycolytic Oscillations in the Pancreatic β-Cell. *Biophysical Journal*, **85**,126-139. https://doi.org/10.1016/S0006-3495(03)74460-9

[8] Riz, M., Braun, M. and Pedersen, M.G. (2014) Mathematical Modeling of Heterogeneous Electrophysiological Responses in Human β-Cells. *PLoS Computational Biology*, **10**, e1003389.

[9] Merrins, M.J., Van Dyke, A.R., Mapp, A.K., Rizzo, M.A. and Satin, L.S. (2013) Direct Measurements of Oscillatory Glycolysis in Pancreatic Islet β-Cells Using Novel Fluorescence Resonance Energy Transfer (FRET) Biosensors for Pyruvate Kinase M2 Activity. *Journal of Biological Chemistry*, **288**, 33312-33322. https://doi.org/10.1074/jbc.M113.508127

[10] Olsen, L.F., Andersen, A.Z., Lunding, A., Brasen, J.C. and Poulsen, AK. (2009) Regulation of Glycolytic Oscillations by Mitochondrial and Plasma Membrane H^+-ATPases. *Biophysical Journal*, **96**, 3850-3861. https://doi.org/10.1016/j.bpj.2009.02.026

[11] Gustavsson, A.K., Adiels, C.B., Mehlig, B. and Goksör, M. (2015) Entrainment of Heterogeneous Glycolytic Oscillations in Single Cells. *Scientific Reports*, **5**, Article No. 9404. https://doi.org/10.1038/srep09404

[12] Gustavson, A.K. (2015) Glycolytic Oscillations in Individual Yeast Cells. Ph.D. Thesis, University of Gothenburg, Gothenburg.

[13] McCollum, P.D. and Henrickson, R.L. (1977) The Effect of Electrical Stimulation on the Rate of Post-Mortem Glycolysis in Some Bovine Muscles. *Journal of Food Quality*, **1**, 15-22.

[14] Song, Y., Wang, J. and Yau, S.T. (2014) Controlled Glucose Consumption in Yeast Using a Transistor-Like Device. *Scientific Reports*, **4**, Article No. 5429. https://doi.org/10.1038/srep05429

[15] Bertram, R., Sherman, A. and Satin, L.S. (2007) Metabolic and Electrical Oscillations: Partners in Controlling Pulsatile Insulin Secretion. *American Journal of Physiology-Endocrinology and Metabolism*, **293**, E890-E900. https://doi.org/10.1152/ajpendo.00359.2007

[16] Hazel, J.R. and Prosser, C.L. (1974) Molecular Mechanisms of Temperature Compensation in Poikilotherms. *Physiological Reviews*, **54**, 620-677. https://doi.org/10.1152/physrev.1974.54.3.620

[17] Cruz, A.L.B., Hebly, M., Duong, G.H., Wahl, S.A., Pronk, J.T., Heijnen, J.J., Daran-Lapujade, P. and van Gulik, W.M. (2012) Similar Temperature Dependencies of Glycolytic Enzymes: An Evolutionary Adaptation to Temperature Dynamics? *BMC Systems Biology*, **6**,151. https://doi.org/10.1186/1752-0509-6-151

[18] Mair, T., Warnke, C., Tsuji, K. and Muller, S.C. (2005) Control of Glycolytic Oscillations by Temperature. *Biophysical Journal*, **88**, 639-646.

[19] Postnikov, E.B., Verveyko, D.V. and Verisokin, Y.A. (2011) Simple Model for Temperature Control of Glycolytic Oscillations. *Physical Review E, Statistical, Nonlinear, and Soft Matter Physics*, **83**, Article ID: 062901. https://doi.org/10.1103/PhysRevE.83.062901

[20] Andocs, G., Renner, H., Balogh, L., Fonyad, L., Jakab, C. and Szasz, A. (2009) Strong Synergy of Heat and Modulated Electromagnetic Field in Tumor Cell Killing. *Strahlentherapie und Onkologie*, **185**,120-126. https://doi.org/10.1007/s00066-009-1903-1

[21] Pennes, H.H. (1948) Analysis of Tissue and Arterial Blood Temperatures in the Resting Human Forearm. *Journal of Applied Physiology*, **1**, 93-122. https://doi.org/10.1152/jappl.1948.1.2.93

[22] Najarian, S. and Pashaee, A. (2001) Improvement of the Pennes Equation in the Analysis of Heat Transfer Phenomenon in Blood Perfused Tissues. *Biomedical Sciences Instrumentation*, **37**,185-190.

[23] Separeto, S.A. and Dewey, W.C. (1984) Thermal Dose Determination in Cancer Therapy. *International Journal of Radiation Oncology*, **10**, 787-800. https://doi.org/10.1016/0360-3016(84)90379-1

[24] Tadayoshi, M. (1993) Cancer Treatment by Hyperthermia, Radiation and Drugs. Taylor & Francis Group, Washington DC.

[25] Yang, K.L., Huang, C.C., Chi, M.S., Chiang, H.C., Wang, Y.S., Andocs, G., *et al.* (2016) *In Vitro* Comparison of Conventional Hyperthermia and Modulated Electro-Hyperthermia. *Oncotarget*, **7**, 84082-84092. https://doi.org/10.18632/oncotarget.11444

[26] Andocs, G., Rehman, M.U., Zhao, Q.L., Tabuchi, Y., Kanamori, M. and Kondo, T. (2016) Comparison of Biological Effects of Modulated Electro-Hyperthermia and Conventional Heat Treatment in Human Lymphoma U937 Cell. *Cell Death Discovery*, **2**, Article No. 16039. https://doi.org/10.1038/cddiscovery.2016.39

[27] Szasz, A. (2015) Bioelectromagnetic Paradigm of Cancer Treatment Oncothermia. In: Rosch, P.J., Ed., *Bioelectromagnetic and Subtle Energy Medicine*, CRC Press, Taylor & Francis Group, Boca Raton, 323-336.

Scientific Research Publishing

Open Journal of Biophysics, 2018, 8, 104-116
http://www.scirp.org/journal/ojbiphy
ISSN Online: 2164-5396
ISSN Print: 2164-5388

The Quantum-Mechanical Sensitivity of Cell Hydration in Mammals

Anna Nikoghosyan, Lilia Narinyan, Armenuhi Heqimyan, Sinerik Ayrapetyan*

Life Sciences International Postgraduate Educational Center, UNESCO Chair in Life Sciences, Yerevan, Armenia
Email: *info@biophys.am

How to cite this paper: Nikoghosyan, A., Narinyan, L., Heqimyan, A. and Ayrapetyan, S. (2018) The Quantum-Mechanical Sensitivity of Cell Hydration in Mammals. *Open Journal of Biophysics*, **8**, 104-116.
https://doi.org/10.4236/ojbiphy.2018.83009

Received: April 12, 2018
Accepted: June 30, 2018
Published: July 3, 2018

Abstract

The elucidation of the mechanism on the biological effects of weak chemical and physical factors on cells and organism is one of the modern problems in life sciences. According to the Receptor Theory of Prof. Bernard Katz the impact of the biological substances on cells is realized through the activation of ligand-gated ion channels in the membrane. However, this theory doesn't provide a satisfactory explanation on the similar biological effects of extremely low concentrations of different chemical substances, which are unable to activate the ionic channels in the membrane and have non-linear dose-dependent effect on cells. Previously we have suggested that the metabolic control of cell hydration serves as a universal quantum-mechanical sensor for different weak physical and chemical signals. For supporting this hypothesis, in this article the comparative study of the effects of low concentrations of both cold (non-radioactive) and [^{3}H]-ouabain (specific inhibitor for Na^+/K^+-ATPase) on the hydration in different tissues of rats has been performed. The obtained data have shown that cold and [^{3}H]-ouabain have different effects on cell hydration and such a difference depends on the initial metabolic state of tissues. On the basis of our previous and present results it is suggested that such a quantum-mechanical sensitivity of cell hydration is realized through the cyclic-nucleotides-dependent Na^+/Ca^{2+} exchange, having a crucial role in the metabolic regulation of cell hydration.

Keywords

Rat, Hydration, Ouabain

1. Introduction

The elucidation of the mechanism on the biological effects of weak chemical and physical factors on cells and organism is one of the modern problems in life

sciences. At present, our knowledge on signal transduction in cells is based on the Membrane Theory which explains this transduction by the changes of cell membrane permeability for inorganic ions leading to generation of transient ionic currents through cell membrane [1]. However, this theory based on classical thermodynamic approaches, cannot explain the biological effects of extremely low concentrations of chemical substances [2] [3] and weak physical signals [4] [5], which are unable to activate ionic channels in the membrane and have non-linear dose-dependent effect.

The main omission of the Membrane Theory is that it does not consider the direct role of cell metabolism in generation of cell membrane potential. Although the existence of the metabolic component of membrane potential in the living cells has been revealed in a number of studies [6] [7], there isn't any reliable theory explaining the sensitivity of cells to weak physical and chemical signals.

Based on our previous research data we have developed a new approach on quantum-mechanical sensitivity of living cells to different weak factors, which are realized through the metabolic control of cell hydration [8] [9] [10]. According to this hypothesis a water molecule, having valence angle with quantum-mechanical sensitivity to different factors, serves as a primary messenger for signal transduction in cells. The metabolically generated water efflux from the cell balances the osmotic water uptake and has inhibitory effect on inward going ionic currents [11] [12] serving as a gate by which the weak signals modulate cell metabolic activity. Therefore, the metabolic control of cell hydration has been suggested as a universal quantum-mechanical sensor through which the biological effects of extremely weak chemical and physical signals on cells and organisms are realized [9]

It is known that the Na^+/K^+ pump is a key mechanism through which the metabolic control of cell hydration is realized. In excitable membranes three isoforms (α_1, α_2, α_3) of α catalytic subunit of Na^+/K^+-ATPase (working molecule for Na^+/K^+ pump) are identified [13]. They are characterized by different affinities to cardiac glycoside ouabain (specific inhibitor for Na^+/K^+-ATPase) as well as functional roles: α_1 (with low affinity) and α_2 (with middle affinity) isoforms are involved in transportation of Na^+ and K^+, while α_3 (with high affinity) is not directly involved in transporting Na^+ and K^+ and has only signaling function [14] [15]. Our previous studies have shown that these isoforms are extremely sensitive not only to ouabain but also to extremely low concentrations of other biologically active substances [2] [3] [16] as well as to weak intensity of electromagnetic fields [17] [18]. From these data it is followed that the same chemical substances with different quantum-mechanical structures (e.g. non-radioactive ouabain and [^{3}H]-ouabain) can have individual effects on cell hydration. It has been shown that Na^+/K^+ pump is a key mechanism in regulation of cell hydration and its age-dependent dysfunction brings to tissue dehydration, which is accompanied by the decrease of α_3 isoform's affinity to ouabain [19]. Therefore,

in the presented article the age-dependent comparative study of the effects of pM (agonist for α_3) and nM (agonist for α_2) concentrations of cold (non-radioactive) ouabain and [^{3}H]-ouabain on the hydration of different tissues was performed.

2. Materials and Methods

2.1. Animals

All procedures performed on animals were carried out following the protocols approved by Animal Care and Use Committee of Life Sciences International Postgraduate Educational Centre (LSIPEC, Yerevan, Armenia).

The experiments were performed on young (6 weeks old) and old (18 months old) Wistar rats. They were regularly examined, kept under control of the veterinarians in LSIPEC and reserved in a specific pathogen-free animal room under optimum conditions of 12 h light/dark cycles, at temperature of 22˚C ± 2˚C, with a relative humidity of 50% and were fed *ad libitum* on a standard lab chow and water.

2.2. Chemicals

Tyrode's Physiological solution (PS) containing (in mM) 137 NaCl, 5.4 KCl, 1.8 $CaCl_2$, 1.05 $MgCl_2$, 5 $C_6H_{12}O_6$, 11.9 $NaHCO_3$, and 0.42 NaH_2PO_4 and adjusted to pH 7.4 with NaOH was used. All chemicals were obtained from "Medisar" Industrial Chemical Importation Company (Yerevan, Armenia). The [^{3}H]-ouabain with specific activity (25.34 Ci/mM) (PerkinElmer, Massachusetts, USA) and cold (non-radioactive) ouabain at pM (10^{-11} M) and nM (10^{-9} M) concentrations dissolved in PS were used for tissue injection and incubation. All ouabain solutions were also adjusted to pH 7.4.

2.3. Experimental Design

It is well known that the anesthetics with different chemical and pharmacological profiles significantly affect metabolic processes, which play an important role in regulation of cell volume [20] [21]. Therefore, in the present experiments animals were sharply immobilized by freezing method (dipping their noses into liquid nitrogen for 3 - 5 sec) and decapitated [22]. After such a procedure the full absence of somatic reflexes on extra stimuli was recorded.

For *in vivo* experiments 15 young and 15 old animals were taken. Each animal group was divided into five subgroups (n = 3). The animals of the control group were injected with PS (according to the animal weight) and the animals of the next four subgroups were injected with 10^{-11} M and 10^{-9} M concentrations of cold and 10^{-11} M and 10^{-9} M concentrations of [^{3}H]-ouabain. After the 15th min the animals were decapitated. Brain cortex, heart muscle and liver tissues were isolated. From each animal 5 samples of each tissue were taken, washed in PS three times and then weighed (15 samples from each tissue). The protocol of experiments was the same for both young and old animals. All data were received from three independent experiments.

For investigation of the water content variations and ouabain effect in *in vitro* conditions 15 young and 15 old animals were taken. After their decapitation 5 samples of the above mentioned tissues were taken from each animal (similar to *in vivo* experiments). These samples (n = 15) were incubated in PS (as sham), cold ouabain solution (10^{-11} M, 10^{-9} M) and [^{3}H]-ouabain solution (10^{-11} M, 10^{-9} M) for 15 min, then washed in PS three times and weighed.

2.4. Definition of Water Content of Brain Tissues

The water content of brain cortex, heart muscle and liver tissues was determined by traditional "tissue drying" method [23]. After measuring the wet weight (w.w.) of tissue samples they were dried in oven (Factory of Medical Equipment, Odessa, Ukraine) for 24 h at 105˚C for determination of dry weight (d.w.). The quantity of water in 1 g of d.w. tissue was counted by the following equation: (w.w. – d.w.)/d.w.

2.5. Counting of [^{3}H]-Ouabain Receptors in the Membrane

The tissue samples from *in vivo* experiments, which were subjected to [^{3}H]-ouabain, were homogenized in 50 µl of 68% HNO_3 solution after determination of wet and dry weights. Then 2 ml of Bray's scintillation fluid was added and chemoluminescence of samples was quantified with 1450-MicroBeta liquid scintillation counter (Wallac, Turku, Finland). The number of [^{3}H]-ouabain molecules' binding with cell membranes was defined per mg of dry weight of samples.

The same procedure (the definition of the number of [^{3}H]-ouabain molecules) was performed on the tissue samples from *in vitro* experiments after removing them from the oven and determining wet and dry weights.

2.6. Statistical Analysis

Microsoft Excel and Sigma-Plot (Version 8.02A, NY, USA) were used for data analyses. The statistical significance in comparison with the sham group was calculated with Student's t-test with the following symbols (*$p < 0.05$; **$p < 0.01$; ***$p < 0.001$).

3. Results

3.1. Investigation of Brain Cortex Tissue Hydration

The comparative study of the hydration sensitivity of excitable (brain cortex, heart muscle) and non-excitable (liver) tissues to pM and nM concentrations of cold and [^{3}H]-ouabain in *in vivo* and in *in vitro* experimental conditions was performed. In i*n vivo* experiments the animals were preliminarily i/p injected with ouabain-free PS and 10^{-11} M and 10^{-9} M concentrations of cold and [^{3}H]-ouabain, while in *in vitro* experiments the tissue samples were incubated in the same solutions for 15 min.

As can be seen from **Figure 1(a)**, after i/p injection with 10^{-11} M cold ouabain

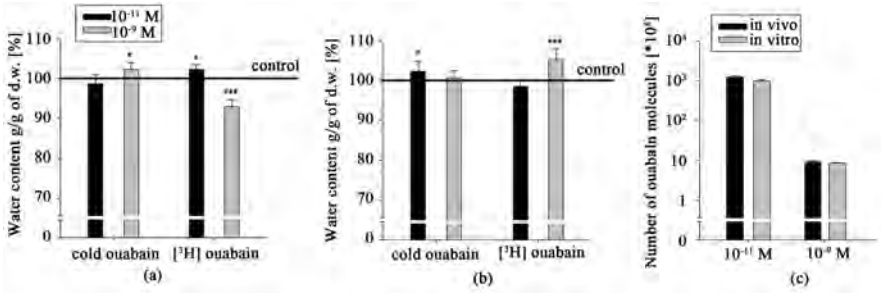

Figure 1. The water contents in cortex tissue of young rats in *in vivo* (a) and in *in vitro* (b) experiments upon the effect of pM and nM concentrations of cold and [^{3}H]-ouabain. The black and gray bars on (a) and (b) indicate the mean value of water contents in the tissues upon the effect of pM and nM ouabain, respectively. The continuous line shows the control value of tissue hydration after PS injection (a) and PS incubation (b). The black and gray bars on (c) show the number of ouabain molecules binding with cell membrane in *in vivo* and in *in vitro* conditions, respectively. Each bar represents the ±SEM (n = 45). The symbols (*) and (***) indicate $p < 0.05$ and $p < 0.001$, respectively. All data were obtained from three independent experiments.

insignificant dehydration in brain cortex tissues of young animals was observed compared with the control (injected with ouabain-free PS), while 10^{-9} M cold ouabain brought to significant hydration. The data on [^{3}H]-ouabain i/p injection (**Figure 1(a)**) revealed the opposite effect on brain tissue hydration, *i.e.* significant hydration at 10^{-11} M and expressed dehydration at 10^{-9} M [^{3}H]-ouabain.

In *in vitro experiments* (**Figure 1(b)**), where the metabolic activity of tissues was impaired, brain tissue hydration sensitivity to ouabain had a reverse character compared with those *in vivo* studies (**Figure 1(a)**): pM cold ouabain had hydration effect, while pM [^{3}H]-ouabain had dehydration effect. In case of nM cold ouabain there was no effect but nM [^{3}H]-ouabain had hydration effect on the tissues. **Figure 1(c)** illustrated that at each concentration of [^{3}H]-ouabain the number of ouabain molecules was higher in *in vivo* experiment compared with *in vitro* one.

According to the fact that aging leads to the depression of the metabolic activity, in the next series of experiments we repeated the above-mentioned protocol on old animals. As can be seen on **Figure 2(a)**, the hydration level in brain cortex tissue of old animals in *in vivo* experiments upon the impact of 10^{-11} M cold ouabain was significantly higher compared with the control, while the same concentration of [^{3}H]-ouabain sharply dehydrated the tissues. In case of 10^{-9} M cold ouabain the dehydration effect was observed, while the same concentration of [^{3}H]-ouabain had slight hydration effect on the tissues compared with the control.

In *in vitro* experiments (**Figure 2(b)**) the hydration levels of brain cortex samples at all concentrations of ouabain were nearly the same. Compared with the control data at both concentrations of cold and [^{3}H]-ouabain the dehydration effect was observed. As indicated on the data presented on **Figure 2(c)** the number of ouabain molecules at 10^{-11} M concentration of [^{3}H]-ouabain in *in vivo* as well as in *in vitro* experiments was the same, while the number of ouabain

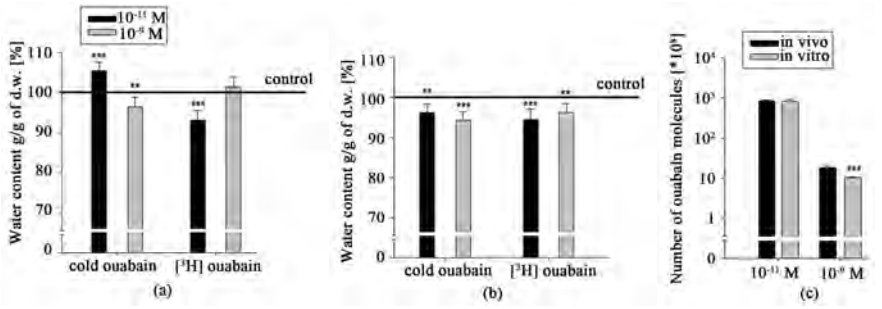

Figure 2. The water contents in cortex tissue of old rats in *in vivo* (a) and in *in vitro* (b) experiments upon the effect of pM and nM concentrations of cold and [^{3}H]-ouabain. The black and gray bars on (a) and (b) indicate the mean value of water contents in tissues upon the effect of pM and nM ouabain, respectively. The continuous line shows the control value of tissue hydration after PS injection (a) and PS incubation (b). The black and gray bars on (c) show the number of ouabain molecules binding with cell membrane in *in vivo* and in *in vitro* conditions, respectively. Each bar represents the ±SEM (n = 45). The symbols (**) and (***) indicate $p < 0.01$ and $p < 0.001$, respectively. All data were obtained from three independent experiments.

molecules at 10^{-9} M concentration of [^{3}H]-ouabain was much higher in *in vivo* experiment than in *in vitro* one.

3.2. Investigation of Heart Muscle Tissue

Considering the fact that unlike brain tissue hydration heart muscle hydration significantly depends on myosin contraction, in the next series of experiments the above mentioned protocol was performed on heart muscle tissues. The data of *in vivo* experiments presented on **Figure 3(a)** showed that the pM cold ouabain had significant dehydration effect on heart muscle tissue of young rats, while the same concentration of [^{3}H]-ouabain had hydration effect.

The effects of both nM cold ouabain and [^{3}H]-ouabain were similar to the effects of pM ouabain, but nM ouabain effect was less pronounced. In *in vitro* experiments the pM cold ouabain had slight hydration effect, while the same concentration of [^{3}H]-ouabain had expressed hydration effect on heart muscle tissue. The nM cold ouabain had more pronounced hydration effect than pM ouabain, while nM [^{3}H]-ouabain had less expressed hydration effect than pM [^{3}H]-ouabain (**Figure 3(b)**). As can be seen from **Figure 3(c)**, the number of ouabain molecules binding with cell membrane in *in vivo* and in *in vitro* experiments was the same.

The investigation of heart muscle tissues in old rats in *in vivo* condition (**Figure 4(a)**) showed significant over hydration at both concentrations (10^{-11} M and 10^{-9} M) and types of ouabain. However at 10^{-9} M [^{3}H]-ouabain the hydration level was higher.

As can be seen from **Figure 4(b)**, 10^{-11} M cold ouabain in *in vitro* experiments led to significant dehydration in old animals, while 10^{-11} M [^{3}H]-ouabain to hydration. As for the effects of 10^{-9} M ouabain the hydration reached to the level recorded at control, but 10^{-9} M [^{3}H]-ouabain brought to significant dehydration.

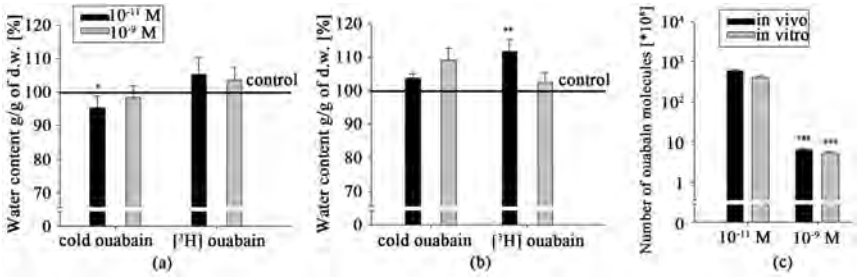

Figure 3. The water contents in heart muscle tissue of young rats in *in vivo* (a) and *in vitro* (b) experiments upon the effect of pM and nM concentrations of cold and [^{3}H]-ouabain. The black and gray bars on (a) and (b) indicate the mean value of water contents in tissues upon the effect of pM and nM ouabain, respectively. The continuous line shows the control value of tissue hydration after PS injection (a) and PS incubation (b). The black and gray bars on (c) show the number of ouabain molecules binding with cell membrane in *in vivo* and in *in vitro* conditions, respectively. Each bar represents the ±SEM (n = 45). The symbols (*) and (**) indicate $p < 0.05$ and $p < 0.01$, respectively. All data were obtained from three independent experiments.

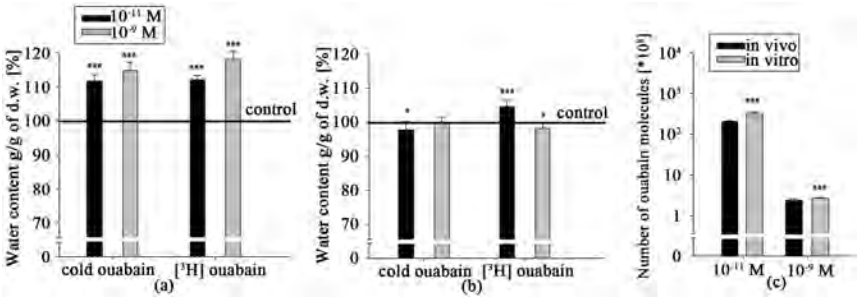

Figure 4. The water contents in heart muscle tissue of old rats in *in vivo* (a) and in *in vitro* (b) experiments upon the effect of pM and nM concentrations of cold and [^{3}H]-ouabain. The black and gray bars on (a) and (b) indicate the mean value of water contents in tissues upon the effect of pM and nM ouabain, respectively. The continuous line shows the control value of tissue hydration after PS injection (a) and PS incubation (b). The black and gray bars on (c) show the number of ouabain molecules binding with cell membrane in *in vivo* and in *in vitro* conditions, respectively. Each bar represents the ±SEM (n = 45). The symbols (*) and (***) indicate $p < 0.05$ and $p < 0.001$, respectively. All data were obtained from three independent experiments.

However, in spite of different effects on tissue hydration in *in vivo* and in *in vitro* conditions the number of ouabain molecules at [^{3}H]-ouabain was approximately the same at two different ouabain concentrations (**Figure 4(c)**).

3.3. Investigation of Liver Tissue

It is known that in soft tissues of healthy animals only a_1 isoform of Na^+/K^+-ATPase with low affinity to ouabain is expressed [24]. At the same time our previous study has shown that nM and pM ouabain concentrations activate cyclic nucleotides-dependent Na^+/Ca^{2+} exchange without any effect on Na^+/K^+ pump activity [25] [26]. Therefore, it was interesting to perform the same protocol used for the previous series of experiments on non-excitable tissues, such as liver.

Although in liver cell membrane a_2/a_3 isoforms of Na^+/K^+-ATPase were not expressed the data presented on Figure 5 indicated the modulation effect of pM and nM ouabain on its tissue hydration. Moreover, the modulation effects of low concentrations of cold and [^{3}H]-ouabain on liver tissue hydration were different compared with the effects on brain cortex and heart muscle tissues.

In i*n vivo* experiments (Figure 5(a)) cold ouabain led to dose-dependent hydration, while [^{3}H]-ouabain brought to dehydration. The significant hydration at 10^{-9} M cold ouabain turned to dehydration at 10^{-9} M [^{3}H]-ouabain. In *in vitro* experiments (Figure 5(b)) the incubation of liver samples at 10^{-11} M cold ouabain brought to more pronounced dehydration, while 10^{-11} M [^{3}H]-ouabain had weak dehydration effect on it. Cold ouabain at 10^{-9} M had no effect on tissue hydration, while [^{3}H]-ouabain at the same concentration had dehydration effect on it. It is worth to note that the ouabain binding with cell membrane at both concentrations was higher in *in vivo* state than in *in vitro* one. In old animals the effects of both cold and [^{3}H]-ouabain i/p injections on liver tissue hydration were more pronounced than in young animals (Figure 6(a)). It is interesting to note that there was no difference between cold and isotope ouabain effects on cell hydration, while 10^{-9} M cold ouabain-induced hydration was more expressed than 10^{-9} M [^{3}H]-ouabain-induced effect.

The incubation of the samples in cold ouabain solutions led to significant dehydration at 10^{-11} M, while at the same concentration of [^{3}H]-ouabain had hydration effect (Figure 6(b)). Both cold and [^{3}H]-ouabain at 10^{-9} M concentration had hydration effect on tissue but [^{3}H]-ouabain effect was less pronounced than the effect of the cold ouabain. It is interesting to note that the ouabain binding with cell membrane in *in vivo* experiment had dose-dependent increasing character, while in *in vitro* experiment it had dose-dependent weakening character (Figure 6(c)).

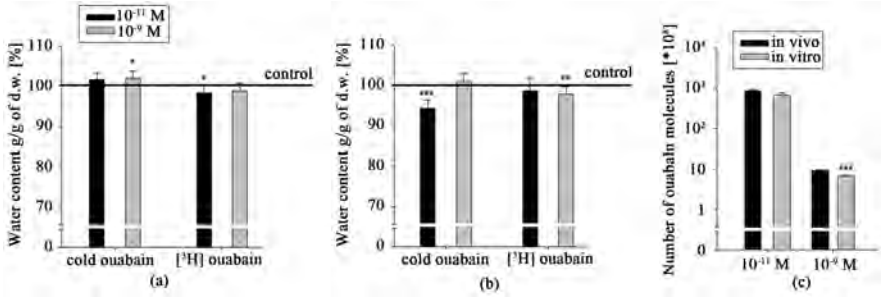

Figure 5. The water contents in liver tissue of young rats in *in vivo* (a) and in *in vitro* (b) experiments upon the effect of pM and nM concentrations of cold and [^{3}H]-ouabain. The black and gray bars on (a) and (b) indicate the mean value of water contents in tissues upon the effect of pM and nM ouabain, respectively. The continuous line shows the control value of tissue hydration after PS injection (a) and PS incubation (b). The black and gray bars on (c) show the number of ouabain molecules binding with cell membrane in *in vivo* and in *in vitro* conditions, respectively. Each bar represents the ±SEM (n = 45). The symbols (*), (**) and (***) indicate $p < 0.05$, $p < 0.01$ and $p < 0.001$, respectively. All data were obtained from three independent experiments.

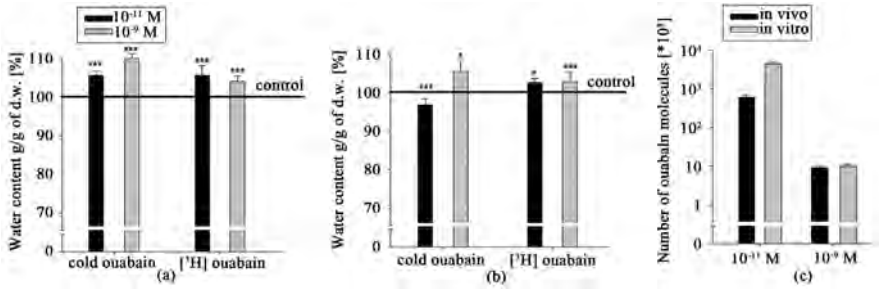

Figure 6. The water contents in liver tissue of old rats in *in vivo* (a) and in *in vitro* (b) experiments upon the effect of pM and nM concentrations of cold and [^{3}H]-ouabain. The black and gray bars on (a) and (b) indicate the mean value of water contents in tissues upon the effect of pM and nM ouabain, respectively. The continuous line shows the control value of tissue hydration after PS injection (a) and PS incubation (b). The black and gray bars on (c) show the number of ouabain molecules binding with cell membrane in *in vivo* and in *in vitro* conditions, respectively. Each bar represents the ±SEM (n = 45). The symbols (*) and (***) indicate $p < 0.05$ and $p < 0.001$, respectively. All data were obtained from three independent experiments.

4. Discussion

Previously it was shown that in brain and heart tissues of rats the pM [^{3}H]-ouabain stimulated the cGMP-dependent Na^+/Ca^{2+} exchange in forward (F) mode [27] which was accompanied by cell dehydration in young and hydration in old animals [26]. The pM [^{3}H]-ouabain-induced cell dehydration in young animals was explained by the activation of Na^+/K^+ pump as a result of Na^+/Ca^{2+} exchange-induced decrease of intracellular contents of $[Ca^{2+}]_i$, while its hydration effect on the tissues of old animal was explained by the direct effect of F Na^+/Ca^{2+} exchange because of high $[Ca^{2+}]_i$ [10]. The nM [^{3}H]-ouabain activated the cAMP-dependent Na^+/Ca^{2+} exchange in reverse mode (R) [28], having age-dependent weakening character which was reversed in old animals [18]. It is worth to note that though [^{3}H]-ouabain has been used in biological experiments for 5 decades [29] [30] the comparative studies of cold and [^{3}H]-ouabain effects on cell metabolism have not been considered. As the metabolic control of cell hydration has quantum-mechanical sensitivity [10] it becomes possible to estimate the different effects of ouabain molecules with different quantum-mechanical structure, such as cold and [^{3}H]-ouabain, on cell hydration. The data presented in this article clearly indicate that the biological effects of cold and [^{3}H]-ouabain are not identical.

The data presented on **Figure 1(a)** showed that the 10^{-11} M and 10^{-9} M cold ouabain, as was noted above (**Figure 1(a)**), had dehydration and hydration effects on brain tissues in *in vivo* experiments, respectively, while their effects were reversed in *in vitro* experiments (**Figure 1(b)**), where the metabolic state of the slices was depressed. The pM and nM concentrations of [^{3}H]-ouabain injection had opposite effects on brain tissue hydration compared with cold ouabain injection. Moreover, the reverse of dose-dependent effect of [^{3}H]-ouabain on tissue hydration in *in vitro* experiments indicated that the modulation effect of the same doses of cold and [^{3}H]-ouabain had different metabolic nature.

Previously it has been shown that [^{3}H]-ouabain binding with cell membrane depends on both the number of ouabain receptors and their affinity: the number of receptors increases with cell swelling [30], while ouabain receptors affinity increases with the decrease of $[Ca^{2+}]_i$ [19]. The data obtained in *in vivo* experiment indicating that the number of ouabain molecules at pM concentration was higher than at nM ouabain (**Figure 1(c)**) can be explained by the pM ouabain-induced activation of F Na^+/Ca^{2+} exchange leading to the decrease of $[Ca^{2+}]_i$ and increase of receptors affinity to ouabain, while the decrease of ouabain binding with cell membrane in *in vitro* experiments can be a result of $[Ca^{2+}]_i$ increase.

The received data allow us to suggest that different effects of pM and nM ouabain as well as the difference in the effects of radioactive and cold ouabain is due to the initial level of $[Ca^{2+}]_i$. This suggestion is consistent with the data of the same protocol of experiments performed on old rats, when the initial level of $[Ca^{2+}]_i$ in brain tissues was higher than in young animals [31].

The data obtained in old animals showed that *in vivo* experiment the pM cold ouabain led to hydration, while [^{3}H]-ouabain had strong dehydration effect on brain cortex tissues (**Figure 2(a)**). In case of the nM ouabain i/p injection we recorded opposite data: cold and [^{3}H]-ouabain had dehydration and slight hydration effect on tissue, respectively. Moreover, in *in vitro* experiments, in which the tissue samples had high Ca^{2+} contents compared with that in *in vivo* experiments, both concentrations of cold and [^{3}H]-ouabain ouabain had dehydration effect on tissues. The differences between the effects of pM and nM as well as between cold and isotope ouabain were inconsistent (**Figure 2(b)**).

The data on dose-dependent binding with membrane in the cortex tissue of old animals indicated that there was dose-dependent increase of ouabain binding (**Figure 2(c)**). These age-dependent differences can be explained by the fact that in old animals $[Ca^{2+}]_i$ is higher. As a result of this, the activation of cGMP-dependent F Na^+/Ca^{2+} exchange had its direct hydration effect on cells [18].

Thus, the obtained data indicating that the same concentrations of cold and [^{3}H]-ouabain had different effects on cortex tissue hydration. The fact that the effect of pM [^{3}H]-ouabain was approximately the same as in case of cold nM ouabain clearly indicates that the existence of [^{3}H] in ouabain molecules increases its effect on cell hydration. This suggestion is supported by the obtained data of the similar study on heart muscle tissues.

It is known that approximately 50% of cardiomyocyte volume consists of myofibrils [32] and $[Ca^{2+}]_i$-dependent contractility of the latter has a determining role in muscle tissues hydration. The data presented on **Figure 3** and **Figure 4** indicate that as in case of cortex tissue (**Figure 1** and **Figure 2**) the cold and [^{3}H]-ouabain at the same concentrations had different effects on heart tissue hydration. The i/p injection of cold ouabain in young animals had dose-dependent dehydration effects on muscle compared with control, while [^{3}H]-ouabain had dose-dependent weakening effect on hydration in heart muscle tissue (**Figure 3(a)**). The data that in heart muscle tissues of old animals (containing higher $[Ca^{2+}]_i$ than in young animals) when the cold and [^{3}H]-ouabain injection led to

the same dose-dependent hydration effect on muscle (**Figure 4(a)**) indicate that their effects on cell hydration is realized by different mechanisms controlling $[Ca^{2+}]_i$. The data on the difference between cold and $[^3H]$-ouabain effects appeared in heart muscle samples incubated in *in vitro* experiments seem extremely interesting. The facts that in *in vitro* experiments where $[Ca^{2+}]_i$ is considered to be higher than in *in vivo* experiments and the increase of $[Ca^{2+}]_i$ activates cGMP-dependent F Na^+/Ca^{2+} exchange through the activation of Ca^{2+}-calmodulin-induced NO production, which in its turn stimulates cGMP formation, allow us to suggest that the modulation effect of $[^3H]$-ouabain on cell hydration is realized through this chain. However, to prove this suggestion more detailed investigation is needed.

It is known that all three isoforms of Na^+/K^+-ATPase are expressed in excitable tissues (nerve and muscle membrane), while in soft tissues of healthy animals only a_1 isoform is expressed [24]. At the same time by our previous experiments performed on snail neurons [28] [30], heart muscles and brain tissues of rats [18] it was shown that pM and nM ouabain-induced modulation of Na^+/Ca^{2+} exchange did not depend on Na^+/K^+ pump and it was realized through the changes of intracellular nucleotides [17] [18].

The data presented on **Figure 5(a)** indicate that after pM and nM cold ouabain injections of young animals the liver tissue hydration increased by dose-dependent manner, while the same concentrations of $[^3H]$-ouabain injections led to dehydration effect. These data support the above suggestion that cold and isotope had different biological effects on cells. It is worth to note that as in case of excitable tissues, the sensitivity of liver tissue hydration to low concentrations of both cold and $[^3H]$-ouabain was higher in old animals as well as in the samples incubated in *in vitro* experiment, when the metabolic activity of tissues was depressed. Therefore, the data that such low concentrations of non-radioactive and radioactive ouabain effects depend on $[Ca^{2+}]_i$ and the data that $[^3H]$-ouabain binding with cell membrane is depressed in *in vitro* experiments allow us to suggest that the modulation of tissue hydration at both concentrations of cold and $[^3H]$-ouabain takes place through the changes of $[Ca^{2+}]_i$.

Thus, the obtained data bring us to the following conclusions:

1) Cold and $[^3H]$-ouabain at pM and nM concentrations have different effects on cell hydration;

2) The different effects of cold and $[^3H]$-ouabain on cell hydration is due to their different activities on cGMP-dependent Na^+/Ca^{2+} exchange controlling intracellular Ca^{2+} concentration. Therefore, these data allow us to conclude that in biological experiments cold ouabain and radioactive ouabain effects cannot be considered as equivalent. These data indicate that Na^+/Ca^{2+} exchange is Na^+/K^+ pump-independent mechanism in the membrane having quantum-mechanical sensitivity.

References

[1] Hodgkin, A.L. (1964) The Ionic Basis of Nervous Conduction. *Science*, **145**,

1148-54. https://doi.org/10.1126/science.145.3637.1148

[2] Ayrapetyan, S.N. and Carpenter, D.O. (1991) Very Low Concentrations of Acetylcholine and GABA Modulate Transmitter Responses. *Neuroreport*, **2**, 563-565. https://doi.org/10.1097/00001756-199110000-00002

[3] Ayrapetyan, S.N. and Carpenter, D.O. (1991b) The Modulatory Effect of Extremely Low Doses of Mediators on Functional Activity of the Neuronal Membrane. *Zhurnal Evoliutsionnoi Biokhimii*, **27**, 146-151. (In Russian)

[4] Devyatkov, N.D. (1973) Influence of Millimeter-Band Electromagnetic Radiation on Biological Objects. *Uspekhi Fizicheskih Nauk*, **110**, 453-454. (In Russian) https://doi.org/10.3367/UFNr.0110.197307l.0453

[5] Adey, W.R. (1981) Tissue Interactions with Non Ionizing Electromagnetic Fields. *Physiological Reviews*, **61**, 435-514. https://doi.org/10.1152/physrev.1981.61.2.435

[6] Ayrapetyan, S.N. (1969) Metabolically Dependent Fraction of Membrane Potential and Electrode Properties of the Membrane of Giant Neurons in Mollusks. *Biofizika*, **14**, 1027-1031. (In Russian)

[7] Thomas, R.C. (1972) Electrogenic Sodium Pump in Nerve and Muscle Cells. *Physiological Reviews*, **52**, 563-594. https://doi.org/10.1152/physrev.1972.52.3.563

[8] Ayrapetyan, S.N., Nasarenko, S.A. and Sorokhina, Z.A. (1971) Dependence of Active Ion Transport in Snail Neurons on the Ionic Composition of Extracellular Medium. *Biofizika*, **16**, 1037-1042. (In Russian)

[9] Ayrapetyan, S. (2015) The Dysfunction of Metabolic Controlling of Cell Hydration Precedes Warburg Phenomenon in Carcinogenesis. *Journal of Bioequivalence & Bioavailability*, **7**, 59. https://doi.org/10.4172/jbb.10000e59

[10] Ayrapetyan, S.N. (2016) The nM Ouabain-Induced Tissue Dehydration as a Novel Diagnostic Marker for Neuronal Pathology. *Global Drugs and Therapeutics*, **2**, 1-2.

[11] Ayrapetyan, S.N., Rychkov, G.Y. and Suleymanyan, M.A. (1988) Effects of Water Flow on Transmembrane Ionic Currents in Neurons of Helix Pomatia and in Squid Giant Axons. *Comparative Biochemistry and Physiology*, **89**, 179-186. https://doi.org/10.1016/0300-9629(88)91076-6

[12] Suleymanian, M.A., Ayrapetyan, V.Y., Arakelyan, V.B., *et al.* (1993) The Effect of Osmotic Gradient on the Outward Potassium Current in Dialyzed Neurons of Helix Pomatia. *Cellular and Molecular Neurobiology*, **13**, 183-190. https://doi.org/10.1007/BF00735374

[13] Juhaszova, M. and Blaustein, M. (1997) Na^+ Pump with Low and High Ouabain Affinity Apha Subunit Isoforms Are Differently Distributed in Cells. *Proceedings of the National Academy of Sciences*, **94**, 1800-1805. https://doi.org/10.1073/pnas.94.5.1800

[14] Xie, Z. and Askari, A. (2002) Na^+/K^+-ATPase as a Signal Transducer. *European Journal of Biochemistry*, **269**, 2434-2439. https://doi.org/10.1046/j.1432-1033.2002.02910.x

[15] Liu, J., Tian, J., Haas, M., Shapiro, J., Askari, A. and Xie, Z. (2000) Ouabain Interaction with Cardiac Na^+/K^+-ATPase Initiates Signal Cascades Independent of Changes in Intracellular Na^+ and Ca^{2+} Concentrations. *The Journal of Biological Chemistry*, **275**, 27838-27844.

[16] Dadalyan, S.S., Azatyan, K.V. and Ayrapetyan, S.N. (1988) Effect of Small Concentrations of Neurotransmitters on the Antigradient Transport of Sodium Ions and on the Intracellular Level of the Cyclic Nucleotide in Helix Pomatia Neurons. *Neurochemistry*, **7**, 18-25. (In Russian)

[17] Narinyan, L., Ayrapetyan, G. and Ayrapetyan, S. (2013) Age-Dependent Magnetosensitivity of Heart Muscle Ouabain Receptors. *Bioelectromagnetics*, **34**, 312-322. https://doi.org/10.1002/bem.21769

[18] Heqimyan, A., Narinyan, L., Nikoghosyan, A. and Ayrapetyan, S. (2015) Age-Dependent Magnetic Sensitivity of Brain and Heart Muscles. In: Markov, M., Ed., *Electromagnetic Fields in Biology and Medicine*, CRC Press, Boca Raton, 217-230. https://doi.org/10.1201/b18148-15

[19] Heqimyan, A., Narinyan, L., Nikoghosyan, A., *et al*. (2012) Age Dependency of High Affinity Ouabain Receptors and Their Magnetosensitivity. *The Environmentalist*, **32**, 228-235. https://doi.org/10.1007/s10669-011-9383-0

[20] Krnjevic, K. (1992) Cellular and Synaptic Actions of General Anaesthetics. *General Pharmacology*, **23**, 965-975. https://doi.org/10.1016/0306-3623(92)90274-N

[21] Heqimyan, A., Deghoyan, A. and Ayrapetyan, S. (2011) Ketamine-Induced Cell Dehydration as a Mechanism of Its Analgesic and Anesthetic Effects. *Journal of International Dental and Medical Research*, **4**, 42-49.

[22] Takahashi, R. and Aprison, M. (1964) Acetylcholine Content of Discrete Areas of the Brain Obtained by a Near-Freezing Method. *Journal of Neurochemistry*, **11**, 887-892. https://doi.org/10.1111/j.1471-4159.1964.tb06740.x

[23] Adrian, R.H. (1956) The Effect of Internal and External Potassium Concentration on the Membrane Potential of Frog Muscle. *Journal of Physiology*, **133**, 631-658. https://doi.org/10.1113/jphysiol.1956.sp005615

[24] Blaustein, M.P. and Lederer, W.J. (1999) Na^+/Ca^{2+} Exchange. Its Physiological Implications. *Physiological Reviews*, **79**, 763-854. https://doi.org/10.1152/physrev.1999.79.3.763

[25] Ayrapetyan, S.N., Suleymanyan, M.A., Saghyan, A.A. and Dadalyan, S.S. (1984) Autoregulation of Electrogenic Sodium Pump. *Cellular and Molecular Neurobiology*, **4**, 367-383. https://doi.org/10.1007/BF00733598

[26] Ayrapetyan, S., Heqimyan, A. and Nikoghosyan, A. (2012) Age-Dependent Brain Tissue Hydration, Ca Exchange and Their Dose-Dependent Ouabain Sensitivity. *Bioequivalence & Bioavailability*, **4**, 60-68. https://doi.org/10.4172/jbb.10000114

[27] Ayrapetyan, S. (2012) The Dysfunction of Metabolic Controlling Cell Hydration Is a Primary Mechanism for Generation of Aging-Related Nerve Disorders. *Bioequivalence & Bioavailability*, **4**, 9-12. https://doi.org/10.4172/jbb.10000e15

[28] Sagian, A.A., Ayrapetyan, S.N. and Carpenter, D.O. (1996) Low Concentrations of Ouabain Stimulate Na:Ca Exchange in Neurons. *Cellular and Molecular Neurobiology*, **16**, 489-498. https://doi.org/10.1007/BF02150229

[29] Baker, P.F. and Willis, J.S. (1970) Potassium Ions and the Binding of Cardiac Glycosides to Mammalian Cells. *Nature*, **226**, 521-523. https://doi.org/10.1038/226521a0

[30] Ayrapetyan, S.N., Suleymanyan, M.A., Saghyan, A.A. and Dadalyan, S.S. (1984) Autoregulation of the Selectrogenic Na Pump. *Cellular and Molecular Neurobiology*, **4**, 367-384. https://doi.org/10.1007/BF00733598

[31] Khachaturian, Z.S. (1989) The Role of Calcium Regulation in Brain Aging: Reexamination of a Hypothesis. *Aging*, **1**, 17-34.

[32] Nakano, S., Muramatsu, T., Nishimura, S. and Senbonmatsu, T. (2012) Cardiomyocyte and Heart Failure. In: Sugi, H., Ed., *Current Basic and Pathological Approaches to the Function of Muscle Cells and Tissues*, Intech, London, 161-182. https://doi.org/10.5772/47772

Scientific Research Publishing

Open Journal of Biophysics, 2018, 8, 117-154
http://www.scirp.org/journal/ojbiphy
ISSN Online: 2164-5396
ISSN Print: 2164-5388

Guided Folding of Life's Proteins in Integrate Cells with Holographic Memory and GM-Biophysical Steering

Dirk K. F. Meijer[1*], Hans J. H. Geesink[2]

[1]University of Groningen, Groningen, The Netherlands
[2]Biophysics Group, Loon op Zand, The Netherlands
Email: *meij6076@planet.nl

How to cite this paper: Meijer, D.K.F. and Geesink, H.J.H. (2018) Guided Folding of Life's Proteins in Integrate Cells with Holographic Memory and GM-Biophysical Steering. *Open Journal of Biophysics*, **8**, 117-154.
https://doi.org/10.4236/ojbiphy.2018.83010

Received: April 26, 2018
Accepted: July 14, 2018
Published: July 17, 2018

Abstract

The current geometric and thermodynamic approaches in protein folding studies do not provide a definite solution to understanding mechanisms of folding of biological proteins. A major problem is that the protein is first synthesized as a linear molecule that subsequently must reach its native configuration in an extremely short time. Hydrophobicity-hydrophilicity models and random search mechanism cannot explain folding to the 3-D functional form in less than 1 second, as it occurs in the intact cell. We propose an integral approach, based on the embedding of proteins in the whole cellular context under the postulate: a life protein is never alone. In this concept the protein molecule is influenced by various long and short distance force fields of nature such as coherent electromagnetic waves and zero-point energy. In particular, the role of solitons is reviewed in relation to a novel GM-scale biophysical principle, revealed by us. This recent finding of a set of discrete EM frequency bands, that either promote or endanger life conditions, could be a key in further studies directed at the morphogenetic aspects of protein folding in a biological evolutionary context. In addition, an alternative hypothesis is presented in which each individual cell may store integral 3-D information holographically at the virtual border of a 4-D hypersphere that surrounds each living cell, providing a field receptive memory structure that is instrumental in guiding the folding process towards coherently oscillating protein networks that are crucial for cell survival.

Keywords

Protein Folding, Coherent Wave Pattern, Electromagnetic Fields, Solitons, Harmonics, Cellular Automata, Quantum Mechanics

1. Introduction

The issue of protein folding is often considered using two different approaches that can be called "biophysical" and "geometrical" [1]. The "biophysical" approach uses concepts such as Gibbs free energy, entropy, and temperature to study protein folding. Simulations of folding are based on statistical physics. In the "geometrical" approach, folding is considered geometrically, as a part of the broader context of the folding of figures of different topologies. A major problem (the so called Levinthal's paradox) is that the protein is first synthesized as a linear molecule that subsequently must reach its native configuration in a short time (on the order of seconds or less, Figure 1). Importantly, the protein can only perform its functions in this (often single) configuration. The problem, however, is that the number of possible conformational states is exponentially large for a long protein molecule. Despite the almost 30 years of attempts to resolve this paradox, a definite solution has not yet been found. In particular, computational biology has shown that the problem of folding based on H-P

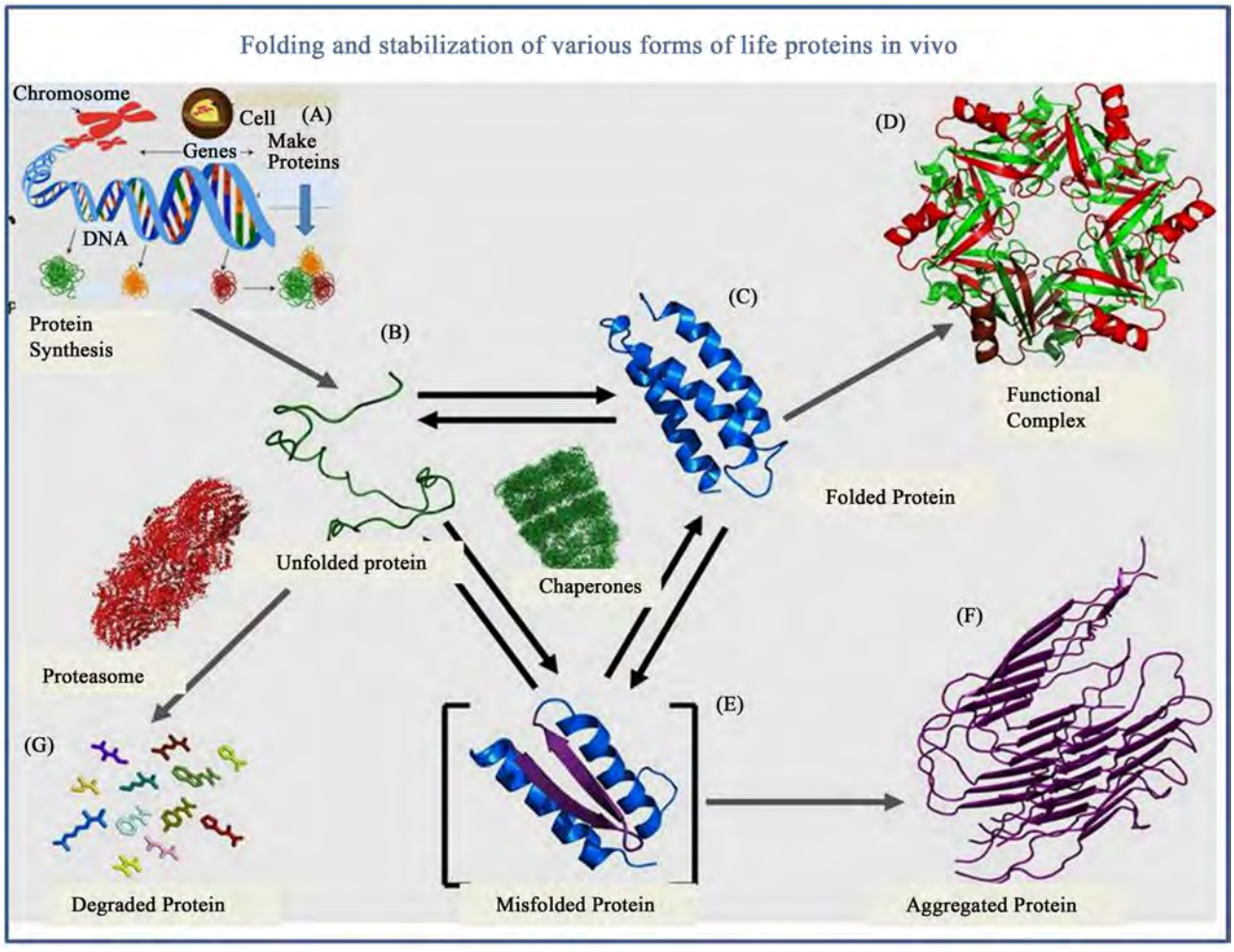

Figure 1. Protein folding in the cell; (A): Ribosomal protein synthesis; (B): Native state; (C): Folded functional conformation; (D): Functional complex; (E): Misfolded form; (F): Toxic aggregate; (G): Degradation products; (modified from Munoz and Cermanara, 2016).

(hydrophobic-hydrophilic) model, is extremely complex (*i.e.*, generally requires an enormous number of steps [2]. Levinthal concluded rightfully that a random search can only be performed in an unrealistic timeframe of billions of years [1]. Thus two major questions remain: what are the actual folding mechanisms and how can this ultra-rapid process be realized in the whole, intact, cell structure?

Martinez noted that the current folding models had weak predictive ability [3]. Natural proteins consist of 100 to 500 building blocks (alpha-amino-acids), but a random search mechanism cannot provide real-time folding on the order of 1 sec. for these proteins. In the framework of a funnel-like energy landscape, the author considers a simple kinetic model of protein folding. However, this kinetic model assumes that once a domain reaches the correct state, it stays there. However, it remains unclear how the domain "knows" that it reached the correct state. After all, an intermediate state is not the minimum energy a state—the minimum is only expected for the whole structure. In the current geometric and thermodynamic approaches in protein folding mechanisms, impressive progress was made, as for instance exemplified by recent papers [4] [5], yet such bottom up approaches fail to provide a satisfactory and generally predictive solution.

Munoz and Cerminara recently reviewed current generation of thermodynamic methods to map ultrafast folding landscapes, interaction networks and various mechanisms at nearly atomic resolution and concluded that folding is tightly coupled to a large number of processes in what they call the protein life cycle (see **Figure 1**), but also stated that there is a deep divide between what theory and simulations predicted and what experiments showed [6]. Bédard *et al.* earlier pointed out that folding should be seen as a heterogeneous process with a spectrum of intermediates that is not so much based on independent and unrelated pathways [2]. Rather, it seems governed by the same step-wise pathway that depends on the cooperative interaction with, so called, foldon units of the target native protein, that is, in a predetermined pathway sequence that however is subject to misfolding errors. All this may be taken as an illustration of the complexity of the folding process in vitro, not to speak of the multi-factorial situation in the intact cell.

2. Alternatives for Classical Approaches

The present study aims at creating a systematic overview of a wide spectrum of EM frequencies that may influence protein folding, in order to unravel the mechanisms by which proteins obtain their functional conformation as parts of integral vibratory networks for inter- and intra-cellular communication.

In order to present a complimentary view to existing theories, a versatile approach to the problem is presented, based on the embedding of proteins in an integral cellular context. This includes, apart from the known genome and proteome modalities, a well defined "electrome" aspect [7]. We consider the protein molecule as being influenced by the various long and short distance

force fields of nature such as gravity, electromagnetism, and zero-point energy, in addition to intrinsic vibratory states of macromolecules that generate coherent excitations in the cell. By defining the condition in which the protein is finally shaped in its 3-D functional configuration in more detail, first of all the interaction of the polypeptide structure with interfacial, potentially structured water dipole molecules and inorganic ions should be taken into account (**Figure 2**). In addition the (partly)-folded polypeptide chain may undergo functional quantum entanglement with (nearly)-identical proteins, specific substrate molecules and chaperones [8] [9]. Special reference should also be given to the permanent influence of magneto-reception, due to the exposure to external and internal electromagnetic fields, that exhibit discrete radiation frequencies and have been shown by us to influence life conditions [10] [11] [12]. These morphogenetic mechanisms can be mediated by phonon/soliton excitations that, according to abundant literature, lead to coherent vibrational domains in cells that also can take the form of wave/particle condensates and non-local multi-boson fields

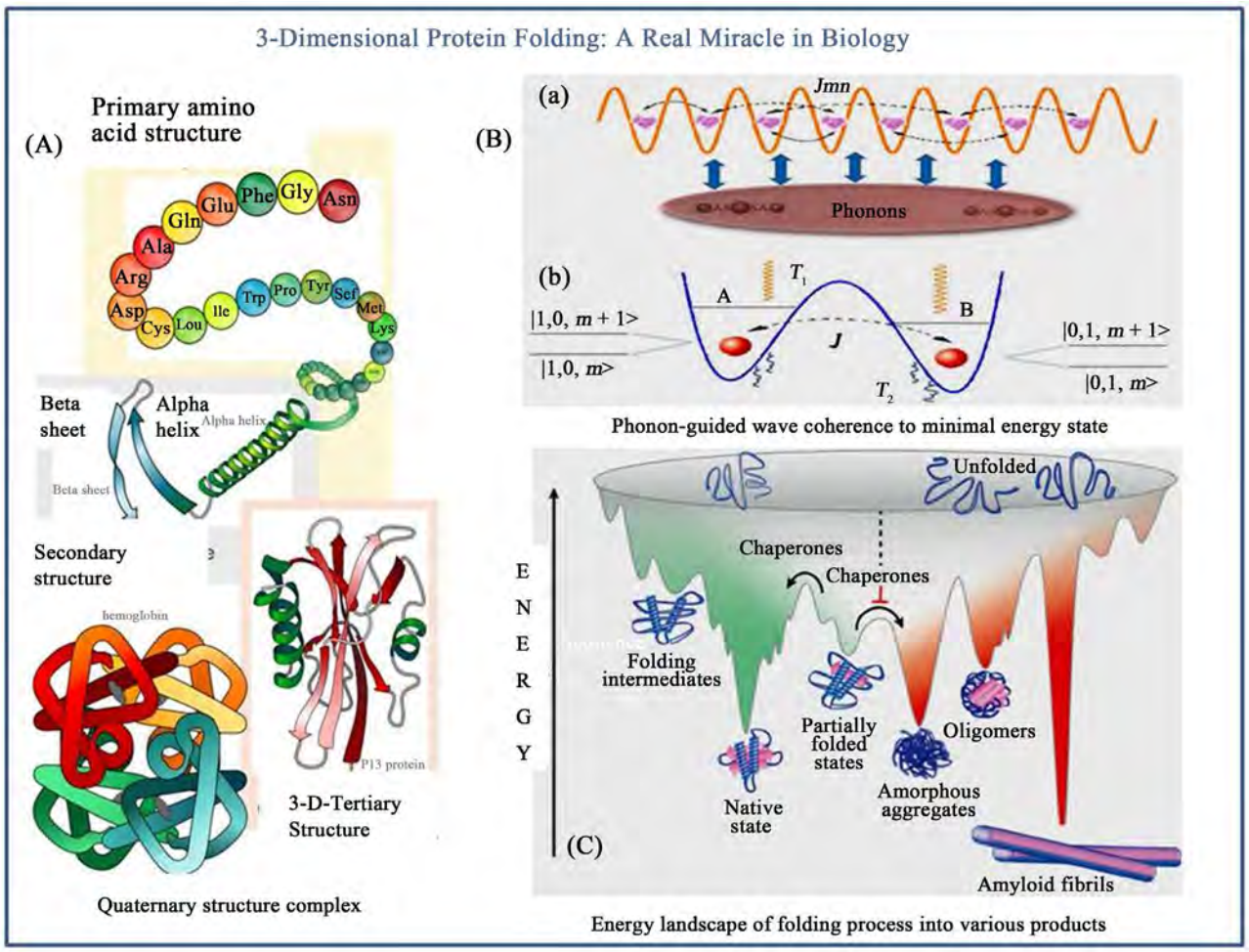

Figure 2. (A): Protein folding from primary to quaternary structure; (B): Influence of phonons on wave coherence, leading to long-lived oscillations through energy dissipation (b) and protection to environmental noise (modified from Zhang and Wang, 2016) (C): Energy landscape with intramolecular (left) and intermolecular aspects (right), producing various endproducts.

(reviewed by Belyaev [13], Brizhik [14], Cifra [15], Cosic *et al.* [16], Hammerschlag *et al.* [17], Levin [18], Muehsam [19], Pokorny [20], Rakovic [21], Tuszynski *et al.* [22]).

In this framework an alternative hypothesis is presented in which we envision a fractal toroidal operator structure to collect and integrate the abovementioned wave information of cells, including their proteins and stores it in a holographic manner on a 3-D virtual screen at the border of a 4-D hypersphere that surrounds each individual cell. This nested torus geometry is fractal at the various organizational levels of the living cell and also provides aspects of error-correction and quality control of the protein folding process. The torus geometry also potentially opens a fourth spatial dimension with a symmetric time aspect, in which the particular protein can be directed to a final functional configuration in the context of the integral cell and whole cell context. This theory finds support in the earlier used computational neural network models, in which integral forward processing of information in a neuronal network, leads to a growing addressable holographic memory space [23]. The global and local excitation mechanisms and the presence of various cytoplasmic factors within the cell, clearly imply that "a life protein molecule is never alone", as depicted in Table 1.

3. Long Range Coherence of Vibrational Mechanisms in Protein Folding

Biomolecular systems exhibit broad vibrational spectral features in the terahertz regime, corresponding to functionally relevant, global, and sub global collective modes [24]. This idea is supported by terahertz absorption spectroscopy, molecular dynamics simulations and normal mode analysis (NMA) that demonstrated the broad terahertz absorption of various proteins in partially solvated

Table 1. A protein molecule in the organism is never alone.

- Proteins bind to transport proteins facilitating nucleus to cytoplasm transport.
- Proteins can be associated with cytoplasmic receptor and chaperone proteins.
- Protein molecules are imbedded in dipole water molecules that can take a clustered form.
- Protein molecules undergo high-frequency spatial changes inducing vibratory conditions.
- Unfolded (parts of) proteins adsorb (hydrated) cytoplasmic alkali cations like K^+ and anions.
- Cytoplasmic proteins bind organic compounds such as ATP and fatty acids.
- Proteins are exposed to various force fields: electromagnetism, gravity, dark energy and zero-point energy.
- Influence of force fields on protein structure is collected and integrated by 4D toroidal geometry.
- Formation of functional 3-D proteins requires a combined genomic/electromic machinery.
- Protein molecules undergo conformational changes that induce vibratory states.
- Different protein molecules can show mutual specific coherent resonance patterns.
- Proteins can communicate in functional networks through their resonant states.
- Protein morphology is influenced by external electromagnetic and geo-magnetic fields.
- Protein molecule folding is influenced by coherent macromolecular vibration domains in the cell.
- Protein geometry can be modeled using space-time with 4 spatial dimensions.
- Protein structure can, in principle, be modified by quantum entanglement as a long-distant aspect.

conditions, as well as in aqueous environments (**Figure 2**) Terahertz vibrational properties of biomolecules resulted in the accessibility of the so-called "terahertz gap" in a water environment. Fröhlich pointed out that energy provided to terahertz modes of a protein may not be completely thermalized but can be redistributed via the nonlinear processes towards specific low-frequency modes of vibration of the biomolecular structure. Fröhlich's description was based upon on a quantum Hamiltonian, also taking into account the dynamics of phonons of each normal mode of vibration, ruled by linear and nonlinear interactions with a thermal environment (e.g., the cell cytoplasm) as well as an external source of energy (biochemical reactions, ATP hydrolysis, endogenous electromagnetic fields). It can be shown that the system of normal modes will rapidly achieve a steady state, characterized by a non-thermal energy distribution, where most of the phonons will adopt modes of lowest frequencies. Applied to biological systems, this effect is equivalent to having the subsystems of a biomolecular structure oscillate cooperatively over long distances at specific frequencies. As emphasized by Reimers *et al.*, if a coherent effect similar to Fröhlich's effect would be experimentally validated, this could lead to numerous applications in physics, biology, and medicine [25].

Similar collective properties of a system such as lasing, superconductivity, and Bose-Einstein condensation have been suggested. Nowadays, several authors have reported the existence of long-lived excited low-frequency modes in protein structures. For example, Lundholm *et al.* used combined terahertz techniques with a highly sensitive X-ray crystallographic method to visualize the low-frequency vibrational modes in the crystal structure of hen-egg white lysozyme [26]. This study was later substantiated in near-field THz absorption spectroscopic studies on in proteins in watery solution [27]. Such studies indicate that 0.4 THz electromagnetic radiation induces non-thermal changes in electron density. In particular, a local increase of electron density in a long alpha-helix motif was observed consistent with a subtle longitudinal compression of the helix at a micro- to milli-second lifetime.

Also, microtubules and cell membranes—for which the hydrolysis of adenosine triphosphate (ATP) or guanosine triphosphate (GTP) provides sources of energy supply—would also be good candidates for Fröhlich's effect. Pokorny, experimentally observed a strong excitation in the spectrum of vibration of microtubules localized in the 10 MHz range that could also be a further evidence of Fröhlich condensation at lower frequencies [20]. Such interactions are thought to play an important role in biomolecular organization, since unlike electrostatic forces, their range could extend far beyond the Debye length. Such interactions occur only when specific modes of the coupled system are strongly excited. Devices such as the Fluorescent Correlation Spectroscopy enable the detection of long-distance interactions between biomolecules in solution by measuring their diffusion coefficient as a function of their concentration [28].

Goushcha explained the idea behind the Davydov's soliton as follows: solitons can be stabilized through the hydrolysis of adenosine triphosphate (ATP) that

creates excited vibrational states in the peptide group, allowing vibrational excitation to propagate to the neighboring groups due to dipole interaction between groups [29].

The excitation interacts also with the hydrogen bond, creating a local deformation that is coupled (self-trapped) to the vibrational excitation through a feedback mechanism. If the feedback is strong enough, a new, non-dissipative state associated with vibrational excitation and hydrogen bond distortion will be created and will propagate coherently along the peptide chain.

Conventional theories cannot explain how the folding protein chooses a single stable structure among billions of others, nor how freely movable ion channel proteins organize themselves into metastable periodic patterns. Rather, such structures may finally evolve into functional clusters, through steering mechanisms of non-thermal biological effects of weak electromagnetic fields with a quantum energy far below the average energy of thermal fluctuations etc. The currently most successful models consider the protein folding as a two-state first-order phase transition triggered by a spontaneous nucleation and progressing along the energy funnel-type landscape by choosing thermodynamically most favorable barrier-crossing steps, facilitated by favorable conformational states. The funnel landscape in the proposed models emerges only for those amino acid sequences for which there is a structure in which nearly all the various interactions are simultaneously minimized; *i.e.*, native proteins are only minimally frustrated (see later).

The self-organization of the protein folding process is supposed to augment itself by enhancing the stability of the core against large-scale motions that would unfold the protein and stabilizing the native state through hydrophobic interaction that drives the overall collapse of the chain robustness of the native structure against mutations, etc. Yet, a unifying concept that combines the basic features governing self-organization of proteins into complex three-dimensional structures both *in vitro* and *in vivo* is still lacking. This may be attributed to a complexity of the folding process that involves a very large number of interactions (with structural feedback), allowing calculation of only relatively small native structures and other critical limitations. Current studies are focused on numerous as yet unresolved questions, such as unfolding-refolding reactions and the role of hidden intermediates such as water dynamics in guiding the chain movements.

Importantly, it should be mentioned here that, very likely, proteins do not adopt their native structure *in-vitro* conditions, but rather require a complete cellular machinery to correctly fold *in vivo* (see Rost, 2003, for many relevant references [30]).

An interesting evolutionary concept on protein folding was put forward by Wolynes in which the folding process is modeled in a energy landscape funnel, and related to the, so called, minimal frustration theory [5]. The author pictures the becoming process of a single functional life protein as an interplay between funnel-shaped information spaces of sequence versus configuration entropies

and thus of an ongoing superposition of information states with regard to protein composition and its final functional 3-D form. In these processes the protein passes several energy barriers that, to various degrees, can frustrate the temporal aspect of the folding. We argue in the following sections, that such frustration modalities, that in fact represent "conflicts" in choice of favorable interactions in the folding process, could be "helped" by local coherent vibrational solitonic states.

4. The Cellular Protein Electrome as Influenced by Discrete EM Frequency Bands

As mentioned above, living cells contain an oscillating macromolecular apparatus, tentatively called the cellular electrome [7] that can be excited by internal as well as by external electromagnetic fields. Through a process of resonance, the various geometry features can become expressed in life systems as coherent vibratory patterns that somehow influence the functional structure and metabolism of the exposed cell systems. The particular internal oscillations may mirror typical mathematical eigenfrequencies of the various external fields over a broad range of frequencies. This resonant coherency is analogue to the principles of Fröhlich-Bose-Einstein condensates as initially postulated by Fröhlich (1975) [31] and later elaborated in a soliton model by Davydov (1977) [32] [33] and Pang *et al.* (2006) [34] and, as mentioned above, more recently identified in cells by spectrometric experimentation [26].

The Fröhlich/Davydov concept has been elaborated and further improved by Pang taking into account that solitons can be largely stabilized, and their life-time increased due to mutual interaction of the particles with lattice vibrations [35]. Consequently the total state of the system has been expressed in three different Hamiltonians. Due to these extensions, the solitons obtain life-times that are more compatible with the ruling biological conditions. This was expressed in Hamiltonians on quasi-coherent two-quantum state wave functions [34].

It is of interest that, for example, coherent longitudinal vibration of micro-tubular proteins may induce electromagnetic fields in the cell [15]. Thus externally applied electromagnetic fields with discrete frequencies may, through resonant mechanisms, interact with endogenous cellular fields that are produced by coherently oscillating macromolecules of the cell, that in concert provide the electrome aspect of the cell [7].

5. Potential Influence of Electromagnetic Fields in Life Systems

An extensive meta-analysis of 500 published biological/medical studies was earlier performed [10] [11], in which living material (tissues, cells, and whole animals) were exposed to external electromagnetic fields, employing a wide spectrum of frequencies. In these studies the various discrete electromagnetic frequency bands were studied as to their life-sustaining, as opposed to detrimental

actions. After collecting and scrutinizing these data, a striking pattern of frequency bands was revealed. The particular bands, representing soliton frequency zones, showed a discrete distribution pattern, plotted on an acoustic scale, in which the separation of the bands was complete and statistically highly significant. The life stabilizing electromagnetic frequency patterns of this "Life algorithm principle" could be modelled as spiral information trajectories using a toroidal geometry, as earlier shown in music theory [11]. The potential EM excitation/resonance of cell components via the detected discrete EM frequency bands were in line with almost identical eigenvalues, calculated by Ritz [36], of the sound-induced geometric/fractal patterns produced by sound excitation of vibrating membranes/plates as reported by Chladny, already in 1817 [37] and three subsequent follow-up studies of others from 1950 up to the present [11].

The actual nature of living cells and potential life supporting effects due to endogenous and exogenous EM field exposition can encompass the following mechanisms:

1) Electromagnetic fields directly influence trans-membrane ion gradients such as for Ca^{2+}, that are pivotal in cellular signalling [11] [38] [39] or perturb collective movements of extracellular (interstitial) ions that can be seen as an active plasma-like workspace [40].

2) Specific EM frequencies can cause vibrational resonance with macromolecules in the cell such as DNA/RNA, ion-channel proteins, microtubular proteins and/or cytosolic proteins, that apart from their chemical signalling may communicate through their vibrational character [16] [26] [41].

3) Cyclic polarized EM fields that can penetrate life tissue promote coherent vibration of various cell components [31] [42].

4) Extended fields of coherent molecules were assumed to be formed by a process called Bose-Einstein condensation that was proposed to occur also at life temperatures [26] [31].

5) EM photon, phonon and electron wave packages can be converted to mixed forms (quasi-particles) such as polarons (phonon/electron modalities, also called solitons), polaritons (photon/electron wave package [38].

6) Solitons in the cells may be able to constitute local quantum fields that both can be involved in intracellular morphogenetic ordering, as well as intercellular communication. For example, solitons have suggested to be instrumental in 3-D folding of proteins and DNA [10] [11] [39].

We found that the different measured typical frequencies in protein systems agree with calculated algorithmic soliton frequencies: oscillations of calcium-binding proteins in the cerebellar cortex of mice [43] and with spectral resonances of signaling proteins alpha-amino acids in the ERK-MAP Pathway [44]. The vibrational features detected by us also are fully in line with the frequencies related to tubulin protein self-assembly [41] [45] [46] [47], the microwave radiation frequencies of green fluorescent proteins [48], the frequencies present during synthesis and protein folding [49] and even to the resonances of aberrant methylation sequences in DNA [50].

Making use of the obtained algorithm of soliton frequencies, the discrete EM frequency bands and corresponding geometries, insight may be given in the patterns of folded proteins by down scaling the soliton patterns of acoustic waves to a (sub) micron level at a Terahertz frequency scale, as once made visible by Chladni (1787) [37] and Ritz (1909) [36], see **Figure 3**. According to the GM scale model of Meijer and Geesink, octave hierarchy of frequency patterns exists, and the revealed geometries are embedded in each other, as made visible by the nested fractal torus model. By selecting the right soliton basic frequencies alignment of patterns, in principle the folding of "proteins" can be made visible. In addition, rotations of structures have been measured [49]. We have recently defined the mathematical basis for the GM-scale [11] and found that the discrete distribution pattern of electromagnetic frequencies perfectly fit literature data for EPR-entanglement promoting EM fields as well as known mass/energies of all of the elementary particles of the Standard model [51] [52].

6. Potential Roles of Electromagnetic Force Fields in Biological Evolution and First Life

The highly reproducible and mathematically defined EMF (electromagnetic field) frequency bands (eigenvalues) that result in life sustainment of living cells, are envisioned as a permanently operating wave pattern phenomenon, [10] [11], and turned out to be strikingly similar to discrete EM (electromagnetic) radiation frequencies of typical clay minerals that have been shown to display semi-conductive properties and act as quantum wave replicators [10] [38]. Such mineral substances may have been instrumental in the creation of first life in relation to the steering influences on overall cell morphology, structure of macromolecules such as proteins, as well as directed synthesis of poly-nucleotides [53].

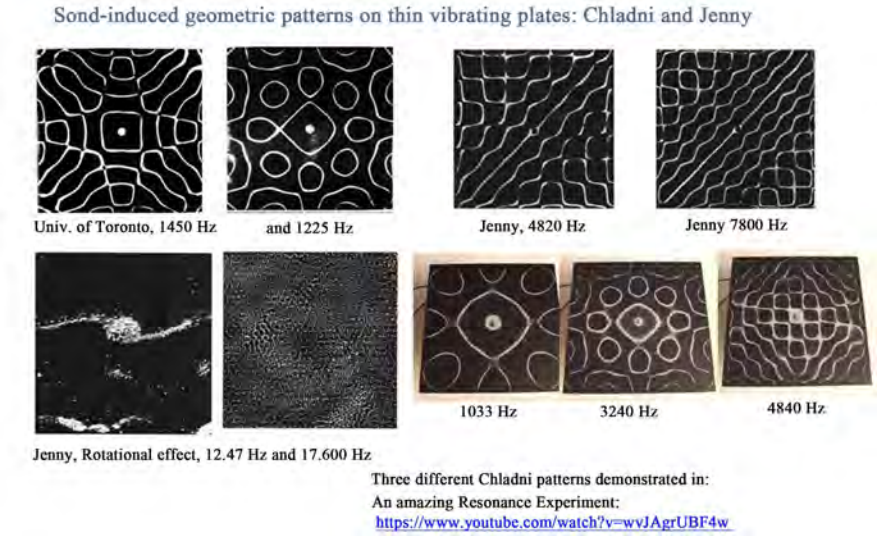

Figure 3. Analogy of phonon-guided protein folding and acoustically induced complex geometric patterns. The latter are evoked on particle covered thin plates, as earlier separately demonstrated by Chladny and Jenny (see also reference: "an amazing resonance experiment" found on internet, see https://www.youtube.com/watch?v=wvJAgrUBF4w).

Of note, this type of minerals, apart from being present in soil, is also abundantly suspended in the earth ionosphere (so called atmospheric dust) and have been suggested to provide a semi-conductive medium that produces selective EM wave patterns following excitation by external energy sources. It is of interest that such silicates have been reported to be candidates for the facilitation of oligo-nucleotide synthesis in the creation of first life in biological evolution [54]. Elements in the universe have seemingly assembled themselves in such a way that the organization of matter resulted into the ability to acquire sufficient life-sustaining information from the environment. Over time, highly complex neg-entropic structures arose that could collect, store, retrieve and communicate essential information to maintain stability and survivability. Such pattern recognition ability may have been directed by combinations of EM radiation frequencies through inducing morphic resonance with coherent vibrational elements (structured water, proteins, oligonucleotides) of proto-cells.

According to Wolynes [5] the integral folding process includes random mutations, potential misfoldings/unfoldings, recombinations and selection by successful competition with less optimal protein species, in which the protein finally obtains sufficient stability in subsequent generations of cells. As such the proteins were seen by the author as non-linear elements in cellular networks that arise from a sort of information spaces that unfortunately, were not further defined. One could also question the supposed random character of this self-organizing process. In other words, how can selection of non-functional precursors of the particular protein be envisioned? And by what physical mechanism is a specific function assigned to the particular protein? As argued by Grandpierre [55] life functions of proteins cannot arise by chance, they can only be assigned by their host cell, but such a cell cannot arise without these functions being already assigned. We propose therefore that a primordial biological principle (register of rules) was operating, that acts as a "recipe for life" [56]. This type of a-priory information must have preceded the development of first life and all known force fields that were present from the birth of the universe should be taken into account (see later). Also quantum processes have probably played an essential role in facilitating the various steps that gave rise to first life and initiation of the first replicating cells [57], see **Figure 4**.

A part of the EM frequencies at stake, were shown by others to be involved in phonon and soliton- (and thus sound-like) mediated steering of cellular functions [32] [33] [34] [58]. It was inferred that the discrete frequency bands (also called eigenfrequency values), as identified in the meta-analysis of the life studies, likely reflect a cellular regulation and communication system that may have an evolutionary origin, realizing that due to the composition of our planet, EM radiation is a basic property of the planetary environment. Life on earth was formed during billions of years, exposed to, and shaped by the original physical forces such as gravitation, cosmic irradiation, atmospheric electric fields and the terrestrial magnetism. The Schumann resonances at 7.8 Hz and a series of other

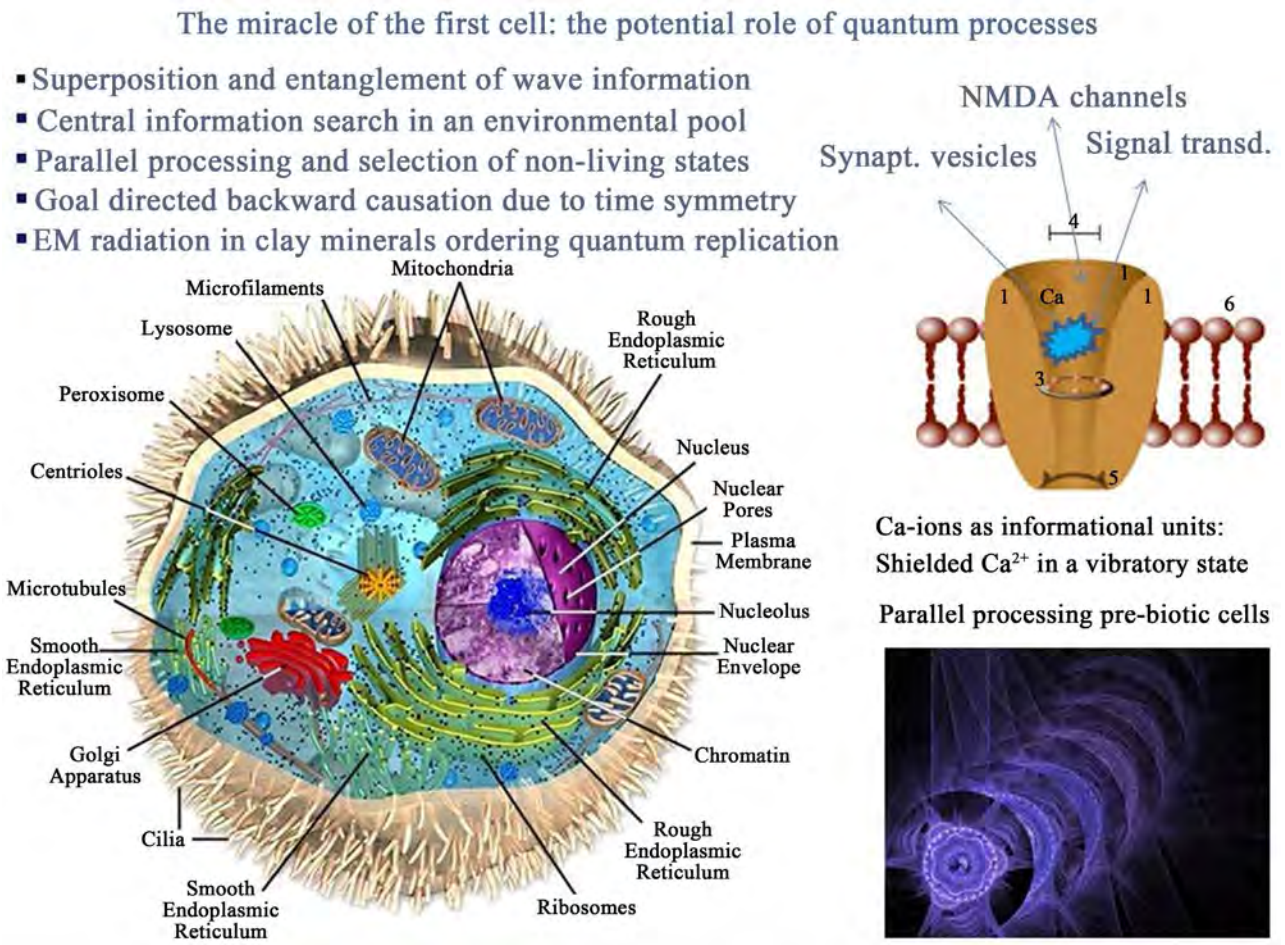

Figure 4. Potential role for quantum processes in biological evolution (listed left above) and the initiation of first life, showing various essential processes. Inset Right above depicts a Ca^{2+} channel protein with Ca^{2+}-ion in a decoherence protected vibratory quantum information state. Inset right below indicate the process of parallel processing of pre-biotic life information as enabled through environmental search of various quantum states.

related frequencies, are an example of oscillation that are potentially important for life. We conclude that the existing organisms are created to function in harmony with the above-mentioned fields and forces which existed when life was born 3 billion years ago.

This collective picture indicated that a distinct biological/physical/mathematical principle may operate in both non-animated and animated systems and that these discrete EM frequencies may have bridged information processing required for the creation of first life at pre-biotic conditions [1] [57] [59] [60].

7. Soliton-Mediated Mechanisms of Protein Folding

The relevant mechanism of electromagnetic wave interaction has been suggested to be spontaneous breakdown of symmetry in the biological, well ordered structures. Such interaction occurs with the dipole moments of the molecules in the cell microtubules [15] [45] [46] [61] [62] [63]. The biophysical aspects of solitons were adequately reviewed by Foletti and Brizhik [64] showing that in cells

the quasi-particle is produced from an electron and a self-induced local lattice deformation of the molecular chain, propagating at constant velocity without energy dissipation, and emits radiative harmonic EM waves that facilitate the creation of coherent states of interfacial water molecules. Interestingly, the energy released under hydrolysis of an ATP molecule, the oscillation energy of the C=O of the peptide groups and the different bending modes of interfacial water molecules fit precisely with the calculated soliton frequencies of the acoustic wave-function, respectively: 0.415 eV, 0.2073 eV and 1660-1693 cm^{-1}. Also the 1.1 THz, mentioned by Brizhik, [14], fits exactly with the calculated algorithm of solitons related to a stabilizing coherent frequency.

Solitons are seen as localized, non-dispersive excitations, which exist in many nonlinear systems [65] [66] and have been proposed to act as an organizing principle in the process of protein folding [67], including membrane proteins [68]. They are very stable, and therefore can propagate without much energy loss or dispersion to much larger distances than wave-packets of linear waves. In proteins, the dipole-dipole interaction between neighboring amide-I (the C=O double bond) quantum modes of vibration gives rise to linear collective modes known as excitons. The dipole-dipole interaction is influenced, however, by lattice vibrations, so the excitons and topological solitons [68] interact with acoustical phonons in the protein and/or provided by quasi-particles. The energy that is carried by the soliton is transferred into the conformation field, and this allows it to overcome energy barrier and reach the desired ground state. It might be that solitons are generated in locations of preferable alpha-amino-acids sequences, while their propagation might be blocked on different sequences. Therefore, the sequence may not only dictate the final conformation, but also the dynamics of the conformational transitions (**Figure 5**).

Among these, collective excitations driven by metabolic activity were hypothesized by H. Fröhlich to account for the huge speed of enzyme reactions and for the fast encounters of the cognate partners of biochemical reactions. In fact, according to this hypothesis, collective oscillations of biomolecules, by bringing about giant oscillating dipole moments, would result in resonant (thus selective) electrodynamic forces acting at a long distance. The particular model assumes that the activation mechanism of collective oscillations can be seen as a Bose-like condensation of the normal vibrational modes of a bio-molecule. In this model a bio-molecule is considered as an open system through which energy flows under the simultaneous action of an external supply and of dissipation due to radiative, dielectric, and viscous energy losses. Such Bose-like condensation, in the lowest vibrational mode, is predicted to occur when the energy input rate exceeds some threshold value.

Recently, Nardecchia [28] highlighted the process of far distance oscillation phenomena in proteins. The authors stipulate that the condensation phenomenon originally proposed by Fröhlich as a quantum process, should be discussed, because the supposed quantum conditions can probably be hardly maintained for biomolecules. In fact, the frequency of collective oscillations is expected in

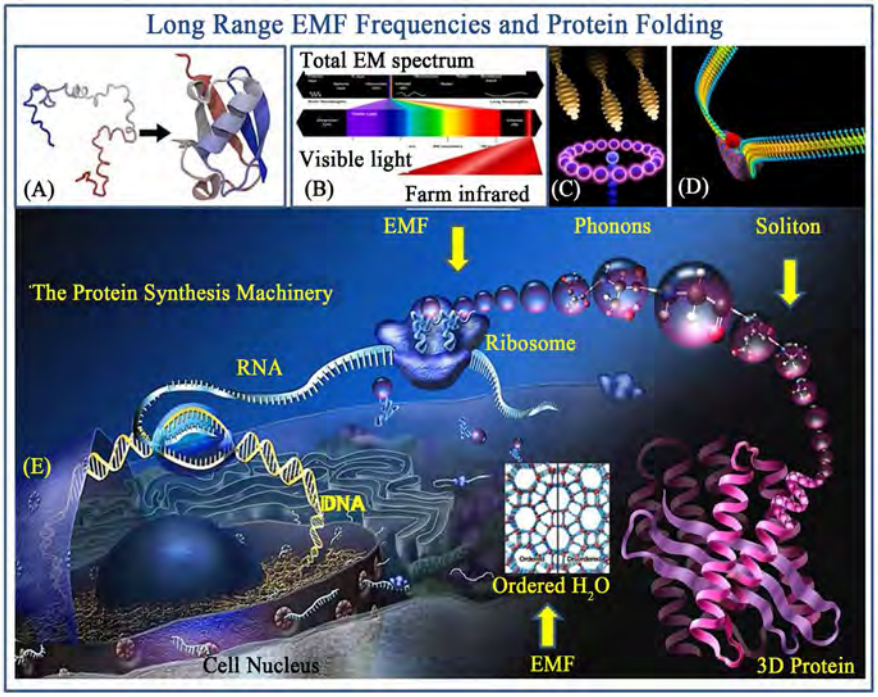

Figure 5. Soliton/phonon guided protein folding, depicting protein synthesis from DNA/RNA (left) to linear amino-acid chain (middle) and final folding to 3-D conformation (right). Inset in the middle shows: EMF-mediated structuring of water in hexagonal geometry, and on top, (A): Protein folding from linear AA chain; (B): electromagnetic field spectrum with visual and far-infrared parts; (C): phonon induced coherent vibration domain (BE-condensation) and (D): soliton/polaron travelling along a protein backbone.

the sub THz domain, around 10^{11} Hz, so that at room temperature kT/hv >> 1, which may rule out a quantum description. An additional, more classical approach on the macromolecular vibratory communication should be considered even though experimental evidence of the existence of collective modes of vibration of biomolecules has been provided at thermal equilibrium by means of Raman spectroscopy already years ago by Lundholm [26]. Yet, this was measured in a quite artificial setting: crystallized proteins. Accordingly, Nardecchia worked out a classical version of the original Fröhlich model, finding that, remarkably, also in a classical context a Fröhlich-like phonon condensation phenomenon is possible. This was illustrated by the authors, for an idealized macromolecule, displaying the deviation from energy equipartition among the normal vibrational modes. Secondly including collective modes of resonances of biomolecules at infrared/light induced electronic transitions may balance kT [11].

Though still representing a biomolecule in a very idealized way, this model predicts a classical condensation phenomenon, that seems worth to be experimentally investigated. Of note, the same group earlier demonstrated long range resonant communication of biomolecules, by measuring their diffusion behavior, indicating an elegant experimental method to probe the activation of resonant electrodynamic interactions among biomolecules [28].

8. The Essential Role of Cell Water in the Protein Folding Processes

Cellular plasma water is generally supposed to act as a transfer medium for external electromagnetic waves to biomolecules for adequate introductions in this field see [69] [70] [71] (**Figure 6**). The cellular plasma was proposed to exhibit a highly arranged 3-D geometric structure as a liquid crystal that exhibits surface interactions with macromolecular structures. The absorption spectrum between 1 THz and 10 THz of solvated biomolecules is sensitive to changes in such fast fluctuations of the water network. There is a long range influence on the hydration bond dynamics of the water around binding sites of proteins, and water is shown to assist molecular recognition processes [72]-[81]. "Biological water" supports itself by coherent dipolar excitations and terahertz/femtosecond infrared interactions and these dynamics extends well beyond the first hydration shell of water molecules. The latter publication makes clear that water molecules in

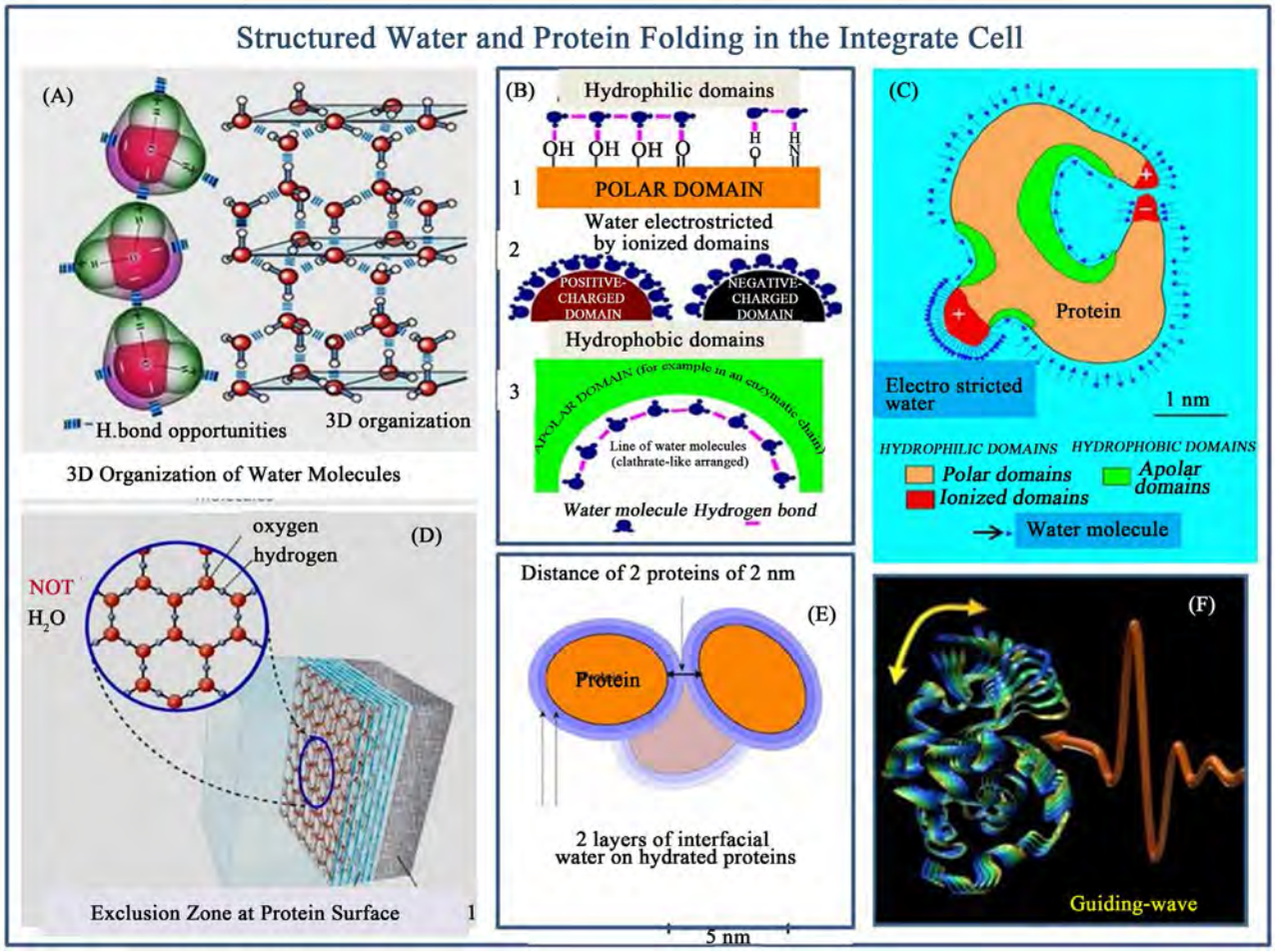

Figure 6. Various aspects of electromagnetically structured water complexes and protein folding. (A): Molecular conformation and 3-D hexagonal organization of water molecules; (B): Dynamical hydration layers in hydrophilic and hydrophobic portions of a protein; (C): The influence of protein hydration in polar and non-polar domains of the protein chain affects folding; (D): Formation of water exclusion zone at the surface of macromolecules (E): The crowded cytoplasm space with adjacent proteins covered with layers of water molecules and hydrated ions (F): EM field guided protein folding (after Mentré, 2012, and Brown, 2016).

the interfacial setting with their dipole character, in combination with cytoplasm inorganic ions, interact with charged groups on the protein backbone, by which surface charges become masked and relatively hydrophobic domains are created that can lead to deformations (see **Figure 2(C)**) and creation of local pockets or cavities, that even may exclude acqueous solvent molecules. This adds up to the natural influence of both hydrophilic and hydrophobic portions of the particular protein chain that are involved in the initial folding process as well as protein stability [82].

Water molecules have typical resonances at Hertz frequencies, and a typical frequency can be expressed in 3-prime-limit tuning. A calculated typical frequency of a water molecule, with a molecular weight M=18 $g \cdot mol^{-1}$, is 54 Hz (2^1, 3^3) according to Henry [49]. This typical frequency of a water molecule, in the centre of our GM-scale, can be derived by using the mass-energy equivalence coupled to the Planck-Einstein relationship: $M \cdot c^2 = h \cdot f \Longrightarrow f\ (Hz) = 2.981 \times M\ (g \cdot mol^{-1})$ (M is molecular weight of water molecule, c = 299,792,458 m/s, h = $6.62606959 \times 10^{-34}$ J·s, f is the frequency of a water molecule). In two papers of Sbitnev [79] [80], a relation between Bohmian pilot wave guiding to toroidal vortex topologies and zero-point energy was discussed in the framework of cell water hydrodynamics.

In this respect, some innovative papers with designed and properly controlled experiments, suggested that electromagnetic fields may reflect macromolecular features of enzymes like DNA-polymerase in water, and that this provides structure specific information storage in aqueous solutions [82] [83] [84]. The electromagnetic radiative properties of DNA and enzyme macromolecules likely depend on the characterization of their electric dipoles. The molecular structure of DNA base pairs and enzyme amino acids, as well as many other bio-molecules, presents aromatic rings containing conjugate planar systems with p electrons delocalized across the structure. It has been argued that London force dipoles in such intra-protein hydrophobic pockets could couple together and oscillate coherently, thus generating a radiative field. Montagnier recently described the fundamental role of water dipole dynamics bridging the interaction between DNA and enzymatic proteins (see **Figure 7**) so as to allow polymerase chain reaction (PCR) processes to occur [84]. They describe the dynamic origin of the high efficiency and precise targeting of *Taq* activity in PCR.

The spatiotemporal distribution of interaction couplings, frequencies, amplitudes, and phase modulations comprise a pattern of fields which constitutes the electromagnetic image of DNA in the surrounding water, which is how the polymerase enzyme actually recognizes in the DNA water environment. The DNA and the enzyme "see" each other's EM images by exchanging quanta of the radiative dipole waves induced by their presence in the water molecular matrix, which thus acts effectively as a bridge between the two, until they are sufficiently close for water exclusion and direct binding to occur (**Figure 7**). This standpoint is consistent with previous experimental work that has shown that some DNAs in water dilutions have electromagnetic waves of low frequency (from hundreds

to 3 kHz) which also could be triggered, as in a resonance phenomenon, by an outside excitation, such as Schumann waves. It is a great interest that macromolecular and drug molecule vibrations can be imprinted and informational encoded in stable ordered coherent water domains by photon EM irradiation, as experimentally demonstrated in various studies with a spectrum of different therapeutic agents (reviewed by Lawrence [85], for potential nontoxic treatment.

We propose in this respect that the cytoplasmic macromolecular aqueous solution is ordered via the the discrete wave frequencies that have been described by us [11], and that this exhibits a fractal self-similar pattern around the central 12-tone octave frequency bands. It is of interest that a fractal-like self-similar structure induces the manifestation of coherent dynamics active at a microscopic level. These (fractal-like) self-similarity properties of the EMS in turn likely induce self-similar organization in the irradiated water. This first step can be followed by a second step consisting of transformation of the signal into an analog form and sending its electric vector to a solenoid which than will generate a magnetic field in the surrounding water. The action of reciprocal "seeing" is described by the exchange of the dipole wave quanta of the collective dynamics induced by DNA and enzyme in the surrounding water dipole field, as derived above. The general process is described by the analysis of two interaction "vertices": the interaction vertex DNA-{water dipole wave}, on the one hand, and the interaction vertex {water dipole wave}-*Taq*, on the other. What this study provides is the dynamical description of the long-range EM correlation modes orchestrating the PCR process, thus accounting for its remarkable efficiency, space-time ordering, and diverse time scales that would be unattainable by otherwise fully stochastic molecular activities.

Of note, divalent cations such as Mg^{2+} and Ca^{2+}, in particular, may enhance or maintain or critically deform the long-range dipole wave fields in water solution. This is supported by recent experimental work that shows that ions can influence up to 100.000 water molecules, which extend roughly 5 nm from the ion radially. This would add another modality of form information regulation. Mc Dermott [86] reported their discovery of a chiral water superstructure surrounding DNA under ambient conditions. They confirmed the existence of a DNA minor groove spine of hydration at room temperature and further showed that the chiral structure of biomolecules can be imprinted on the surrounding solvation structure. The observation reported in of the robustness of the DNA's chiral spine of hydration, and the fact that "a change in the hydration state can lead to dramatic changes to the DNA structure" also indicate that such a water superstructure actually constitutes a detailed mold or "electromagnetic image".

All this highlights the crucial role of water as a connecting modality in the EM vibrational steering of 3-D macromolecules and also in the realization of holographic memory of the cell and entangled information transfer in the universe as a whole [76]. In the latter study it was emphasized that in the interfacial water layer of proteins both permittivity and viscosity of water is largely different from bulk water. Previously it was reported that long-range radiant energy excludes

colloidal and molecular solutes from hydrophilic zones of proteins in a wavelength dependent manner [75].

It can thus be conceived that multiple bio-solitons of different discrete energies, facilitated by their quasi-particle phonon features, travel along the primary protein backbone (**Figure 5**), thereby providing essential long or short range information, that leads to the final conformational shape of the molecule (see for folding mechanisms later on). The various solitons could arise from external EM fields, preferably in the polarized form in relation to a more optimal tissue penetration or being formed internally and organized in coherent domains or collective modes in the cell. The question should be raised here how the particular series of travelling solitons translate the fine-tuning forces that finally shape the protein in its functional 3-D configuration. If special combination of solitonic wave frequencies would play a role, some sort of premordial or evolutionary harmonic information could be responsible (see later). Alternatively, the discrete EM energies may be derived from an addressable memory space for geometric forms of life macromolecules that have been build up in biological evolution.

The latter aspect will be treated in the following from the point of view of holographic memory space models. It should be mentioned here that apart from the coherence promoting soliton waves, also soliton frequency bands were identified by us that produce detrimental and de-coherent influences. Thus misfolding or destabilization of proteins could be related to such de-coherent EM radiation fields as have been suggested for cancer [87], and even in cataract and Alzheimer disease [88]. The general properties of solitons are solitary waves (waves localized in space) with the following properties: 1) they preserve their shape and velocities; 2) they are extremely stable to perturbations (in particular collisions with small amplitude linear waves); 3) they are even stable with respect to collisions with other solitons. In such collusion they pass through each other and recover their speed and shape after interaction. It should be noted here that phonon density on electrons can largely determine the harmonic versus an-harmonic features of such polarons and thereby their diffusebility in life tissues and macromolecules [89].

9. Protein Folding in the Intact Cell: Do We Need More Integral and Holistic Approaches?

It has been firmly established that *in vitro* protein folding models do not correctly predict *in vivo* folding in the whole cell context (references in [30]). In fact the many factors depicted in **Table 1**, to some extent may contribute to the final 3-D functional structure, depending on the particular protein at stake. This addresses the general item how nature makes use of neg-entropic information related to the wide variety of life systems, including the morphology of crucial macromolecules that were created during biological evolution. It stands to reason that somehow this information is registered and re-used to prevent redundancy [59] [90] [91]. This would require a addressable quantum register or a

dynamically build memory space that allows a versatile searching modality and potential parallel processing of information of very different structures in the various contexts that nature offers (see **Figure 4**). For example such a search procedure could integrate genomic and proteomic knowledge on the basis of wave interference patterns that can be stored through holographic memory processes probably related to a background quantum field. This not only introduces a huge memory space, but also implies that a holistic framework is created, in which any small fraction of the hologram reflects the total information pattern. Interestingly, such a mechanism was earlier used for the holographic storage of information in the human brain [92] [93], and is currently also used in physics and cosmology for the geometric description of radiating black holes, with the known assumption that quantum information cannot be lost. Such processes could play a role at any fractal scale if the universe, including the cells that constitute life organisms and their macromolecular components. As Schrödinger stated for living matter in general, the attempt to explain the high efficiency in terms of ordering generated by "statistical mechanisms" would be "the classical physicist's expectation that far from being trivial, is wrong", and "it needs no poetical imagination but only clear and sober scientific reflection to recognize that we are here obviously faced with events whose regular and lawful unfolding is guided by a mechanism entirely different from the probability mechanism of physics".

10. Steering by Holographic Memory Hypersphere of the Individual Cell

Each individual cell in our body is not a "stand alone" information processing unit: it acts as a part of our integral organism with recurrent information exchange or permanent feedback coupling with the entire organism. Such an integral context attracts much attention in cosmology, physics and also in life studies and is often approached with, what is called, the holographic principle [94] [95]. The holographic principle states that everything that is embedded in a space region can be described by bits of information at its border. In view of this basic definition there is no reason whatsoever not to apply it to complex life cells that obviously can be seen as bundles of integrated neg-entropic information. Holographic principles may clearly provide the information channel required for any biological system, in order to keep track of all essential information at once, and creating a dedicated memory space for sustaining life [96].

In this respect it was postulated earlier that the intrinsic information that defines the living condition of organisms may be holographically stored on a virtual screen associated with the particular life system [97]. The idea of a holographic organization of memory even in single cells was earlier proposed by Anjamroos in relation to preventing reprogramming of differentiated cells and activation of immune responses [98] [99]. This non-genetic memorization was claimed to be generated in the cell both endogenously and exogenously at several

levels of the cell such as atoms, molecules including proteins, cellular water, microtubules and electromagnetic fields. The collective information may be projected in a holographic manner in a memory space from which every part of the cell is informed about the integrate hologram information of the particular tissue type (Figure 7). This information is considered to be non-local, a feature that in quantum physics is related to the phenomenon of entanglement. We have recently shown that discrete EM frequency pattern precisely fit earlier EPR experimentation in which such EM radiation promotes states of quantum entanglement [51].

Hales pointed out that the plasma membrane of the cell contains a high density of ion-channels that, in a collective action, can produce a major migration of charged ions, a phenomenon that may induce local magnetic forces [100].

These take the form of toroidal organized force vectors that even may extend the cellular membrane surface. This process could be enhanced due to GM-like coherent vibrations that, as mentioned above, have been shown to increase the degree of quantum entanglement [51]. Such a process can especially be anticipated in the quantum de-coherence protected channel interior [101]. This kind of external magnetic domain could provide the opportunity for wave interference with EM fields in the environment, and could in a holographic manner

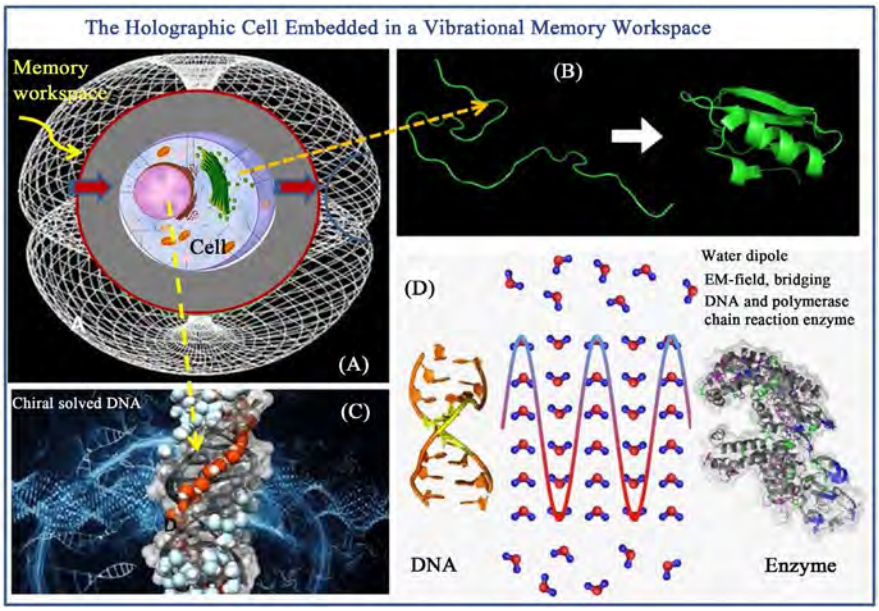

Figure 7. Toroidal hypersphere mediated morphogenesis of the integral cell. (A): The nested torus structure with an outer surface of the torus (red circle and arrows) represents the event horizon memory space surrounding the cell; (B): Depicts the 3-D folding of life macromolecules as it occurs following primary synthesis in the cell; (C): Shows the fractal attractor structure of H_2O around DNA, steered by quantum information of the toroidal hypersphere memory workspace; (D): Shows the dipole radiative EM field of arranged water molecules that bridges the DNA molecule and PCR enzyme as essential for realization of the PCR activity. The coherency of cytoplasmic domains may be steered by externally applied EM fields in a resonance state with the various cellular vibratory elements (modified from Montagnier, 2017).

build up a dedicated memory space for each cell, containing stored and updated life-information for cell survival. Such a cell bound memory space could also be responsible for long-distance, non-local, communication between different cells, as reviewed by Cifra [102] and experimentally shown by Fahradi [103].

A bio-photon type of information transfer was suggested in the latter paper and Persinger and Dotta even demonstrated that cell-specific wave information can be spatially stored for quite some time, although the physical mechanism of this space-time phenomenon remained unknown [104].

Several studies have implied that in pre-biotic evolution various force fields may have been instrumental in the creation of fist life [1] [47] [59] [60]. If a cellular holographic memory space would be involved it may imply that discrete EM wave-frequencies from the photon sea of zero-point energy can directly influence cell function by wave interference and holographic storage and thereby can also guide the 3-dimensional folding of life macromolecules into functional units of the information networks of the cell. In relation to this it was earlier stipulated by Gough and Shacklett that a knowledge domain beyond the Planck scale could provide characteristics of the well known implicate order of David Bohm [105].

There is recent evidence that such a domain outside known space-time could be constituted by a spin-liquid network [106], later pictured as a geometry of relations coined as the amplituhedron [107] [108]. This underlying domain contains information expressed in mathematical and geometric wave relations and can be inferred from a mathematical operation through transformation into twistor space. By some this is called a frequency domain that could function as a source of Bohmian pilot waves [12]. Such a pilot wave-frequency domain could contain a primordial recipe for the representation of neg-entropic information that may have led to the constitution of first life and also as proper information space for the maintenance of present life (see **Figure 8**). It was recently shown that a photon that is removed from our physical world can still become entangled with another photon with similar features in the present world, in spite of the fact that they never co-existed [108].

This is strongly indicative for an information domain beyond our local 3D-space time in which information of the destroyed photon is somehow stored. Thus material particles in general should be seen as excitations of an underlying non-material matrix that behave as vortices or perhaps as tori in a 4-D setting, also producing quasi-particles such as polarons/solitons. A deeper (geometric) information domain was also implied in "Our Mathematical Universe" by Tegmark [109] (discussed by Butterfield [110]) as well as for the life world by Azevedo and Filho [111] and Fleming [112], the latter postulating a fractal circular wave guide, involved in intra- and inter-cellular communication.

This cellular memory aspect was coupled to the assumption that cells are embedded in a 4-D toroidal structured topology (as proposed by Tozzi [113], Haramein [114]), that interacts with resonant sensitive energy structures in the various cell compartments, including their proteins (**Figure 8**). This idea of

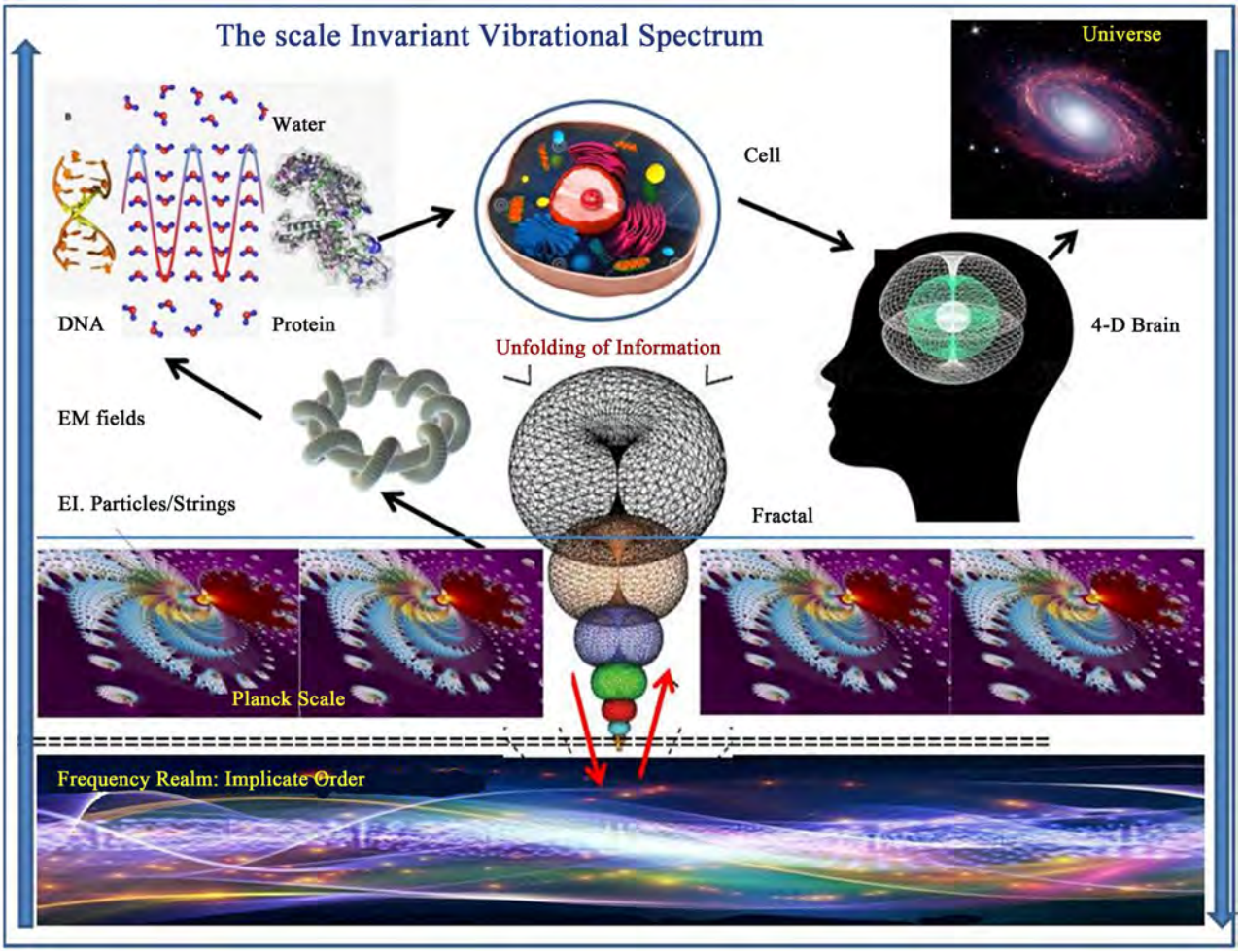

Figure 8. Morphogenesis of reality seen as a fractal process of information processing (collection, compression and subsequent unfolding), either (bottom up) from an implicate order frequency domain (below) up to the level of the Planck scale, and at higher levels producing elementary particles, atoms, life molecules for the build-up of whole structure of the cells and organs such as the brain. All elements are equipped with a toroidal memory workspace (consciousness) that is scale invariant (see Meijer and Gessink, 2017). In this manner it finally results in to black hole/white hole structure that (top-down) transmits information for the fabric of reality, thereby constituting a circular (rebound) type of information universe (see large arrows at the sides for bottom up and top-down information processing).

extended spacetime was earlier agreed upon by many others in physics, and implies that our reality and thus life processes are considered to be embedded in a 4th spatial dimension that we cannot observe but through symmetry breaking can infer from shadow energies in our world [10] [114]. In this respect, the geometry of the nested torus that also accommodates 4-D aspects, is envisioned as a scale invariant basic unit (operator) of spacetime, with unique collecting, coupling and integrating properties for a wide variety of wave information (**Figure 8**). These include photons, phonons and quasi-particle/waveforms such as polarons/solitons and polaritons, as recently discussed in our studies on phonon- and soliton-guided biology [48] [115].

Bio-photons have been widely proposed as information carriers in brain [63] [115] [116] [117], but also in other tissues [118] [119]. Recently it has been

shown that incubation of brain slices with glutamate (a major neurotransmitter in the brain) results in the release of red-shifted bio-photons [120] and in a recent PNAS paper that the degree of bio-photon induction in brain slices of various species is highly correlated with the relative intelligence of the species studied [121]. These studies confirm the idea that bio-photons are instrumental in ultra-fast cellular communication, in addition to the known action potential mediated messaging and may even be central in building up of consciousness. We infer that the communication between a holographic memory space of the cell with its components could be bio-photon mediated, and that coherent soliton/polaron activities, indicated above, can lead to guiding of protein folding against the background of a bio-photon equipped hologram of the entire functional structure of the cell.

The cell, within such a memory hypersphere, is conceived as a dedicated multi-cavity network that for instance can convert ZPE wave information as well as states of gravity, dark energy and earth-magnetism, in an attractor type of fractal energy fields. The hypothesized external, field-receptive memory domain, may store wave interference patterns as defined by the abovementioned holographic principles. This generalized principle also implies that every small part of the hologram contains all the information of the whole picture [101] [102], and thus a large number of holographic fractal planes or octaves [10] [122]. We have earlier applied this holograhic concept to the entire brain [104] and in view of the known fractal character of the neuronal system [96] [122]. We consequently assume this to occur also at the various brain scales (neuronal networks, individual neurons, membrane and cytoplasmic proteins and ions, as well as constituting atoms and elementary particles).

As treated above, we therefore have postulated a self-similar, fractal, type of holographic information processing to be expressed in a holonomic entangled matrix of the whole complex neural structure including the various cell types of the brain [10] [122]. We assumed that a toroidal geometry that facilitates self-referential and spiral energy trajectories, functions as a basic operator unit for information integration processing and transfer 122, as was previously proposed for the mathematical transition to twistor space [123]. As mentioned earlier, by Persinger and Dotta showed that patterns of photon emissions can be stored and retrieved after some days from the same defined space and that collections of cells in culture in different loci can share the same complex magnetic fields, suggesting a non-local geomagnetic space time connection, that was explained by involvement of optical holograms [104].

Although the step that we take here from the whole brain to individual cells seems huge, it should be realized that even single neurons have been suggested to be able to develop conscious states [93] [124] [125] [126]. Also in biological evolution the first primitive proto-cells required a dedicated and addressable memory space to store stimulus/reception/action type of information in a learning process to cope with problem solving in the survival in very hostile environments [57]. Since, even in pre-biotic times, all the known force fields were

present and the becoming cells should gather essential ecological information from their direct surroundings and planetary atmosphere, such an integral memory space would be a prerequisite for survival. We argue that such a memory workspace associated with life cells should be field-receptive and apart from containing the integral cellular information for life, can collect and integrate external information from the mentioned force fields in which all life organisms are permanently embedded.

How would such a quantized memory unit, associated with the cell, communicate in a bi-directional manner (see **Figure 8**)? It is likely that wave resonance and wave interference represent viable mechanisms for this purpose, in which cellular energy stimulates coherent vibration states of intracellular components. This electrome background of the cell can in this manner undergo a holographic interaction with external and integrated wave information. Among others, the cellular architecture could be guided by discrete patterns of eigen-frequencies of solitonic waves directed at the cell and backwards. The latter process serves for updating a time-symmetric global memory space of the individual cell. Solitons or polarons are electrons "dressed" by phonons and are sensitive to cyclotron resonance [127]. It is well known that sound (noise) can largely facilitate effective transport of charged particles [93] [128].

If each cell would be surrounded by such a "memory space" that houses wave/particles with discrete wave frequencies, a toroidal coupling of phonons and electrons could provide soliton waves that may function as pilot waves in the Bohmian sense. If the cell contains coherently vibrating macromolecules, influenced by cyclotron resonance [127] and/or stochastic resonance soliton information from the proposed hypersphere memory workspace, could lead to guiding wave interference [129]. This can than lead to perturbation of the 3-dimensional protein molecule structures, in this way being instrumental in the transfer of crucial life information that is stored in the 3-D conformation of proteins and poly-nucleotides. Using such a "memory mirroring", an individual cell could in this way build up a holographic endo-memory of the exo-world. Through the evident fractal character of the cell structure this could not only play a role on the molecular level but even at more deeper atomistic levels up to elementary particles and could even provide qualia-like information at the Planck scale [62] [96], see **Figure 7**.

At the atomic level, Ca^{2+} ions/waves could play a central messenger role since the ion is supposed to be an excellent information carrier [130], and is involved in a spectrum of regulatory processes in the cell. Ca^{2+}-ions, noise protectively enclosed in Ca-channels and K^{+}-ions in K-channels in the cell membranes, for instance, may produce quantum wave coherence states that endure long enough to transmit entangled information in and between cells [108]. Ca^{2+}-ion trans-membrane gradients have also been shown to be very sensitive to cyclotron electromagnetic radiation [131]. In the dynamic, field sensitive, electrome state of the cell, directed protein folding to a functional 3-D conformation, would in this way be steered by an integral biophysical recipe. This

recipe, in principle, encompasses all the necessary in-formation of the metabolic networks in which the particular protein functions in the intact cell, taking into account all the factors as listed in **Table 1**. A similar memory workspace as described here for an individual cell, was coined for the whole brain as "global workspace" [132], or "cloud" [93], or "event horizon", [97]. Electromagnetic field aspects of brain function are extensively reviewed [133] and with regard to consciousness [79] [80] [97] [134]. Sbitnev [79] [80], discussed the relation between Bohmian pilot wave guiding to toroidal vortex topology and zero-point energy in the framework of cell water hydrodynamics. The relation with photon emission of the human brain was highlighted [104] [120] [121] [135]. Interestingly, it follows that a "proto-conscious" state can in this manner be ascribed to each cell in the organism through continuous information matching with the supervening holographic field-receptive memory space, just like the permanent reading of genetic information that is intrinsically present in each cell in the organism. Holographic associative memory for pattern recognition and information completion in which a weighing function is included to ensure dominance profiles and focus, have been earlier described for neural networks [131].

The general concept is that this piloting process functions at any fractal scale of the cell-system and, more general, as an informative vortex principle that operates from the Planck scale to macro-scales of organisms [122]. Einstein and Minkowsky originally proposed a 3 + 1 dimensional space-time (3 spatial and 1 symmetric time dimension), in which all time is laid out, while later in physics 4 + 1 models were adopted, including an extra spatial dimension (Kaluza-Klein theory). More recently, Randall (see [136]), postulated the Randall-Sundrum model (also called 5-dimensional warped geometry theory) imagining that the real world is living in a higher-dimensional universe, described by warped geometry. In this generally accepted space-time concept, time has a bi-directional (symmetric) character that allows aspects of backward- or retro-causation. In the framework of protein folding, this implies that a primary structure of the protein can also anticipate a future (final functional) structure. This aspect obviously would drastically speed up the folding process and may explain some of the questions raised before in the present paper (see evolutionary aspects). The aspect of top-down causation (process feed-back) by information control is extensively discussed [137].

If in single cells such a memory steered mechanism would operate, a crucial question is how the integral information with regard to single cell constitution would be translated in a multi-cellular context. One possibility is that discrete EM wave frequencies promote states of entanglement that than could explain long distance correlation of information in any tissue or even organisms and thereby would obtain a distributed character. In a recent study such non-locality inducing effects of discrete EM fields were revealed in a meta-analysis of so called EPR experiments [51]. Alternatively the EM vibratory character of cells may produce electromagnetic magnetic fields in which the form information is shared in a long distance manner [97]. The fractal or holographic property of cell structure cell (many copies at different sites) can in principle imply that mo-

lecular state information is also expressed in the fine-structure of cells like the components of membranes and organelles. As treated before, such processes could also be helped by stochastic resonance and/or phonon/soliton (acoustic) mediated flexibility of the cellular matrix [131] [134]. In this manner a convergent correlation matrix of information would become manifest that can guide the whole architecture of life systems.

Our hyperspace information concept of cell memory may have some correspondence with the known quantum holographic Hopfield-like biomolecular recognition models [138] [139].

This computational approach was applied in the framework of protein folding [30] [140], among others. Incidentally, the successful prediction of protein secondary structure was one of the first examples for applications of neural networks in which these significantly exceeded the performance of all other systems and even that of experts. This principle provides quantum computing an advantage in processing huge data sets. An example of the latter is the Hopfield model of content-addressable memory using the concept of attractor states. This content addressable memory allows to compute even incomplete input information, which forms the basis for memory and learning. In the Hopfield network each update of a neuron minimizes the network energy if possible. Memorized firing patterns are thus stored as stable attractors that become holographically coupled at fractal layers in a process of multi-level information processing. In this manner, also pattern recognition can be attained from very different biophysical and bio-informational aspects of proteins, so that the prediction of 3-D structure can be highly facilitated. The earlier mentioned work of Chen *et al*., for example, uses hybrid data of atomistic associative memory and data base memory in structural predictions [4].

Finally, we emphasize that the soliton mediated processes mentioned in our pa-per should be seen as a steering of the balance of folding and unfolding activities: Unfolded or disordered protein regions play a crucial role in flexibility and in-teraction of proteins and can largely bind inorganic ions such as K^+ and Ca^{2+} as well as organic compounds such as ATP. This, in turn, can lead to polarization of the associated and structured water layers. The resulting fractal "cell matrix" supports coherent vibrations and harmonic resonance and may induce bio-photon discharge that can produce holographic properties (reviewed in [141] [142]).

11. Final Conclusion

It is postulated that the problem of folding of bio-molecules, theoretically, requires an unrealistically large number of steps to find the correct state. Perspectives for solving this paradox are associated with an explicit incorporation of topology in the physical models of folding. This condition can perhaps be achieved through the construction of hybrid models based on the geometrical and physical approaches [1]. However, it is necessary to perform future experiments to identify the specific mechanisms underlying the actual forces between molecules (atoms). In particular, the actual problem is the possible existence of a collective

action at a distance between the molecules. The presence of such long-range interaction can substantially change the folding model. Moreover, it could lead to a complete revision of our understanding not only of the folding of proteins but also of the work of molecular biological structures in the broadest sense.

In our opinion, therefore, it is crucial to approach the item of protein folding from a more "holistic" standpoint, in which all the interacting factors and intrinsic conditions of the intact cell should be taken into account (as depicted in Table 1). These include long-range force fields and local cell biological conditions such as structured water complexes, among many other factors. In particular, we show that abundant information is available in the literature on the role of soliton waves (phonon/electron quasi particles) that can be instrumental as guiding elements in the various steps in the folding process. This, by crucial energy transitions in their interaction with the semi-conducting protein lattices. Our recent finding of a set of discrete EM frequency bands that either promote or endanger life conditions (see Figure 9), could be a key in further studies

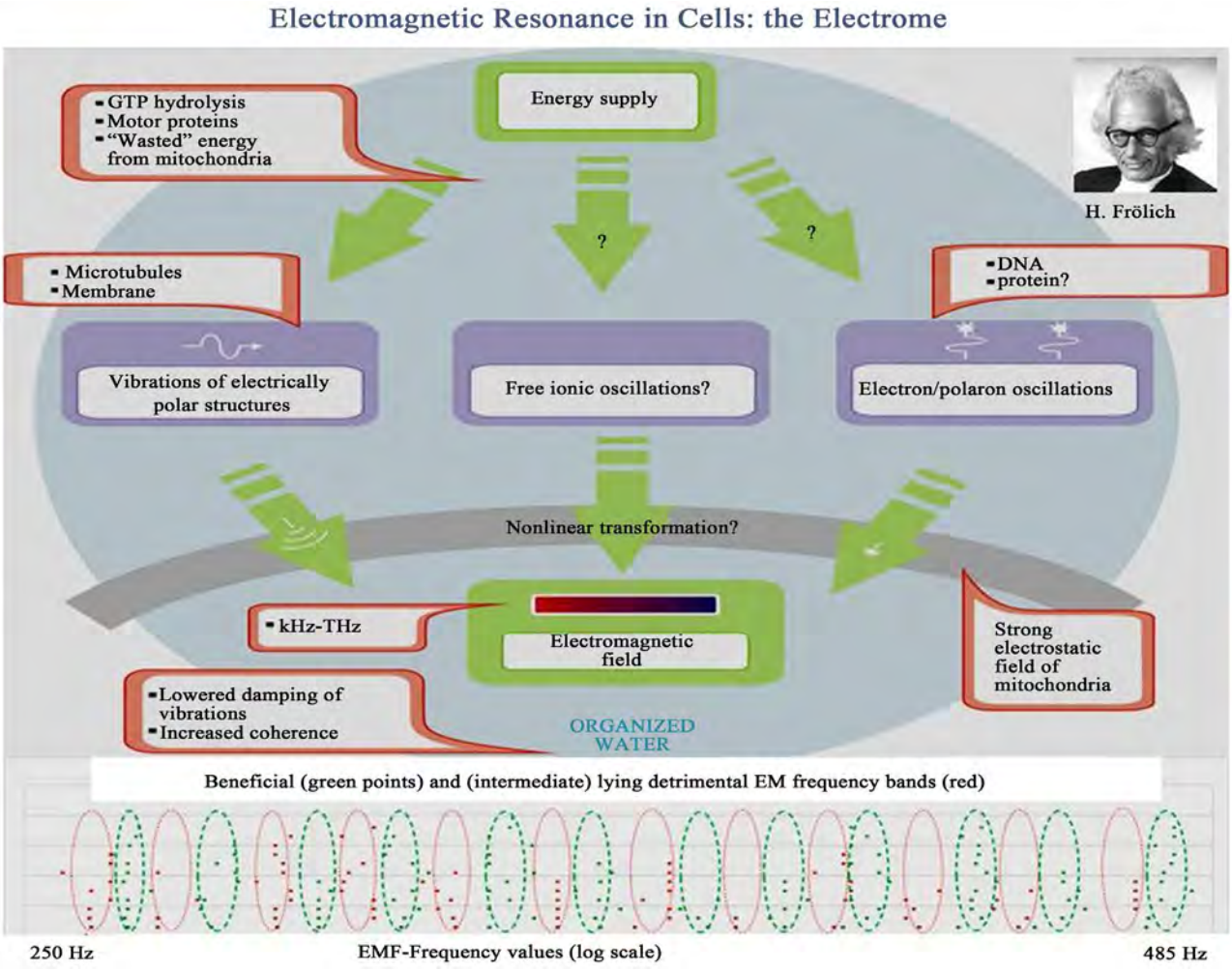

Figure 9. The EM resonance aspect of the integrate cell (electrome) with oscillating constituents at various intracellular sites (green arrows). Bottom part: EM field frequency band pattern of coherent (green points) and non-coherent values, as revealed in a meta-analyses of biomedical literature (see Geesink and Meijer, ref, nr 10, 11, 12).

directed at the morphogenetic aspects of biological evolution. This also implies the requirement of a field receptive memory structure that can faithfully collect and store the integral history and present state of the particular cell, would be required.

In this respect, a toroidal space-time unit (hypersphere), encompassing a fourth spatial dimension and time symmetry is proposed. This represents an integral and updated holographic endo-memory of the exo-world that is instrumental in guiding the required life-architecture of cell structure and conformation of macromolecules to an optimal functional state for survival. For the latter aspect, potential retro-causality, through probing future viable states may be necessary. In this manner crucial a-priory information for the unfolding of life processes can be detected and the final function of the protein in the cellular protein networks can be anticipated and assigned

In conclusion: proteins in life-systems indeed are never alone: they are guest in a multi-layered energy landscape, yet faithfully coupled with a memory modality. This supervening information can coordinate the fine tuning through constant feed-back and quality control on the basis of the representation of a versatile network of force fields that interact with those of the cell. Toroidal geometry of discrete electromagnetic wave frequency patterns, reflecting soliton (polaron) energies at the fractal scales of life systems is proposed to be instrumental in this respect. Distinct life information can be derived from the all pervading zero-point energy field, that is seen as a stochastic electro-dynamic system, but partly functions as a strongly correlated information matrix with dominating collective effects that can drive coherence and attractor states in cell components. Such a piloting steering system seems to provide a deterministic aspect to quantum mechanics [12], yet it should be realized that this kind of quantum transfer includes a back-reaction into the vacuum field and is a symmetric process [143], by which the field is continuously updated. This implies that the information flow cannot be fully deterministic, since the overall background is never the same.

We stipulate in the present paper that the recognition of resonant frequencies can lead to modulation of form and function of proteins and DNA, but that, associated with each cell, an integrated information processing center is required for an orchestrated effort to maintain cell viability and proper intercellular communication. It remains to be established whether a collective cellular memory workspace of the organism contributes to epigenetic perturbations and/or organ- and total body-memory. In this sense such a holographic memory space, as described by us for the human brain [97] may, in certain special stages of tissue development and regeneration, supplement known transcriptional mechanisms [144] and be instrumental in encoding distinct life information of non-neural nature.

The semi-harmonic GM-scale, of EM fields that influence a wide spectrum of oscillating systems in nature (see **Figure 9**), as revealed by us, may therefore

represent a generalized biophysical principle with a "musical" signature that provides an interplay of electromagnetic waves, highlighting the electro-tonal features that underlies life and the fabric of reality in general. It is of interest that Niemetz [145] reviewed the recent findings of micro-musical aspects of whole cells, DNA and proteins by atomic force microscopy ("tactoscope"), also mentioning the scale invariant recorded, discrete, sounds of in-animated physical structures, up to black holes in the universe. All this points at a deeper layer of a harmonically guided evolution [146], as was also revealed by Frank Wilczek, in his book "A Beautiful Question, on Finding Nature's Deep Design" [147].

References

[1] Melkikh, A.V. and Meijer, D.K.F. (2018) On a Generalized Levinthal's Paradox: The Role of Long- and Short Range Interactions on Complex Bio-Molecular Reactions, including Protein and DNA Folding. *Progress in Biophysics and Molecular Biology*, **132**, 57-79. https://doi.org/10.1016/j.pbiomolbio.2017.09.018

[2] Bédard, S., Krishna, M.M.G., Mayne, L. and Englander, W.S. (2008) Protein Folding: Independent Unrelated Pathways or Predetermined Pathway with Optional Errors. *PNAS*, **105**, 7182-7187. https://doi.org/10.1073/pnas.0801864105

[3] Martinez, L. (2014) Introducing the Levinthal's Protein Folding Paradox and Its Solution. *Journal of Chemical Education*, **91**, 1918-1923. https://doi.org/10.1021/ed300302h

[4] Chen, M., Lin, X., Zheng, W., Onuchic, J.N. and Wolynes, P.G. (2016) Protein Folding and Structure Prediction from the Ground Up: The Atomistic Associative Memory, Water Mediated, Structure and Energy Model. *The Journal of Physical Chemistry B*, **120**, 8557-8565. https://doi.org/10.1021/acs.jpcb.6b02451

[5] Wolynes, P.G. (2015) Evolution, Energy Landscapes and the Paradoxes of Protein Folding. *Biochimie*, **119**, 218-230. https://doi.org/10.1016/j.biochi.2014.12.007

[6] Muñoz, V. and Cerminara, M. (2016) When Fast Is Better: Protein Folding Fundamentals and Mechanisms from Ultrafast Approaches. *Biochemical Journal*, **473**, 2545-2559. https://doi.org/10.1042/BCJ20160107

[7] De Loof, A. (2016) The Cell's Self-Generated "Electrome": The Biophysical Essence of the Immaterial Dimension of Life? *Communicative & Integrative Biology*, **9**, e1197446. https://www.researchgate.net/publication/304712940 https://doi.org/10.1080/19420889.2016.1197446

[8] Tamulis, A. (2008) Quantum Mechanical Control of Artificial Minimal Living Cells. *NeuroQuantology*, **6**, 311-322. https://doi.org/10.14704/nq.2008.6.3.188

[9] Tamulis, A. and Tamulis, V. (2008) Quantum Mechanical Design of Molecular Electronics OR Gate for Regulation of Minimal Cell Functions. *Journal of Computational and Theoretical Nanoscience*, **5**, 545-553. https://doi.org/10.1166/jctn.2008.2497

[10] Geesink, J.H. and Meijer, D.K.F. (2016) Quantum Wave Information of Life Revealed: An algorithm for EM Frequencies That Create Stability of Biological Order, with Implications for Brain Function and Consciousness. *NeuroQuantology*, **14**, 106-125. https://doi.org/10.14704/nq.2016.14.1.911

[11] Geesink, J.H. and Meijer, D.K.F. (2016) Electromagnetic Frequency Patterns That Are Crucial for Health and Disease Reveal a Generalized Biophysical Principle: The GM Scale. *Quantum Biosystems*, **8**, 1-16.

[12] Geesink, J.H. and Meijer, D.K.F. (2018) Structure for Electromagnetic Frequencies That May Reflect Pilot Waves of Bohm's Implicate Order. *Journal of Modern Physics*, **9**, 851-897. http://www.scirp.org/journal/jmp https://doi.org/10.4236/jmp.2018.95055

[13] Belyaev, I. (2015) Biophysical Mechanisms for Nonthermal Microwave Effects. In: Markov, M.S., Ed., *Electromagnetic Fields in Biology and Medicine*, CRC Press, Boca Raton, 49-68. https://doi.org/10.1201/b18148-6

[14] Brizhik, L. (2013) Biological Effects of Pulsating Magnetic Fields: Role of Solitons.

[15] Cifra, M., Fields, J.Z. and Farhadi, A. (2011) Electromagnetic Cellular Interactions. *Progress in Biophysics and Molecular Biology*, **105**, 223-246.

[16] Cosic, I., Cosic, D. and Lazar, K. (2015) Is It Possible to Predict Electromagnetic Resonances in Proteins, DNA and RNA? *Nonlinear Biomedical Physics*, **3**, 5.

[17] Hammerschlag, R., Levin, M., Mc Craty, R., Bat, B.A., Ives, J.A., Lutgendorf, S.K. and Oschman, J.L. (2015) Biofield Physiology: A Framework for an Emerging Discipline. *Global Advances in Health and Medicine*, **4**, 35-41.

[18] Levin, M. (2012) Molecular Bioelectricity in Developmental Biology: New Tools and Recent Discoveries: Control of Cell Behavior and Pattern Formation by Transmembrane Potential Gradients. *BioEssays*, **34**, 205-217. https://doi.org/10.1002/bies.201100136

[19] Muehsam, D. and Ventura, C. (2014) Life Rhythm as a Symphony of Oscillatory Patterns: Electromagnetic Energy and Sound Vibration Modulates Gene Expression for Biological Signaling and Healing. *Global Advances in Health and Medicine*, **3**, 40-55. https://doi.org/10.7453/gahmj.2014.008

[20] Pokorny, J. (2004) Excitation of Vibrations in Microtubules in Living Cell. *Bioelectrochemistry*, **63**, 321-326. https://doi.org/10.1016/j.bioelechem.2003.09.028

[21] Rakovic, D., Dugic, M. and Cirkovic, M.M. (2004) Macroscopic Effects in Biophysics and Consciousness. *NeuroQuantology*, **2**, 237-262.

[22] Tuszynski, J.A., Wenger, C., Friesen, D.E. and Preto, J. (2016) An Overview of Sub-Cellular Mechanisms Involved in the Action of TTFields. *International Journal of Environmental Research and Public Health*, **13**, 1128. https://doi.org/10.1016/j.bioelechem.2003.09.028

[23] Redozubov, A. (2017) Holographic Memory: A Novel Model of Information Processing by Neuronal Microcircuits. In: Opris, Ioan, Casanova and Manuel, F., Eds., *The Physics of the Mind and Brain Disorder*s, Springer Series in Cognitive and Neural Systems Chapter 13, Springer, Berlin, 271-295.

[24] Preto, J. (2016) Classical Investigation of Long Range Coherence in Biological Systems. *Chaos*, **26**, Article ID: 123116. https://doi.org/10.1063/1.4971963

[25] Reimers, J.R., McKemmish, L.K., McKenzie, R.H., Mark, A.E. and Hush, N.S. (2009) Weak, Strong, and Coherent Regimes of Fröhlich Condensation and Their Applications to Terahertz Medicine and Quantum Consciousness. *PNAS*, **106**, 4219-4224. https://doi.org/10.1073/pnas.0806273106

[26] Lundholm, I.V., Rodilla, H., Wahlgren, W.Y., Duelli, A., Bourenkov, G., Vukusic, J., Friedman, R., Stake, J., Schneider, T. and Katona, G. (2015) Terahertz Radiation Induces Non-Thermal Structural Changes Associated with Fröhlich Condensation in a Protein Crystal. *Structural Dynamics*, **2**, Article ID: 054702. https://doi.org/10.1063/1.4931825

[27] Nardecchia, I., Torres, J., Lechelon, M., Giliberti, V., Ortolani, M., Nouvel, P., Gori, M., Donato, I., Preto, J., Varani, L., Sturgis, J. and Pettini, M. (2017) Out-of-Equilibrium

Collective Oscillation as Phonon Condensation in a Model Protein. https://arxiv.org/pdf/1705.07975.pdf

[28] Nardecchia, I., Spinelli, L., Preto, J., Gori, M., Floriani, E., Jaeger, S., Ferrier, P. and Pettini, M. (2014) Experimental Detection of Long-Distance Interactions between Biomolecules through Their Diffusion Behavior: Numerical Study. *Physical Review* E, **90**, Article ID: 022703. https://doi.org/10.1103/PhysRevE.90.022703

[29] Goushcha, A.O., Hushcha, T.O. and Christophorov, L.N. (2014) Self-Organisation and Coherence in Biology and Medicine. *Open Journal of Biophysics*, **4**, 119-146. https://doi.org/10.4236/ojbiphy.2014.44014

[30] Rost, B. (2003) Neural Network Predict Protein Structure: Hype or Hit? In: Frasconi, P. and Shamir, Eds., *Artificial Intelligence and Heuristic Methods in Bioinformatics*, IOS press, Amsterdam, 34-50.

[31] Fröhlich, H. (1975) The Extraordinary Dielectric Properties of Biological Materials and the Action of Enzymes. *PNAS*, **72**, 4211-4215. https://doi.org/10.1073/pnas.72.11.4211

[32] Davydov, A.S. (1977) Solitons and Energy Transfer along Protein Molecules. *Journal of Theoretical Biology*, **66**, 379-387. https://doi.org/10.1016/0022-5193(77)90178-3

[33] Davydov, A.S. (1973) The Theory of Contraction of Proteins under Their Excitation. *Journal of Theoretical Biology*, **38**, 559-569. https://doi.org/10.1016/0022-5193(73)90256-7

[34] Pang, X.F., Chen, S., Wang, X. and Zhong, L. (2016) Influences of Electromagnetic Energy on Bio-Energy Transport through Protein Molecules in Living Systems and Its Experimental Evidence. *International Journal of Molecular Sciences*, **17**, 1130. https://doi.org/10.3390/ijms17081130

[35] Cruzeiro, L. (2009) The Davydov/Scott Model for Energy Storage and Transport in Proteins. *Journal of Biological Physics*, **35**, 43-55. https://www.ncbi.nlm.nih.gov/pmc/articles/PMC2660397

[36] Ritz, W. (1909) Theorie der Transversalschwingungen einer quadratischen Platte mit freien Rändern. *Annalen der Physik*, **333**, 737-786.

[37] Chladni, E.F.F. (1817) Neue Beyträge zur Akustik, by Ernst Florens Friedrich Chladni. Breitkopf und Härtel, Leipzig.

[38] Geesink, J.H. and Meijer, D.K.F. (2017) Bio-Soliton Model That Predicts Non-Thermal Electromagnetic Frequency Bands, That Either Stabilize or Destabilize Living Cells. *Electromagnetic Biology and Medicine*, **36**, 357-378. https://doi.org/10.1080/15368378.2017.1389752

[39] Salford, L.G., Nitty, H., *et al.* (2017) The Mammalian Brain in the Electromagnetic Fields Designed by Man with Special Reference to Blood-Brain Barrier Function, Neuronal Damage and Possible Physical Mechanisms. *Progress of Theoretical Physics Supplement*, **173**, 283-309. http://ptp.ipap.jp/link?PTPS/173/283

[40] Tozzi, A. and Peters, J. (2017) Plasma-Like Brain: Collective Movements in the Extracellular Nervous Spaces. https://www.researchgate.net/publication/304777768_PLASMALIKE_BRAIN_COLLECTIVE_MOVEMENTS_IN_THE_EXTRACELLULAR_NERVOUS_SPACES

[41] Sahu, S., Ghosh, S., Ghosh, B., Aswani, K., Hirata, K., Fujita D., *et al.* (2013) Atomic Water Channel Controlling Remarkable Properties of a Single Brain Microtubule: Correlating Single Protein to Its Supramolecular Assembly. *Biosensors and Bioelectronics*, **47**, 141-148. https://doi.org/10.1016/j.bios.2013.02.050

[42] Zioutas, K. (1996) On the Interaction of Extreme-Low-Frequency (ELF) Radiation with Living Matter's Coherent Spiral States. https://arxiv.org/pdf/patt-sol/9601001

[43] Cheron, G., Gall, D., Servais, L., Dan, B., Maex, R. and Schiffmann, S.N. (2004) Inactivation of Calcium-Binding Protein Genes Induces 160 Hz; Oscillations in the Cerebellar Cortex of Alert Mice. *The Journal of Neuroscience*, **24**, 434-441. https://doi.org/10.1523/JNEUROSCI.3197-03.2004

[44] Persinger, M.A., Murugan, N.J. and Karbowski, L.M. (2015) Combined Spectral Resonances of Signaling Proteins' Amino Acids in the ERK-MAP Pathway Reflect Unique Patterns That Predict Peak Photon Emissions and Universal Energies. *International Letters of Chemistry, Physics and Astronomy*, **43**, 10-25. https://doi.org/10.18052/www.scipress.com/ILCPA.43.10

[45] Sahu, S., Ghosh, S., Fujita, D. and Bandyopadhyay, A. (2014) Live Visualizations of single Isolated Tubulin Protein Self-Assembly via Tunneling Current: Effect of Electromagnetic Pumping during Spontaneous Growth of Microtubule. *Scientific Reports*, **4**, Article No. 07303. https://doi.org/10.1038/srep07303

[46] Ghosh, S., Sahu, S., Agrawal, L., Shiga, T. and Bandyopadhyay, A. (2016) Inventing a Co-Axial Atomic Resolution Patch Clamp to Study a Single Resonating Protein Complex and Ultra-Low Power Communication Deep inside a Living Neuron Cell. *Journal of Integrative Neuroscience*, **15**, 403-433. https://doi.org/10.1142/S0219635216500321

[47] Copty, A.B., Neve-Oz, Y., Barak, I., Golosovsky, M. and Davidov, D. (2006) Evidence for a Specific Microwave Radiation Effect on the Green Fluorescent Protein. *Biophysical Journal*, **91**, 1413-1423. https://doi.org/10.1529/biophysj.106.084111

[48] Meijer, D.K.F. and Geesink, J.H. (2016) Phonon Guided Biology: Architecture of Life and Conscious Perception Are Mediated by Toroidal Coupling of Phonon, Photon and Electron Information Fluxes at Discrete Eigenfrequencies. *Neuro-Quantology*, **14**, 718-755. https://doi.org/10.14704/nq.2016.14.4.985

[49] Gerner, C., Haudek, V., Schandl, U., Bayer, E., Gundacker, N., Hutter, H.P. and Mosgoeller, W. (2010) Increased Protein Synthesis by Cells Exposed to a 1,800-MHz Radio-Frequency Mobile Phone Electromagnetic Field, Detected by Proteome Profiling. *Archives of Occupational and Environmental Health*, **83**, 691-702. https://doi.org/10.1007/s00420-010-0513-7

[50] Cheon, H., Yang, H.J., Lee S.H., Kim, Y.A. and Son, J.H. (2016) Terahertz Molecular Resonance of Cancer DNA. *Scientific Reports*, **6**, Article No. 37103. https://doi.org/10.1038/srep37103

[51] Geesink, J.H. and Meijer, D.K.F. (2018) A Semi-Harmonic Frequency Pattern Organizes Local and Non-Local States by Quantum Entanglement in both EPR-Studies and Life Systems. *Journal of Modern Physics*, **9**, 898-924. http://www.scirp.org/journal/jmp https://doi.org/10.4236/jmp.2018.95056

[52] Geesink, J.H. and Meijer, D.K.F. (2018) Semi-Harmonic Scaling Enables Calculation of Masses of Elementary Particles of the Standard Model. *Journal of Modern Physics*, **9**, 925-947. http://www.scirp.org/journal/jmp https://doi.org/10.4236/jmp.2018.95057

[53] Adamatzky, A. (2013) Game of Life on Phyllosilicates: Gliders, Oscillators and Still Life. *Physics Letters*, **377**, 597-1605.

[54] Hashizume, H. (2012) Role of Clay Minerals in Chemical Evolution and the Origins of Life. http://uu.diva-portal.org/smash/get/diva2:935529/FULLTEXT01.pdf

[55] Grandpierre, A. (2001) Phenomenology of Space and Time. Book 1. The Forces of the Cosmos and the Ontopoietic Genesis of Life. In: Tymieniecka, A.-T. Ed., *Analecta Husserliana*. http://www.springer.com/philosophy/book/978-3-319-02014-3

[56] Meijer, D.K.F. (2012) The Information Universe. On the Missing Link in Concepts on the Architecture of Reality. *Syntropy Journal,* **1**, 1-64.

[57] Walker, S.I. and Davies, P.C.W. (2013) The Algorithmic Origin of Life. *Journal of the Royal Society Interface*, arXiv:1207.4803. https://doi.org/10.1098/rsif.2012.0869

[58] Dotta, B.T., Mulligan, B.P., Hunter, M.D. and Persinger, M.A. (2009) Evidence of Macroscopic Quantum Entanglement during Double Quantitative Electroencephalographic Measurements of Friend's vs Strangers. *NeuroQuantology*, **7**, 548-551. https://doi.org/10.14704/nq.2009.7.4.251

[59] Melkikh, A.V. (2014) Quantum Information and the Problem of Mechanisms of Biological Evolution. *BioSystems*, **115**, 33-45. https://doi.org/10.1016/j.biosystems.2013.10.005

[60] Melkikh, A.V. and Mahecha, D.S. (2018) On the Broader Sense of Life and Evolution: Its Mechanisms, Origin and Probability across the Universe. *Journal of Astrobiology and Outreach*, **6**, 1-13.

[61] Tuszynski, M.H., *et al.* (2015) Nerve Growth Factor Gene Therapy: Activation of Neuronal Responses in Alzheimer Disease. *JAMA Neurology*, **72**, 1139-1147. https://doi.org/10.1001/jamaneurol.2015.1807

[62] Hameroff, S. and Penrose, R. (2014) Consciousness in the Universe: A Review of the "Orch OR" Theory. *Physics of Life Reviews*, **11**, 39-78. https://doi.org/10.1016/j.plrev.2013.08.002

[63] Craddock, T.J.A., Friesen, D., Mane, J., Hameroff, S. and Tuszynski, J. (2014) The Feasibility of Coherent Energy Transfer in Microtubules. *Journal of the Royal Society Interface*, **11**, Article ID: 20140677.

[64] Foletti, A. and Brizhik, L. (2017) Non-Linearity Coherence and Complexity: Biological Aspects Related to Health and Disease. *Electromagnetic Biology and Medicine*, **36**, 315-324. https://doi.org/10.1080/15368378.2017.1371034

[65] Laurell, H. (2016) A Summary on Solitons in Quantum Field Theory. http://uu.diva-portal.org/smash/get/diva2:935529/FULLTEXT01.pdf

[66] Molkenthin, N., Hu, S. and Niemi, A.J. (2010) Discrete Nonlinear Schrodinger Equation, Solitons and Organizing Principles for Protein Folding. https://arxiv.org/abs/1009.1078

[67] Halgamuge, M.N., Perssont, B.R.R. and Salford, G. (2009) Comparison between Two Models for Interactions between Electric and Magnetic Fields and Proteins in Cell Membranes. *Environmental Engineering Science*, **26**, 1473-1480. https://doi.org/10.1089/ees.2009.0014

[68] Chernodub, M., Hu, S.W. and Niemi, A.J. (2010) Topological Solitons and Folded Proteins. *Physical Review E*, **82**, Article ID: 011916. https://doi.org/10.1103/PhysRevE.82.011916

[69] Jerman, I. (2016) The Origin of Life from Quantum Vacuum, Water and Polar Molecules. *American Journal of Modern Physics*, **5**, 34-43.

[70] Henry, M. (2016) Hofmeister Series: The Quantum Mechanical Viewpoint. *Current Opinion in Colloid & Interface Science;* **23**, 119-125. https://doi.org/10.1016/j.cocis.2016.08.001

[71] Levy, Y. and Onuchie J.N. (2006) Water Mediation in Protein Folding and Molecular Recognition. *Annual Review of Biophysics and Biomolecular Structure*, **35**,

389-415. https://doi.org/10.1146/annurev.biophys.35.040405.102134

[72] Chaplin, M.F. (2000) A Proposal for the Structuring of Water. *Biophysical Chemistry*, **83**, 211-221. https://doi.org/10.1016/S0301-4622(99)00142-8

[73] Johnson, K. (2009) "Water Buckyball" Terahertz Vibrations in Physics, Chemistry, Biology, and Cosmology. https://arxiv.org/ftp/arxiv/papers/0902/0902.2035.pdf

[74] Tielrooij, K.J., Garcia-Araez, N., Bonn, M. and Bakker, H.J. (2010) Cooperativity in Ion Hydration. *Science*, **328**, 1006-1009. https://doi.org/10.1126/science.1183512

[75] Chai, B., Yoo, H. and Pollack, G.H. (2009) Effect of Radiant on Near-Surface Water. *The Journal of Physical Chemistry B*, **113**, 13953-13958. https://doi.org/10.1021/jp908163w

[76] Carniello, T.N., Vares, D.A.E. and Persinger, M.A. (2015) Quantitative Support for Water as the Conduit of Interaction for Universal Entanglement. *Journal of Consciousness Exploration & Research*, **6**, 738-749.

[77] Havenith, M. (2010) Water and Biological Molecules Probed by Terahertz-Spectroscopy. http://www.hfsp.org/frontier-science/hfsp-success-stories/water-and-biological-molecules-probed-terahertz-spectroscopy

[78] Ball, P. (2017) Water Is an Active Matrix of Life for Cell and Molecular Biology. *PNAS*, **114**, 13327-13335. https://doi.org/10.1073/pnas.1703781114

[79] Sbitnev, V.I. (2016) Quantum Consciousness in Warm, Wet, and Noisy Brain. *Modern Physics Letters B*, **30**, 25 p. https://arxiv.org/abs/1606.00258 https://doi.org/10.1142/S0217984916503292

[80] Sbitnev, V.I. (2017) Hydrodynamics of Superfluid Quantum Space: De Broglie Interpretation of Quantum Mechanics.

[81] Mentré. P. (2012) Water in the Orchestration of the Cell Machinery. Some Misunderstandings: A Short Review. *Journal of Biological Physics*, **38**, 13-26. https://doi.org/10.1007/s10867-011-9225-9

[82] Graziano, G. (2013) A View on the Dogma of Hydrophobic Imperialism in Protein Folding. *Journal of Biomolecular Structure and Dynamics*, **31**, 1016-1019. https://doi.org/10.1080/07391102.2012.748545

[83] Montagnier, L., *et al.* (2015) Transduction of DNA Information through Water and Electromagnetic Waves. *Electromagnetic Biology and Medicine*, **34**, 106-112. https://doi.org/10.3109/15368378.2015.1036072

[84] Montagnier, L., *et al.* (2017) Water Bridging Dynamics of Polymerase Chain Reaction in the Gauge Theory Paradigm of Quantum Fields. *Water*, **9**, 339. https://doi.org/10.3390/w9050339

[85] Lawrence, D.S. and Shell, T.A. (2015) Vitamin B_{12}: A Tunable, Long Wavelength, Light-Responsive Platform for Launching Therapeutic Agents. *Accounts of Chemical Research*, **48**, 2866-2874. https://doi.org/10.1021/acs.accounts.5b00331

[86] Mc Dermott, M.L, Vanselous, H., Corcelli, S.A. and Petersen, P.B. (2017) DNA's Chiral Spine of Hydration. *ACS Central Science*, **3**, 708-714. https://doi.org/10.1021/acscentsci.7b00100

[87] Plankar, M., Jerman, I. and Krasovec, R. (2011) On the Origin of Cancer: Can We Ignore Coherence*? Progress in Biophysics and Molecular Biology*, **106**, 380-390. https://doi.org/10.1016/j.pbiomolbio.2011.04.001

[88] Todorova, N., Bentvelzen, A., English, N.J. and Yarovsky, I. (2016) Electromagnetic-Field Effects on Structure and Dynamics of Amyloidogenic Peptides. *The Journal of Chemical Physics*, **144**, Article ID: 085101. https://doi.org/10.1063/1.4941108

[89] Pouthier, V. (2009) Narrow Band Excitation Coupled with Acoustical Anharmonic

Phonons: Application to the Vibrational Energy Flow in Lattice of H-Bonded Peptide Units. *Journal of Physics*: *Condensed Matter*, **21**, Article ID: 185404. https://www.utinam.cnrs.fr/IMG/pdf/exciton.pdf https://doi.org/10.1088/0953-8984/21/18/185404

[90] Davies, P.C.W. (2014) Does Quantum Mechanics Play a Non-Trivial Role in Life? *BioSystems*, **78**, 69-79. https://doi.org/10.1016/j.biosystems.2004.07.001

[91] Farnsworth, K.D., Nelson, J. and Gershenson, C. (2013) Living Is Information Processing: From Molecules to Global Systems. *Acta Biotheoretica*, **61**, 203-222. https://doi.org/10.1007/s10441-013-9179-3

[92] Pribram, K.H. (2004) Consciousness Reassessed. *Mind and Matter*, **2**, 7-35.

[93] Bieberich, E. (2012) Introduction in Fractality Principle of Consciousness and Sentyon Postulate. *Cognitive Computation*, **4**, 13-28. https://doi.org/10.1007/s12559-011-9104-5

[94] Susskind, L. (1994) The World as a Hologram.

[95] 't Hooft, G. (2001) The Holographic Principle. In: Zuchichi, A., Ed., *Basics and Highlights in Fundamental Physics*, World Scientific, Singapore, 72-100. https://doi.org/10.1142/9789812811585_0005

[96] Bieberich, E. (2014) Synthesis, Processing, and Function of N-Glycans in N-Glycoproteins. *Glycobiology of the Nervous System*, **9**, 47-70. https://doi.org/10.1007/978-1-4939-1154-7_3

[97] Meijer, D.K.F. and Geesink, J.H. (2017) Consciousness in the Universe Is Scale Invariant and Implies an Event Horizon of the Human Brain. *NeuroQuantology*, **15**, 41-79.

[98] Anjamrooz, S.H. (2013) The Cellular Memory Disc of Reprogrammed Cells. *Stem Cell Reviews and Reports*, **9**, 190-209. https://doi.org/10.1007/s12015-013-9429-4

[99] Anjamrooz, S.H. (2015) Cell Memory-Based Therapy. *Journal of Cellular and Molecular Medicine*, **19**, 2682-2689. https://doi.org/10.1111/jcmm.12646

[100] Hales, C.G. (2014) The Origin of Brain's Endogenous Electromagnetic Field and Its Relation with Consciousness. *Journal of Integrative Neuroscience*, **13**, 313-361. https://doi.org/10.1142/S0219635214400056

[101] Bernroider, G. (2003) Quantum Neurodynamics and the Relationship to Conscious Experience. *NeuroQuantology*, **1**, 163-168.

[102] Cifra, M., Pokorny, J., Havelka, D. and Kucer, O. (2010) Electric Field Generated by Axial Longitudinal Vibration Modes of Microtubule, *BioSystems*, **100**, 122-131. https://doi.org/10.1016/j.biosystems.2010.02.007

[103] Farhadi, A., Forsyth, C., Banan, A., Shaikh M., Engen, P., Fields, J.Z. and Keshavarzian, A. (2007) Evidence for Non-Chemical, Non-Electrical Intercellular Signaling in Intestinal Epithelial Cells. *Bioelectrochemistry*, **71**, 142-148. https://doi.org/10.1016/j.bioelechem.2007.03.001

[104] Persinger, M.A. and Dotta, B.T. (2011) Temporal Patterns of Photon Emission Can Be Stored and Retrieved Several Days Later from the "Same Space": Experimental and Quantitative Evidence. *NeuroQuantology*, **9**, 605-613. https://doi.org/10.14704/nq.2011.9.4.467

[105] Gough, W.C. and Shacklett R.L. (1993) "Physics, Parapsychology and Religion"—Part I: The Reality Beyond Space-Time, Part II: The Quantum Linkage, Part III: The Human Implications. *Journal of Religion and Psychical Research*, **16**, 65-77, 126-134, 196-209.

[106] Levin, M.A. and Wen, X.-G. (2005) String-Net Condensation: A Physical Mechanism for Topological Phases. *Physical Review B*, **71**, Article ID: 045110

[107] Arkani-Hamed, N. (2013) Beyond the Standard Model Theory. *Physica Scripta*, **2013**, T158.

[108] Merali, Z. (2017) The Universe Is a String-Net Liquid. http://dao.mit.edu/~wen/NSart-wen.html

[109] Tegmark, M. (2014) Our Mathematical Universe. My Quest for the Ultimate Nature of Reality. Penquin Books Ltd., London.

[110] Butterfield, J. (2014) Our Mathematical Universe. Book Review in Plus Magazine of the UK Mathematics Millenium Project.

[111] Azvedo, E. and Filho, J.P. (2017) Is There an Information Field in the Life World? Empirical Approach Using Electrophotonic Analysis. *Journal of Life Sciences*, **11**, 191-201.

[112] Fleming, A.H.J. (2017) A Range of Fields over the Spectrum in a Cell Colony May Control the Timing of Its Cell Cycle. 2017 *Progress* in *Electromagnetics Research Symposium—Spring* (*PIERS*), St. Petersburg, 22-25 May 2017. https://doi.org/10.1109/PIERS.2017.8262346

[113] Tozzi, A. and Peters, J.F. (2016) Towards a Fourth Spatial Dimension of Brain Activity. *Cognitive Neurodynamics*, **10**, 189-199. https://doi.org/10.1007/s11571-016-9379-z

[114] Haramein, N, Brown, W.D. and Val Baker, A. (2016) The United Space Memory Network: From Cosmogenesis to Consciousness. *NeuroQuantology*, **14**, 1-15. https://doi.org/10.14704/nq.2016.14.4.961

[115] Geesink, J.H. and Meijer, D.K.F. (2017) Bio-Soliton Model That Predicts Non-Thermal Electromagnetic Frequency Bands, That Either Stabilize or Destabilize Living Cells. *Electromagnetic Biology and Medicine*, **36**, 357-378. https://doi.org/10.1080/15368378.2017.1389752

[116] Rouleau, N. and Dotta, B.T. (2014) Electromagnetic Fields as Structure Function Zeitgebers in Biological Systems: Environmental Orchestration and Consciousness. *Frontiers in Integrative Neuroscience*, **8**, 84.

[117] Salari, V., Vallian, H., Bassereh, H., Bókkon, I. and Barhordari, A. (2015) Ultraweak Photon Emission in the Brain. *Journal of Integrative Neuroscience*, **14**, 1-11. https://doi.org/10.1142/S0219635215300012

[118] Laager, F. (2015) Light Based Cellular Interactions: Hypotheses and Perspectives. *Frontiers in Physics*, **3**, 55. https://doi.org/10.3389/fphy.2015.00055

[119] Mayburov, S.N. (2012) Photonic Communication and Information Encoding in Biological Systems. arXiv:1205.4134.

[120] Tang, R. and Dai, J. (2014) Spatiotemporal Imaging of Glutamate-Induced Biophotonic Activities and Transmissions in Neural Circuits. *PLoS ONE*, **9**, e85643. https://doi.org/10.1371/journal.pone.0085643

[121] Wang, Z., Wang, N., Li, Z., Xiao, F. and Dai, J. (2016) Human High Intelligence Is Involved in Spectral Redshift of Biophotonic Activities in the Brain. *PNAS*, **113**, 8753-8758. https://doi.org/10.1073/pnas.1604855113

[122] Meijer, D.K.F. (2014) The Extended Brain: Cyclic Information Flow in a Quantum Physical Realm. *NeuroQuantology*, **12**, 180-200.

[123] Penrose, R. (2014) On the Gravitization of Quantum Mechanics 1: Quantum State Reduction. *Foundations of Physics*, **44**, 557-575. https://doi.org/10.1007/s10701-013-9770-0

[124] Edwards, J.C.W. (2015) Is Consciousness only a Property of Individual Cells? *Journal of Consciousness Studies*, **12**, 60-76.

[125] Edwards, J.C.W. (2016) Distinguishing Representations as Origin and as Input: Roles for Individual Neurons. *Frontiers in Psychology*, **7**, 1537. https://doi.org/10.3389/fpsyg.2016.01537

[126] Sevush, S. (2004) Single-Neuron Theory of Consciousness. https://www.ncbi.nlm.nih.gov/pubmed/16083912 http://cogprints.org/3891/1/snt-9html.htm

[127] Lisi, A., Ledda, M., De Carlo, F., Foletti, A., Giuliani, L., D'Emilia, E. and Grimaldi, S. (2008) Calcium ion Cyclotron Resonance (ICR) Transfers Information to Living Systems: Effects on Human Epithelial Cell Differentiation. *Electromagnetic Biology and Medicine*, **27**, 230-240. https://doi.org/10.1080/15368370802269135

[128] Huelga, S.F. and Plenio, M.B. (2013) Vibartion, Quanta and Biology. *Contemporary Physics*, **54**, 181-207.

[129] Stoop, R., Buchli, J., Keller, G. and Steeb, W.-H. (2003) Stochastic Resonance in Pattern Recognition by a Holographic Neuron Model. *Physical Review E*, **67**, Article ID: 061918. https://doi.org/10.1103/PhysRevE.67.061918

[130] Pereira, A. and Furlan, F.A. (2007) Biomolecular Information, Brain Activity and Cognitive Function. *Annual Review of Biomedical Sciences*, **9**, 12-29. https://doi.org/10.3389/fpsyg.2013.00200

[131] Sutherland, J.G. (1994) The Holographic Cell: A Quantum Perspective. In: Plantamura, V.L., *et al.*, Eds., *Frontier Decision Support Concepts*, John Wiley & Sons, New York.

[132] Baars, B.J., Franklin, S. and Zoege Ramsoy, T. (2013) Global Workspace Dynamics: Cortical "Binding and Propagation" Enables Conscious Contents. *Frontiers in Psychology*, **4**, 1-22.

[133] Fröhlich, F. and McCormick, D.A. (2010) Endogenous Electric Fields May Guide Neocortical Network Activity. *Neuron*, **67**, 129-143. https://doi.org/10.1016/j.neuron.2010.06.005

[134] Keppler, J.A. (2013) A New Perspective on the Functioning of the Brain and the Mechanisms behind Conscious Processes. *Frontiers in Psychology*, **4**, 242.

[135] Persinger, M.A. and Lavallee, C.F. (2010) Theoretical and Experimental Evidence of Macroscopic Entanglement between Human Brain Activity and Photon Emissions: Implications for Quantum Consciousness and Future Applications. *Journal of Consciousness Exploration & Research*, **1**, 785-807.

[136] Gabella, M. (2006) The Randall-Sundrum Model.

[137] Auletta, G., Ellis, G.F.R. and Jaeger, L. (2008) Top-Down Causation by Information Control: From Philosophical Problem to Scientific Research Program. *Journal of the Royal Society Interface*, **5**, 1159-1172. https://doi.org/10.1098/rsif.2008.0018

[138] Perus. M. and Bishof, H. (2003) A Neural-Network Quantum Information Processing System. *Neural Network World*, **10**, 1001-1013.

[139] Ezhov, A.A. and Ventura, D. (2000) Quantum Neural Networks. In: Nikola, K., Ed., *Future Directions for Intelligent Systems and Information Sciences*, 213-235.

[140] Rakovic, D., Dugic, M., Jeknic-Dugic, M., Plavicik, M., Jacimovski, S. and Setracic, J. (2014) On Macroscopic Quantum Phenomena in Biomolecules and Cells: From Levinthal to Hopfield. *BioMed Research International*, **2014**, Article ID: 580491. https://www.hindawi.com/journals/bmri/2014/580491 https://doi.org/10.1155/2014/580491

[141] Ling, G.N. (2014) Can We See Living Structures in a Cell. *Physiological Chemistry and Physics and Medical NMR*, **43**, 1-71.

[142] Jaeken, L. (2017) The Neglected Functions of Intrinsically Disordered Proteins and the Origin of Life. *Progress in Biophysics and Molecular Biology*, **126**, 31-46. https://doi.org/10.1016/j.pbiomolbio.2017.03.002

[143] Sutherland, R.I. (2006) Causally Symmetric Bohm Model. https://pdfs.semanticscholar.org/c5f0/8198ef854f5fd824110d9aab05101879d63c.pdf

[144] Burrill D.R. and Silver, P.A. (2010) Making Cellular Memories. *Cell*, **140**, 13-18. https://doi.org/10.1016/j.cell.2009.12.034

[145] Niemetz, A. (2004) Singing Cells, Art, Science and Noise in between. MFA Thesis, UCLA Department of Design/Media Arts, University of California, Los Angeles.

[146] Merrick, R. (2010) Harmonically Guided Evolution. Fairview.

[147] Wilczek, F. (2016) A Beautiful Question, Finding Nature's Deep Design. Penquin Books, London.

Scientific Research Publishing

Open Journal of Biophysics, 2018, 8, 155-162
http://www.scirp.org/journal/ojbiphy
ISSN Online: 2164-5396
ISSN Print: 2164-5388

Live *C. elegans* Diffraction at a Single Point

Jenny Magnes[1], Cheris Congo[1], Miranda Hulsey-Vincent[1], Harold Hastings[2], Kathleen M. Raley-Susman[1]

[1]Departments of Physics and Astronomy, and Biology, Vassar College, Poughkeepsie, NY, USA
[2]Division of Science, Mathematics and Computing, Bard College at Simons Rock, Great Barrington, MA, USA
Email: jemagnes@vassar.edu

How to cite this paper: Magnes, J., Congo, C., Hulsey-Vincent, M., Hastings, H. and Raley-Susman, K.M. (2018) Live *C. elegans* Diffraction at a Single Poi. *Open Journal of Biophysics*, **8**, 155-162.
https://doi.org/10.4236/ojbiphy.2018.83011

Received: June 19, 2018
Accepted: July 16, 2018
Published: July 19, 2018

Abstract

Using coherent light, we analyze the temporal diffraction at a single point from real-time living *C. elegans* locomotion in three-dimensional space. We describe the frequency spectrum of single swimming nematodes in an optical cuvette at a single sampling point in the far-field diffraction pattern. An analytical expression of the double slit is used to model the frequency spectra of nematodes as oscillating segments. The frequency spectrum in the diffraction pattern expands discretely and linearly as a multiple of the fundamental frequency with increasing distance from the central maximum. The frequency spectrum of a worm at a single point in the frequency spectrum contains all the frequencies involved in the locomotion and is used to characterize and compare nematodes. The occurrence of resonant frequencies in the dynamic diffraction pattern increases with the distance from the central maximum. The regular spacing of the resonant frequencies is used to identify characteristic swimming frequencies.

Keywords

C. elegans, Nematode, Temporal Diffraction, Live Diffraction, Locomotion

1. Introduction

Tracking the three-dimensional (3D) movement of microscopic species over larger distances is developing with the availability of optical components and increasing computing power [1]. These techniques are highly compact, fast and avoid the issue of the species moving out of the focal plane by using diffraction and holographic methods [2]. Ozcan *et al.*, for example use holographic shadowing to track the path of sperm over a distance of about 10 μm [3]. However, the right and left-handed helical path could not be determined with a two-dimensional (2D) imaging technique where the species travels on a micro-

scope slide.

We have used the transparent nematode, *Caenorhabditis elegans*, to develop methodologies for examining microscopic organismal shape and locomotion in real-time in 3 dimensions without using microscopes [1] [4] [5]. The simple rhythmic motions and small size of these free-living organisms have allowed us to develop techniques and mathematical reconstruction processes to allow us to explore locomotion dynamics.

The analysis of the locomotion of microscopic species typically involves the filming of the species followed by a computationally intense processing of the video [6]. This type of analysis has proven to be useful in characterizing the locomotion of nematodes and comparing to other species by sight. Using these traditional microscopic methods, waveforms, oscillating movement frequencies, etc. can be established with the precision corresponding to the resolution of the microscope and the precision of the specifications associated with the optics. Using diffraction and shadowing methods forces [1] [4], movements on the order of the wavelength are used. The frequency analysis of a live diffraction signal contains information about the cumulative movements of every single point on the microscopic object as the Fraunhofer diffraction pattern is proportional to the magnitude of the Fourier transform (FT) squared of the diffracting nematode shape containing a superposition of the EM radiating from all points on the diffracting object's outline. This point is especially well illustrated by the discrete FT (DFT) [7]:

$$\mathbf{X}_{\vec{k}} = \sum_{\vec{n}=0}^{\vec{N}-1} \mathrm{e}^{-2\pi i \vec{k} \frac{\vec{n}}{\vec{N}}} \boldsymbol{x}_{\vec{n}} \tag{1}$$

where $\mathbf{X}_{\vec{k}}$ is the element in Fourier space denoted by $\vec{k}$, $\vec{n}$ is the element in object space, N represents the total number of elements in a particular dimension and $\boldsymbol{x}_{\vec{n}}$ is the element in Fourier space denoted by $\vec{n}$. The phase sensitivity is on the order of the wavelength of the coherent radiation.

In this paper, we present the single point temporal diffraction model explaining the frequency spectra as related to the locomotion of the nematode; *i.e.*, frequency and amplitude of worm oscillations. The relationship between the worm thickness and thrashing amplitude is related to the number of resonance frequencies as a function of the single point location, where the single point simulates a photodiode (PD) placed in the dynamic diffraction pattern.

2. One Dimensional Single Point Diffraction Model

The *C. elegans* width-to-length ratio is about 1/10 [8] so that the dimensions are similar to a single slit typically discussed in introductory physics texts. The intensity of the Fraunhofer diffraction pattern is proportional to the modulus of the Fourier transform squared [9]:

$$I(p) \propto \left| 2d \operatorname{sinc}(\pi p d) \right|^2 \tag{2}$$

where d is the slit width and p is the position in reciprocal space. Two segments of a *C. elegans* can then be represented by using the shift theorem [9]:

$$F(x+a)+F(x-a) \rightleftharpoons 2\Phi(p)\cos(2\pi pa) \tag{3}$$

where F is the function in object space and Φ its Fourier transform; while x represents position in object space, p the reciprocal variable in Fourier space and a is the distance by which the function F has been displaced. In the case of a dynamic system a is time-dependent a(t).

C. elegans tend to move using a sinusoidal waveform [6] so that there are segments on the worm which move out of phase. To start with a simplified model, the motion of two corresponding segments out of phase can be modeled using a double slit in one dimension (1D), similar to the well-known Young's experiment. Two slits oscillating out of phase produce an oscillating diffraction pattern with an oscillating intensity (**Figure 1**):

$$I(p,t) \propto \left(2d\,\mathrm{sinc}(\pi pd)\cos(2\pi pa_0\sin(2\pi ft))\right)^2 \tag{4}$$

where a_0 is the amplitude of oscillation and f the frequency at which the oscillations of the segments occur.

Placing a photodiode (PD) in the diffraction pattern fixes the position p in the diffraction pattern. The time-dependent signal at $p = 0$ will not vary as the frequency inside the cosine term (Equation (4)) equals zero. Holding the oscillation amplitude steady as the distance of the PD from the central maximum increases the frequency range increases matching the increments of the fundamental frequency; *i.e.*, integer multiples of the frequency at which the slits are oscillating. The amplitude can also increase the frequency of in the diffraction pattern since larger amplitudes will span a larger number of wave-fronts.

Placing a photodiode (PD) in the diffraction pattern fixes the position p in the diffraction pattern. The time dependent signal at the central maximum, $p = 0$, will not vary as the frequency inside the cosine term (Equation (4)) equals zero. Holding the oscillation amplitude steady as the distance of the PD from the central maximum increases the frequency range increases matching the increments of the fundamental frequency; *i.e.*, integer multiples of the frequency at which the slits are oscillating since the sine term inside the cosine term (Equation (4)) in the diffraction pattern dominates. The oscillation amplitude of the worm can also increase the frequency of in the diffraction pattern since a larger amplitude will span a larger number of wave-fronts.

The expected number of higher dominant frequencies is indicated by n in the spectrum can then be determined using the location of the PD at point p is then a factor of the worm thickness, sinusoidal locomotion amplitude and the value of p:

$$n \geq a_0 p/(\pi d) \tag{5}$$

The number of frequencies is indicated by n if n is an integer; otherwise the next larger integer indicates the number of fundamental frequencies included in the signal from the PD. The remaining fraction in n indicates the amplitude of the highest frequency contributing to the cosine while the sine function (Equation (4)) provides the envelope, which can be attributed to the nematode's width.

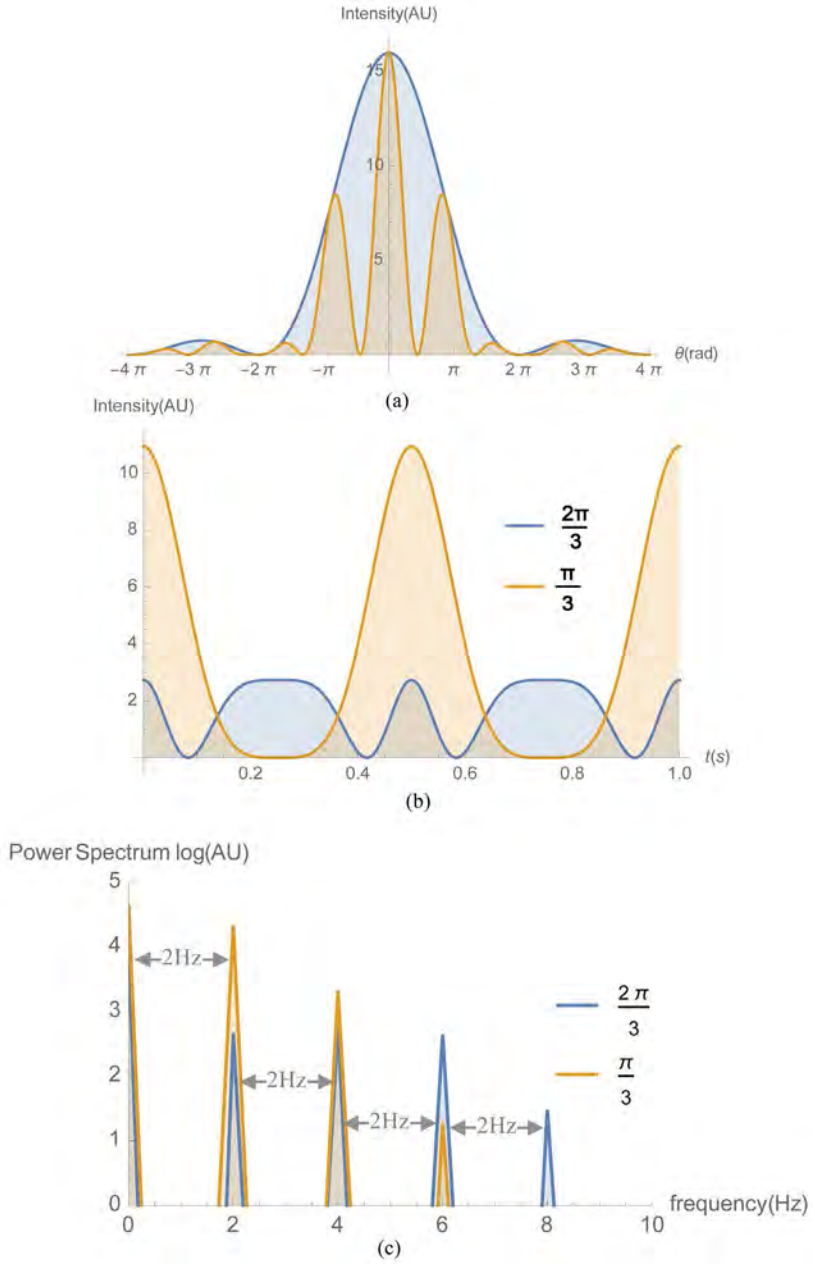

Figure 1. (a) The diffraction pattern due to two single slits oscillating out of phase at a frequency of 1 Hz. The slit width is a third of the slit separation. The outside envelope corresponds to the starting position of overlapping single slits drifting apart at t = 0 s with the spatial frequency of the diffraction pattern increasing as evident in the inner pattern at t = 0.15 s; (b) A PD placed at a phase angle of π/3 produces a 2 Hz signal. The frequency doubles for a PD placed at 2π/3 doubles the frequency. The relative intensities are larger at smaller frequencies for π/3; (c) The frequency spectrum stretches out as the PD is further away from the central maximum.

Overall, the number of frequency components increase with the phase angle as indicated in Figure 2. The resonant frequencies are spaced uniformly as dictated by the fundamental frequency. Note that the amplitude corresponds to the maximum worm oscillation (slit separation in our simplified model).

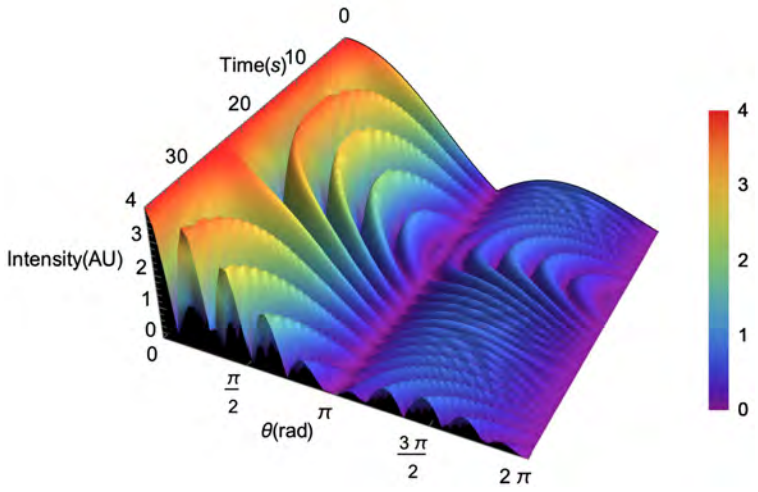

Figure 2. Intensity of PD shown as a function of phase and time. As the sensor moves away from the central maximum, intensity decreases with more frequency components.

3. Experimental Setup and Results

The optical setup was constructed to collect data at one point of the diffraction pattern (**Figure 3**). The Helium-Neon (HeNe) laser at 632.8 nm avoids the blue frequencies, which are known to influence the behavior of the nematodes [10]. The NDF prevents the PD from saturating. An adult (L4) *C. elegans* is placed in a water-filled cuvette. The cuvette is centered between Mirror 1 and Mirror 2 so that the nematode is within the laser beam's path. Mirror 2 and the translational stage control the distance of the PD from the central maximum. Measurements were taken at the 0.18 cm, 0.30 cm, and 0.42 cm away from the central maximum.

The distance from the nematode to Mirror 2 is 3.65 ± 0.05 cm. Mirror 2 is located 18.75 ± 0.05 cm from the photodiode so that the total distance from the diffracting worm to the photodiode is 22.4 ± 0.1 cm. The experimental data sets in **Figure 4** demonstrate that the frequency spectrum spreads out as the distance from the PD from the central maximum increases as indicated by the increasing mean frequency. The mean frequency is estimated using:

$$\langle f \rangle = \frac{\sum f_n \cdot PSD_n}{\sum PSD_n} \tag{6}$$

where f is the frequency, PSD represents the Power Spectral Density and n indicates the matrix element. The experimental spectra are not as distinct in their resonances as the simplified sinusoidal model; nevertheless, the resonances are consistent with known experimental locomotory frequencies of swimming and crawling *C. elegans* [11]. The bottom spectrum in **Figure 4** at 0.42 cm near the third minimum from the central maximum shows a consistent spacing of 0.602 Hz in the major peaks while finding a pattern for the spectrum closer to the central maximum at 0.18 cm near the first minimum is not possible because lower frequencies obscure the fundamental frequency. Placing the PD past the third maximum allows for enough resonances to use the spacing between resonances

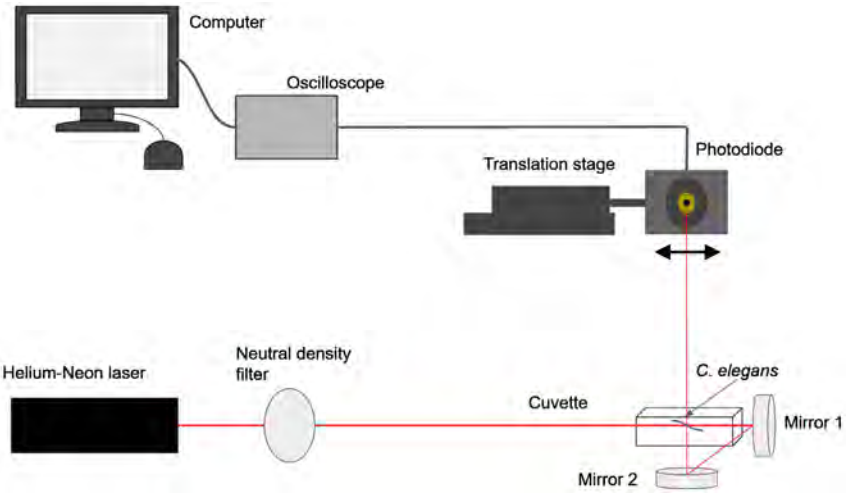

Figure 3. In the optical setup the laser beam travels through a neutral density filter (NDF) to prevent saturating the photodiode. Mirror 1 and Mirror 2 steer the laser beam through the cuvette containing the worm towards the PD. The *C. elegans* diffract the laser beam. Part of the diffraction pattern forms on the PD off center in the diffraction pattern.

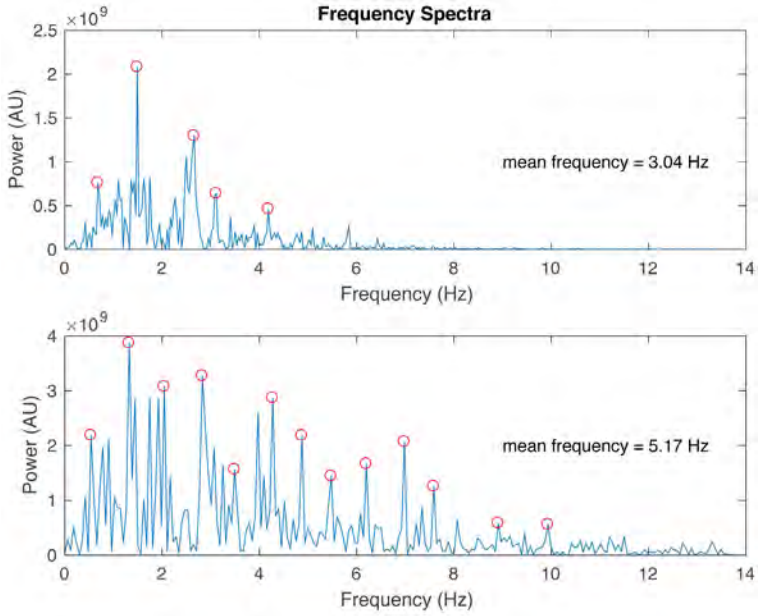

Figure 4. Frequency of intensity at 0.18 cm and 0.42 cm from the central maximum of a single wild type *C. elegans*. The mean frequency was calculated using Equation (6) and increases with distance from the central maximum and the resonance frequencies become more pronounced. The regular spacing of the resonance frequencies becomes apparent, as the PD is placed further away from the central maximum.

to determine the fundamental frequency. Destructive interference can eliminate resonance peaks so that placing the PD strategically allows for a maximum signal. Various worm movements such as head movement and the changing in direction or speed of the nematode can create frequencies. Some of these movements tend to show up in the slower frequencies, diffusing the dominant swimming or crawling frequency.

4. Conclusions

In this case study, we have demonstrated an efficient method for measuring dominant frequencies by strategically placing the PD in a dynamic diffraction pattern. Using this method, the locomotion of various phenotypes and in various environments can be characterized by frequency. A point in the diffraction pattern is used to record the superposition of all locomotory oscillations of the nematode allowing for the analysis of all frequencies embedded in the worm motion through a single time series. The intensities are sensitive to motion on the order of the wavelength of light used in the experiment so that subtle movements that might be missed in a microscopic analysis are detected and measured. Even the newest work in locomotion of *C. elegans* involves traditional microscopy rather than diffraction so that the work published by this group is the only work involving live diffraction of *C. elegans* [12] [13].

Collecting the signal at a distance from the central maximum allows for enough resonant peaks in the FT spectrum to use the spacing to measure the fundamental frequency. The regular spacing of the resonant peaks in the FT helps to identify dominant frequencies in the locomotion precisely. Further studies on separating movements of various worm parts are promising future projects. Dynamic diffraction using power spectral analysis complements traditional microscopic methods. Frequency filters can be employed to isolate various movements and switching mechanisms.

References

[1] Jago, A., Kpulun, T., Raley-Susman, K.M. and Magnes, J. (2014) Single Wavelength Shadow Imaging of *Caenorhabditis elegans* Locomotion Including Force Estimates. *Journal of Visualized Experiments*, **86**, e51424.

[2] Ozcan, A. and McLeod, E. (2016) Lensless Imaging and Sensing. *Annual Review of Biomedical Engineering*, **18**, 77-102. https://doi.org/10.1146/annurev-bioeng-092515-010849

[3] Su, T.-W., Choi, I., Feng, J., Huang, K. and Ozcan, A. (2016) High-Throughput Analysis of Horse Sperms' 3D Swimming Patterns Using Computational On-Chip Imaging. *Animal Reproduction Science*, **169**, 45-55. https://doi.org/10.1016/j.anireprosci.2015.12.012

[4] Magnes, J., Hastings, H.M., Raley-Susman, K.M., Alivisatos, C., Warner, A. and Hulsey-Vincent, M. (2017) Fourier-Based Diffraction Analysis of Live *Caenorhabditis elegans*. *Journal of Visualized Experiments*, **127**, e56154.

[5] Magnes, J., Susman, K. and Eells, R. (2012) Quantitative Locomotion Study of Freely Swimming Micro-Organisms Using Laser Diffraction. *Journal of Visualized Experiments*, **68**, e4412, https://doi.org/10.3791/4412

[6] Korta, J., Clark, D.A., Gabel, C.V., Mahadevan, L. and Samuel, A.D.T. (2007) Mechanosensation and Mechanical Load Modulate the Locomotory Gait of Swimming *C. elegans*. *Journal of Experimental Biology*, **210**, 2383-2389. https://doi.org/10.1242/jeb.004572

[7] Brigham, E.O. (1974) The Fast Fourier Transform. Prentice-Hall, Englewood Cliffs.

[8] Moore, B.T., Jordan, J.M. and Baugh, L.R. (2013) WormSizer: High-Throughput

Analysis of Nematode Size and Shape. *PLoS ONE*, **8**, e57142. https://doi.org/10.1371/journal.pone.0057142

[9] James, J. F. (1995) A Student's Guide to Fourier Transforms with Applications in Physics and Engineering. University Press, Cambridge.

[10] Edwards, S.L., Charlie, N.K., Milfort, M.C., Brown, B.S., Gravlin, C.N., Knecht, J.E. and Miller, K.G. (2008) A Novel Molecular Solution for Ultraviolet Light Detection in *Caenorhabditis elegans. PLoS Biology*, **6**, e198. https://doi.org/10.1371/journal.pbio.0060198

[11] Magnes, J., Raley-Susman, K., Melikechi, N., Sampson, A., Eells, R., Bello, A. and Lueckheide, M. (2012) Analysis of Freely Swimming *C. elegans* Using Laser Diffraction. *Open Journal of Biophysics*, **2**, 101-107.

[12] Gagnon, D.R. and Montenegro-Johnson, T.D. (2018) Thrifty Swimming with Shear-Thinning: A Note on Out-of-Plane Effects for Undulatory Locomotion through Shear-Thinning Fluids. *The ANZIAM Journal*, **59**. https://doi.org/10.1017/S1446181118000032

[13] Rahman, M., Hewitt, J.E., Van-Bussel, F., Edwards, H., Blawzdziewicz, J., Szewczyk, N.J., Driscoll, M. and Vanapalli, S.A. (2018) NemaFlex: A Microfluidics-Based Technology for Standardized Measurement of Muscular Strength of *C. elegans*. *Lab on a Chip*. https://doi.org/10.1039/C8LC00103K

Scientific Research Publishing

Open Journal of Biophysics, 2018, 8, 163-175
http://www.scirp.org/journal/ojbiphy
ISSN Online: 2164-5396
ISSN Print: 2164-5388

Specific Radius Change of Quantum Dot inside the Lipid Bilayer by Charge Effect of Lipid Head-Group

Soon Ki Sung[1,2*], Hyuk Kyu Pak[3*], Jong Hyeok Kwak[4], Sang Weon Lee[1], Young Ha Kim[1], Beong Ik Hur[5], Seong Jin Jin[6], Gyeong Rip Kim[1,2#†]

[1]Department of Neurosurgery, Pusan National University Yang-san Hospital, Yang-san, Korea
[2]Research Institute for Convergence of Biomedical Science and Technology, Yang-san, Korea
[3]Department of Physics, Ulsan National Institute of Science and Technology, Ulsan, Korea
[4]Department of Radiology, Pusan National University Yang-san Hospital, Yang-san, Korea
[5]Department of Neurosurgery, Pusan National University Hospital, Busan, Korea
[6]Haeundae Paik Hospital, Busan, Korea
Email: [†]sjkim76@pusan.ac.kr

How to cite this paper: Sung, S.K., Pak, H.K., Kwak, J.H., Lee, S.W., Kim, Y.H., Hur, B.I., Jin, S.J. and Kim, G.R. (2018) Specific Radius Change of Quantum Dot inside the Lipid Bilayer by Charge Effect of Lipid Head-Group. *Open Journal of Biophysics*, **8**, 163-175.
https://doi.org/10.4236/ojbiphy.2018.83012

Received: June 12, 2018
Accepted: July 22, 2018
Published: July 25, 2018

Abstract

We studied the quantum dot-liposome complex (QLC), which is the giant unilamellar vesicle with quantum dots (QDs) incorporated in its lipid bilayer. A spin coating method in conjunction with the electroformation technique yielded vesicles with highly homogeneous unilamellar structure. We observed QD size dependence of the QLC formation: QLCs form with blue, green and yellow-emission QD (core radius ~1.05 nm, 1.25 nm and 1.65 nm) but not with red-emission QD (core radius ~2.5 nm). In order to explain this size dependence, we made a simple model explaining the QD size effect on QLC formation in terms of the molecular packing parameter and the lipid conformational change. This model predicts that QDs below a certain critical size (radius ≈ 1.8 nm) can stably reside in a lipid bilayer of 4 - 5 nm in thickness for Egg-PC lipids. This is consistent with our previous experimental results. In the case of red-emission QD, QD-aggregations are only observed on the fluorescent microscopy instead of QLC. We expected that the reduction of packing parameter (P) would lead to the change of specific QD radius. This prediction could be verified by our experimental observation of the shift of the specific QD size by mixing DOPG.

Keywords

Quantum Dot-Liposome Complexes (QLCs), The Interface Energy at Optical Head Area, Packing Parameter, DOPC/DOPG QLC

*Contributed equally to this work.
#Corresponding author earlier know as Seong Jin Kim.

1. Introduction

Labeling biomolecules and cells with organic fluorophores are representative tools for studying the underlying complex interactions and the dynamics in metabolic processes in various time and length scales. Recently, these organic fluorophores have been gradually replaced by nano-size semiconductor nanocrystals [1] such as quantum dots (QDs).

This preference for QDs results from several remarkable optical properties of QDs. In contrast to organic fluorophores, QDs have a higher quantum yield, and a narrower and more symmetric emission spectrum which can be controlled by tuning the core size of the QDs during synthesis procedures. Furthermore, the photo-bleaching effect of QDs is much weaker compared to organic fluorophores. However, before introduction into biological environments, the surface of QDs should be transformed to hydrophilic with the help of amphiphilic molecules or other surface-capping materials due to the hydrophobic surface property of QDs. In recent years, several groups reported passivation of QDs by phospholipid, which is a building unit of the cell membrane [2]-[11]. One good example is QLC (Quantum dot-Liposome Complex) which is a giant unilamellar vesicle with QDs incorporated in the lipid bilayer [12] [13] [14] [15].

QLC is good candidate for biomedical imaging in site of specific drug delivery. For instance, biological fusion area between QLCs and biological targets can be fluorescent by conjugating with QDs and macromolecules such as cell membrane [12]. In addition, if QDs coexist with organic fluorophores in the lipid bilayer of QLCs, fluorescence resonance energy transfer (FRET) signal can be observed in a nano-scale confined system of a lipid bilayer [16].

In spite of the various potential applications of QLCs, we still lack detailed knowledge and quantitative approaches regarding the interactions and dynamics between QDs and lipids during QLC formation. And there is still no reliable experimental data regarding the exact position of QDs in the lipid bilayer. In this work, we assume that QDs are approximated as hydrophobic hard spherical particles, and there are no specific interactions other than hydrophobic interactions. Therefore, QDs are spontaneously incorporated into the lipid bilayer of lipsomes during the self-assembly process due to strong hydrophobic interactions between QDs and phospholipids in hydrophilic environment and are positional at the center of the lipid bilayer.

In our previous work, we proposed a theoretical model by interfacial energy for a quantum dot (QD)-lipid mixed system based on a simple geometrical assumption for a single-component lipid (DOPC) monolayer deformation profile [13] [14]. And we studied the stability problem of QDs inside the lipid bilayer depending on the size of QD as shown **Figure 1** and experimentally proposed QLCs, which are GUVs (Giant Unilamellar Vesicles) with QDs below critical QD size loaded into the DOPC lipid bilayer. But, in our previous study, we did not observe any QLCs for the orange-emission QDs (2 - 2.15 nm) and red-emission ones (~2.5 nm) above specific QD size [15].

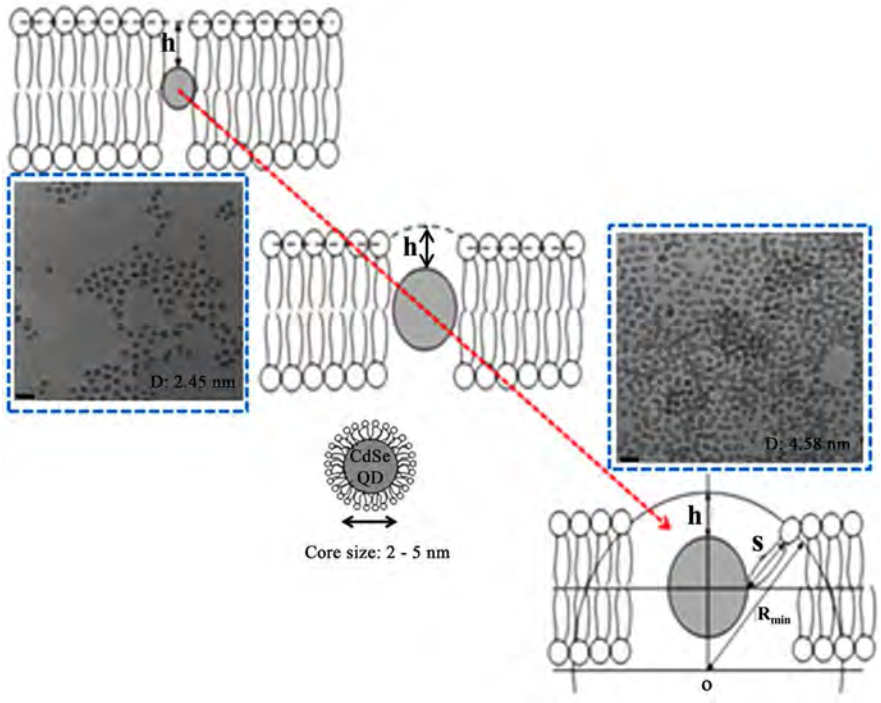

Figure 1. QD is embedded in the thin lipid bilayer depending on the size of QD. Box dotted line shows TEM image of CdSe-QD: left QD size D: 2.45 nm and right QD size D: 4.58 nm. This scale bar is about 10 (nm).

In the present work, however, we do detect a fluorescent signals from orange-emission QDs (~2 - 2.15 nm) and red-emission QDs (~2.5 nm) above critical QD size in the mixture of DOPC and DOPG. To interpret these experimental results, we propose a simple theoretical model based on geometric considerations of deformed lipid monolayer surrounding a QD in terms of the molecular packing parameter and the conformational change of the lipid chain instead of complicated elastic free energy calculations. This model explains our experimental observation of shift of the specific QD size.

2. Background and Model

According to Israelachvili's work [17], given the packing parameter P of a given lipid, the minimum radius $R_{\min}$ of the special liposome is determined as follow. **Figure 2** shows a uni-bilayer liposome with the in-outer layer (R_0) and the outer layer thickness (t_0) in a single liposome. For liposome of the outer layer volume V_0 and the outer surface area S_0 with N_0 molecules, there are following relations between them [18].

$$V_0 = N_0 v = \frac{4}{3}\pi\left[R_0^3 - \left(R_0 - t_0\right)^3\right] \tag{1}$$

$$S_0 = 4\pi R_0^2 = N_0 a\,,\quad N_0 = \frac{4}{3v}\pi\left[R_0^3 - \left(R_0 - t_0\right)^3\right] \tag{2}$$

Here, v is the volume of simple hydrocarbon molecule. The area per head group (a) is

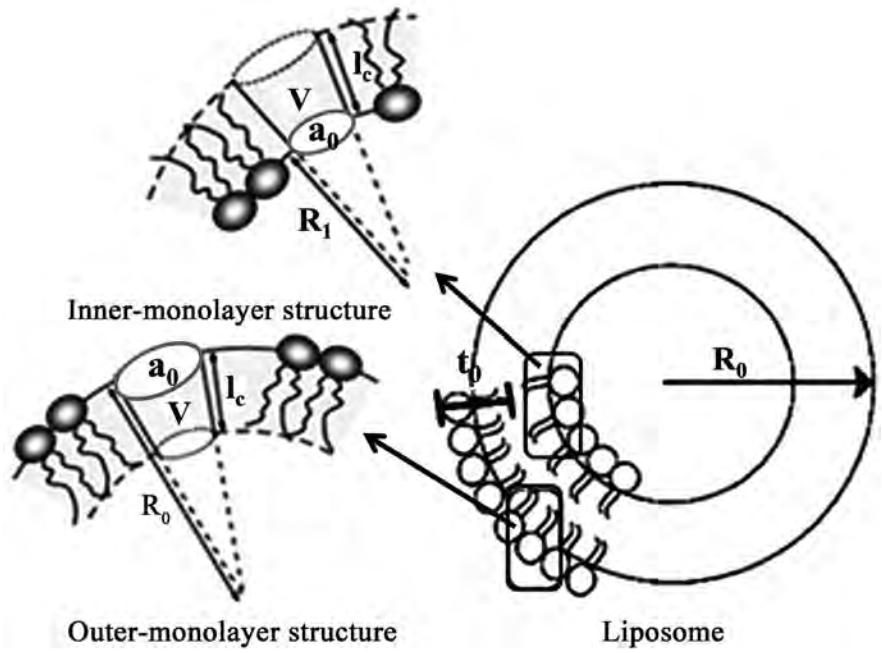

Figure 2. Uni-bilayer liposome and inner and outer monolayer structures.

$$a = 4\pi R_0^2 / N_0 = 3vR_0^2 \Big/ \left[R_0^3 - \left(R_0 - t_0 \right)^3 \right] \tag{3}$$

Here, ($a \neq a_0$) is the actual area per head group. If Equation (3) is divided by a_0, the ratio of the actual area a to the optimal area a_0 is given by

$$\frac{a}{a_0} = 3\left(\frac{v}{a_0 l_c} \right) l_c \frac{R_0^2}{\left[R_0^3 - \left(R_0 - t_0 \right)^3 \right]} \tag{4}$$

Here, a_0 is referred to as the optimal surface area per molecule, defined at the hydrocarbon-water interface.

Equation (4) gives the area ratio as a function of the packing parameter ($P = v/a_0 l_c$), the critical chain length (l_c), the out radius (R_0), and the thickness of the outer layer (t_0). If the packing parameter and critical chain length are fixed, the ratio of the area to the optima head area (a/a_0) will approaches 1 with a decrease of the out radius (R_0). This condition approaches to the lower possibility for liposome formation. When the minimum value of R_0 is reached, the smallest liposome can be formed. The out radius (R_0) replace the value of $R_{\min}$, we refers to $t_0 = l_c$. Substituting $a/a_0 = 1$, and $t_0 = l_c$, expressed as a formula according to $R_{\min}$,

$$\left(1 - \frac{v}{a_0 l_c} \right) R_{\min}^2 - l_c R_{\min} + \frac{l_c^2}{3} = 0 \tag{5}$$

From Equation (5), the minimum radius is

$$R_{\min} = \frac{3 + \sqrt{3(P-1)}}{6(1-P)/l_c} \tag{6}$$

Here, the packing parameter is $P = v/a_0 l_c$.

For truly fluid hydrocarbon chains, meanwhile, the optimal head area should not depend strongly on the chain length or on the number of chains. We can define the critical chain l_c as the maximum effective length of the hydrocarbon chain in the liquid state. The semi-empirical definition of the hydrocarbon chain length was theoretically interpreted by Israelachvili [17] Tanford [19] and Lindman [20]. l_c for the saturated hydrocarbon chains is

$$l_c \le l_{\max} = (0.154 + 0.1265n)\ \text{nm} \tag{7}$$

Here, $l_{\max}$ stands for the length of the fully extended hydrocarbon chain, and n is number of carbon atom for each hydrocarbon tail. However, as may be expected, l_c is of the same order as, though somewhat less than, the fully extended molecular length of the chain $l_{\max}$. It can be seen that the minimum size of a liposome ($R_{\min}$) depends on the packing parameter ($P = v/a_0 l_c$) and on the critical chain length (l_c). Since v and l_c are fixed, the only way to reduce the packing parameter ($v/a_o l_c$) is increasing the optimal head area (a_0).

Modeling

The key point of this model would define the critical QD radius by limiting the $l_{\max}$ to cover part of the void around the QD $S_{\max}$ at graph. For the definition of $S_{\max}$ in this model, we considered only the size of QD core excluding ligand (hexadecylamine).

Equation (6) shows the minimum possible radius $R_{\min}$ of the spherical liposome, which is composed of the lipids with the packing parameter *P*. We first assumed that the maximum possible curvature of the lipid monolayer with thickness *d* around the QD of radius *r* has its limit at the value $1/R_{\min}$ to evade any unfavorable surface energy penalties. In other words, $R_{\min}$ is the critical radius below which a bilayer cannot curve without introducing unfavourable packing strains such as QD inside the lipids. Therefore, when the size of each QD is smaller than $R_{\min}$, as in our experiment, the curvature of the monolayer around the QD is approximated as $1/R_{\min}$, and the deformed monolayer profile is a circular arc of radius as $R_{\min}$ shown in **Figure 4**. In the case of Egg-PC lipid liposome, the packing parameter value is known to be 0.85 ($v/a_0 l_c$; $a_0 \approx 0.717\ \text{nm}^2$, $v \approx 1.063\ \text{nm}^3$ and $l_c \approx 1.75\ \text{nm}$) [17]. Therefore, we know that $R_{\min}$ of Egg-PC liposome can get the value of 10.8 nm from Equation (6).

We can also introduce two parameters related to the conformational variation of the hydrocarbon chain around the QD: the compressing extent *h* of the hydrocarbon chain and the maximum stretching extent *S* of the hydrocarbon chain in order to remove void formation around the QD. In the case of Egg-PC lipid, a saturated hydrocarbon chain is approximately composed of n = 18 of carbon number about 70%. When the number of carbon is n = 18, we defined $l_{\max} = 2.43\ \text{nm}$ form Equation (7). If S has only to contact with ligand, as shown in **Figure 3(a)**, we can also assume that the most stretched (longest) chain is

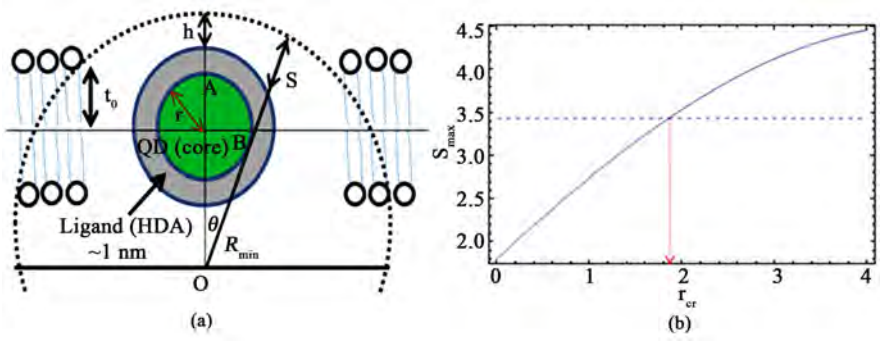

Figure 3. (a) A model representing the deformed monolayer due to the incorporation of a QD inside the lipid bilayer (b) A plot of chain length of the most stretched lipid, S_{max} as a function of the QD radius, r; The dotted line corresponds to the minimum radius R_{min} of deformed lipid monolayer around QD.

located in a corner of the QD direction (point B in **Figure 3(a)**) to remove the void formation between lipid and QD. Here, we approximately considered the distance between point B and C as ligand length (~1 nm). For the maximum extent, we can define S_{max} as 3.43 nm (the ligand length plus l_{max}). And we assumed that the compression of the chain occurs at the top of the QD, as shown in **Figure 3(a)**. In the case of maximum compression, the lipid monolayer thickness at point A is represented by $h_{min} = 1.22$ nm from the Egg-liposome thickness due to $l_{max} = 2.43$ nm [21].

The distance S from the corner of the QD to the point on the circular arc of radius R_{min} for a given θ can be expressed as

$$S = \sqrt{\left(R_{min}\sin\theta - r\right)^2 + \left(R_{min}\cos\theta - R_{min} + h_{min} + r + 1\right)^2} \quad (8)$$

Equation (8) is differentiated with respect to θ to obtain the minimum S_{max} that is required to be equal to the chain length of the most stretched lipid among the lipids around the QD of radius r. **Figure 3(b)** shows a plot of S_{max} as a function of the QD radius r. S_{max} can't exceed the maximally stretched chain length, ligand length (~1 nm) plus l_{max}, which is 3.43 nm in this case [17]. Otherwise, there would be a void formation at the ligand portion that is connected with corner of the QD. Therefore, the critical QD size is $r_{cr} \approx 1.8$ nm, where the chain is maximally stretched to S_{max} (corresponding to the horizontal dashed line in **Figure 3(b)**).

In **Figure 3(a)**, at point S, the curvature is divided by positive and negative. In the case of this model, we took only positive curvature into account. The part of negative curvature does not fully need to stretch because one of the principal curvatures is close to the monolayer spontaneous curvature of the DOPC. In other words, the regions of positive curvature require the highly curved lipids to cover the rapid increase of the area above critical, while the parts of negative curvature which have non-charged head-group can be decreasing the mechanical stress generated by a packing constraint between ligands and the head-group above critical size.

3. Experimental Methods and Materials

3.1. Materials

In this experiment, we used four different kinds of lipid molecules: L-α-phosphatidylcholine (Egg-Pc), 1,2-dioleoyl-sn-glycero-3-phosphocholine (DOPC), 1,2-dioleoyl-sn-glycero-3-[phospho-rac-(1-glycerol)] (DOPG), and 1,2-dipalmitoyl-sn-glycero-3-phosphocholine (DPPC), which were purchased from Avanti Polar Lipids. In the case of DOPC and DOPG, number of carbon atom for each hydrocarbon tail is $n = 18$ and DPPC is $n = 16$.

Before sample preparation, they were dissolved into chloroform at a determined concentration. Deionized water was obtained from a Milli-Q plus 185 (Millipore, Molsheim, France) ultra-pure water system with a resistivity of ≥18 MΩ/cm. Five different sizes of hexadecylamine (~1 nm)-coated CdSe QDs dispersed in toluene were purchased from Sigma-Aldrich. Each of them has a different core radius; blue (~1.05 nm), green (~1.25 nm), yellow (~1.65 nm), orange (2.0 - 2.15 nm) and red-emission (~2.5 nm).

3.2. Preparation of QLC

QLCs were synthesized by using the mixed solutions of QDs and phospholipids via the electroformation method [22] in conjunction with spin-coating technique [23], as shown in **Figure 4**. Egg-PC (10 mg/1ml) and a mixture of DOPC lipid: DOPG lipid = 1: 1 (5 mg/1ml, molecular weight) and QD (5 mg/1ml) was prepared with the volume ratio of mixed DOPC and DOPG lipid solution:QD solution = 700 μl:25 μl. This well-mixed solution was deposited onto the ITO substrate, then spin-coated at 600 rpm for 100 s under a stream of nitrogen gas. This QD/lipid thin film was immediately dried out in a vacuum oven for 2 h to remove excess organic solvents. A home-made chamber for electroformation was built by combining two transparent conducting indium tin oxide (ITO) substrates (4 × 4 cm^2, <50 Ω); one is clean and the other has a dried thin film

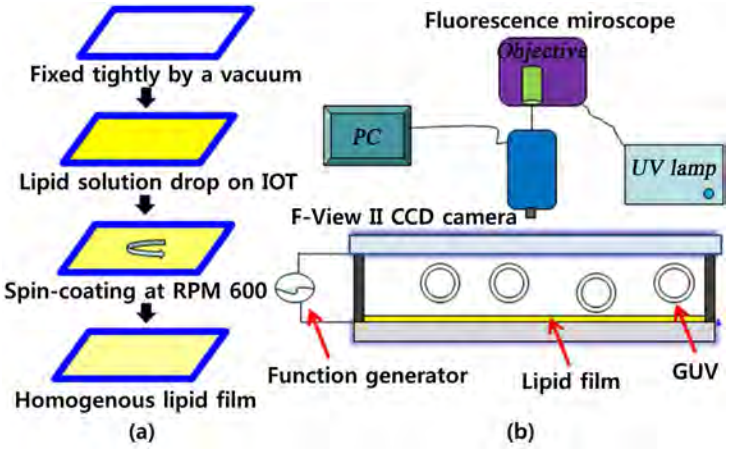

Figure 4. Preparation of QLCs in the order of spin-coating, drying-out QD/lipid thin film, and electro-swelling under an AC field. (a) Spin coating procedure (b) Schematic diagram of the electroformation setup.

with a spacer (~1 mm), then sealed with a vacuum grease (Dow Corning, High vacuum Grease). The chamber for was then filled with 2 ml of room-temperature deionized water. An AC signal of 10 Hz and 1.2 V (peak-to-peak) using a function generator (model 33250 A, Agilent, USA) was applied to the chamber for 2 h. During this process, lipiosomes grew on the substrate. Then, the AC signal was set to 4 Hz and 2.0 V (peak-to-peak) for 10min to detach the liposomes from the substrate in order to make an easy observation on a confocal microscope (Axiovert 100 M, Zeiss, German).

4. Experimental Results and Discussions

4.1. Egg-PC QLC

In order to checking this model, we checked over the QD size dependence for QD stabilization inside the lipid bilayer of liposome. The QLC is expected to be observed only for the QD size smaller than a certain specific size. We successfully obtained the blue-, green-and yellow-emission Egg-PC QLCs with clear and sharp fluorescent signals, as shown in **Figure 5(a)**. However, when red-emission QDs were used with the same concentration as the blue-, green- and yellow-emission QDs during the QLC preparation, we did not obtain the red-emission DOPC QLCs. Instead, we observed some aggregation kind of image, as shown in **Figure 5(b)**. The results are similar to those of previous DOPC experiments [15].

It means that the aggregated several QDs prefer to be surrounded by lipid instead of QLC. In other words, red-emission QDs were not incorporated into the bilayer of liposome. The experimental results are supporting the predictions of our theoretical model.

We believe that, if the QD radius is larger than r_{cr}, the QLC structure is no longer stable due to the high energy cost in the formation of either the lipid voids or increase of hydrophobic interface contacting with water, as shown in **Figure 6**. It means that the mono-layer curvature of surrounding the QD is highly required to form the QLC. In other words, we consider that hydrocarbon chain $l_{\max}$ of Egg-PC lipids is not long enough, wetting a void formation at the ligand

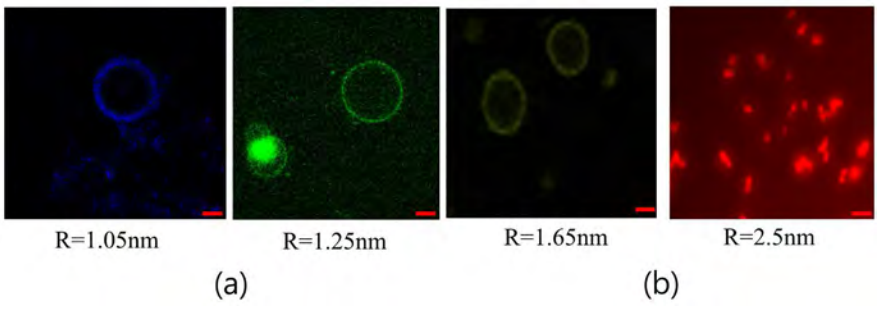

Figure 5. (a) Confocal microscope image of the blue-, green-and yellow-emission QLC with core radius ~1.05 (nm), 1.25, 1.65 (nm) (b) Aggregated QD with core radius ~2.5 (nm) surrounding lipids is observed on the fluorescent microscopy. This scale bar is about 20 (μm).

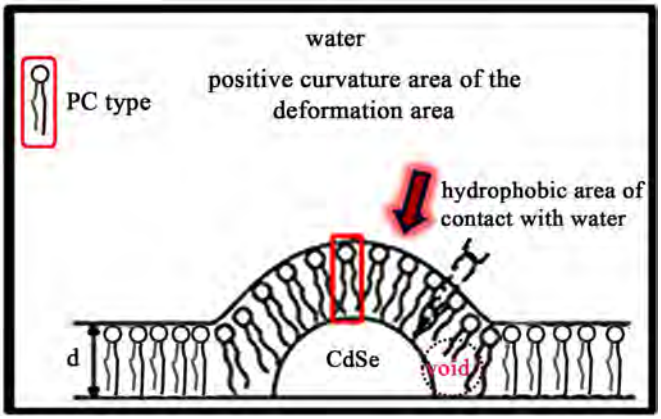

Figure 6. The mono-layer deformation of positive curvature area induced CdSe surrounding by PC-type lipid.

portion that is connected with corner of the QD and the geometric shape of them don't pack fully hydrophobic area deformed above r_{cr}. As a result, the QDs only below a certain specific size (core radius ≈ 1.8 nm) can stably reside in the lipid bilayer.

If lipids of large mono-layer curvature surrounding QD exist, they will reduce the deformation area and cover the void by highly curvature lipid. According to this model, r_{cr}, the specific radius of QD, is affected by a change in the minimum radius $R_{\min}$. In the case of Egg-PC lipid, the minimum of radius ($R_{\min}$:10.8 nm) is given by Equation (6) and thus the maximum of radius curvature is $1/R_{\min}$. For forming the QLC above r_{cr}, it is necessary to use lipid having large monolayer curvature more than $1/R_{\min}$. It is theoretically difficult to reduce the curvature value of $1/R_{\min}$ more than 1/10.8 nm^{-1} for a single lipid molecule of the PC type.

According to the experimental result by Israelachvili [17], they have experimentally seen that it reduced the $P \approx 0.37$ (non-spherical micelle) to the $P \approx 0.33$ (spherical micelle) for sodium dodecyl sulphate surfactant (SDS) in water. Since v and l_c are fixed, the only way to reduce is to raise a_0 by raising the pH of the solution. In practice, this could be achieved by increasing the pH of the solution. This would increase the degree of ionization of the negatively charged head-groups which increases the repulsion between them, resulting in an increase in a_0. It means that the spherical micelle is more high curvature than non-spherical micelle. By Israelachvili's experiment, in this study, we think that charged lipids (DOPG) with large optimal head area (a_0) is able to from a highly mono-layer curvature more than $1/R_{\min}$ by mixing the DOPC and DOPG.

4.2. DOPC/DOPG QLC

Figure 7 shows that r_{cr} is changed by the reduction of P value. **Figure 7** is not a measured value but a calculated value by **Figure 3(b)**, which the decrease of P resulted in the decrease of $R_{\min}$ from Equation (6). The graph of **Figure 3(b)** shifted to the right due to the decrease of $R_{\min}$. This caused r_{cr} to shift to the

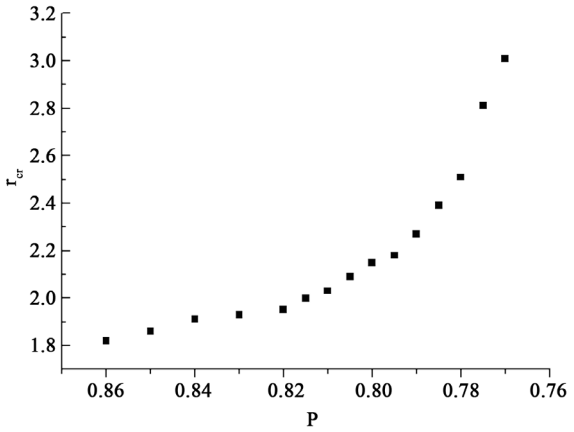

Figure 7. The change of critical point r_{cr} according to changing P.

right. In other words, the reduction of $R_{\min}$ can cause high curvature. It means that an increase in optimal head area (a_0) results in highly curvature.

We seek to increase the large optimal head area (a_0) to form a highly mono-layer curvature for checking the change of r_{cr}. In this study, if v and l_c are fixed, the only way to reduce $P = v/a_0 l_c$ is to raise optimal head area (a_0) by using the DOPG. We have the following experiment to confirm the increase of r_{cr} such as **Figure 7**.

As we mentioned earlier, QLC above r_{cr} will be formed by mixing DOPG with a charged heap-group and DOPC a neutral head-group for charge effect [17] [24].

We expected that this mixing would will be larger curvature than $1/R_{\min}$ because of the increase of effective head-group area (a_{e0}), which arises from the repulsive interaction between the like-charged head-groups. It causes the geometry shape such as **Figure 8(a)**. The phenomenon of effect head-group area explains as follows. For example, the micelle-forming lysolecithin ($v/a_0 l_c < 0.5$) and non-aggregate forming cholesterol ($v/a_0 l_c > 1.0$) will mix in certain proportions to form liposome ($0.5 < v/a_0 l_c < 1$). If we mix DOPC and DOPG, we will expect that the mono-layer of the mixture of DOPC/DOPG lipids can form more a highly curvature mono-layer than Egg-PC mono-layer.

In this experiment, we observed the orange (radius; 2.0 - 2.15 nm) and red-emission QDs (radius ~2.5 nm) were successfully incorporated in the bilayer of the mixture of DOPC/DOPG lipids, as shown in **Figure 8(b)**. This experiment result shows that the radius of curvature is increased by DOPG.

As we have anticipated the change of a specific point r_{cr}, this experimental result explains the increase in r_{cr} by the increase of a_{e0} by charge effect.

4.3. DOPC/DPPC QLC

In order to confirm charge effect of lipid head-group, experiments were conducted by mixing DPPC, a neutral lipid molecule, as a control experiment in the same manner as the above experiment. **Figure 9** shows only the QLC below a specific QD size similar to the DOPC QLC experiment results.

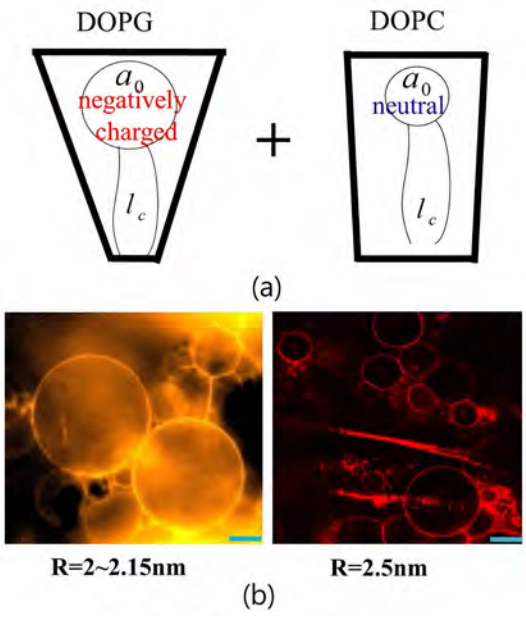

Figure 8. (a) Geometric shapes of DOPG (truncated shape) and DOPC (truncated shape close to cylindrical shape) at a_0; (b) Confocal microscopy image of the QLCs prepared with the same ratio of two lipids DOPC/DOPG (1:1) by using the orange and red-emission QDs (2 - 2.15 (nm) and ~2.5 (nm)). This scale bar is about 10 (μm).

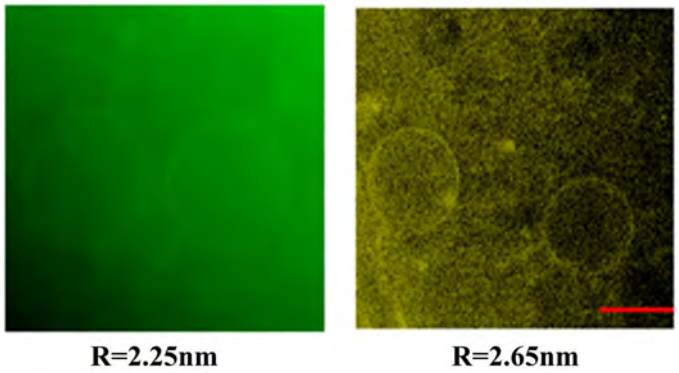

Figure 9. QLC structure using DOPC/DPPC mixed lipid molecules in fluorescence microscopy. This scale bar is about 50 (μm).

In conclusion, it can be expected that the role of charge effect at the head-group is an important factor to form QLC structure above the specific QD size. In this study, unlike previous experimental results, we can observe the orange and red-emission QLC due to highly curvature mono-layer.

5. Conclusion

We proposed a simple model to describe the stability of QDs embedded in lipid bilayer in terms of molecular packing parameter and the conformational change of the lipid chain. The existence of QDs in the lipid bilayer was confirmed using confocal microscopy. QLC formation was found to be dependent on the size of QDs: Egg-QLCs formed with blue, green and yellow-emission QDs (core radius

~1.05 nm, 1.25 nm and 1.65 nm) but not with red-emission QDs (core radius ~2.5 nm). When DOPG lipids, which have a larger head group area, were mixed with DOPC lipids, QLCs were formed with orange-emission QDs as well as with red-emission QDs. The model predicts that 1) QDs below a certain critical size can stably reside in the lipid bilayer, and 2) the specific QD size increases as the head group area of the lipids increases. These predictions agree well with our experimental results in spite of a lack of exact information about the change of effect optimal head area and the conformational changes of the hydrocarbon chain around the QD.

Acknowledgements

This work was supported by a Research Institute for Convergence of Biomedical Science and Technology (30-2018-007), Pusan National University Yang-san Hospital.

References

[1] Park, J., Joo, J., Kwon, S.G., Jang, Y. and Hyeon, T. (2007) Synthesis of Monodisperse Spherical Nanocrystals. *Angewandte Chemie International Edition*, **46**, 4630-4660. https://doi.org/10.1002/anie.200603148

[2] Dubertret, B., Skourides, P., Norris, D.J., Noireaux, V., Brivanlou, A.H. and Libchaber, A. (2002) *In Vivo* Image of Quantum Dots Encapsulation in Phospholipid Micelles. *Science*, **298** 1759-1762. https://doi.org/10.1126/science.1077194

[3] Fan, H., Leve, E.W., Scullin, C., Gabaldon, J., Tallant, D., Bunge, S., Boyle, T., Wilson, M.C. and Brinker, C.J. (2005) Surfactant-Assisted Synthesis of Water-Soluble and Biocompatible Quantum Dot Micelles. *Nano Letters*, **5**, 645-648. https://doi.org/10.1021/nl050017l

[4] Park, S.H., Oh, S.G., Mun, J.Y. and Han, S.S. (2006) Loading of Gold Nanoparticles inside the DPPC Bilayers of Liposome and Their Effects on Membrane Fluidities. *Colloids and Surfaces B*: *Biointerfaces*, **48**, 112-118. https://doi.org/10.1016/j.colsurfb.2006.01.006

[5] Bothun, G.D., Rabideau, A.E. and Stoner, M.A. (2009) Hepatoma Cell Uptake of Cationic Multifluorescent Quantum Dot Liposome*s. Journal of Physical Chemistry Letters B*, **113**, 7725-7728. https://doi.org/10.1021/jp9017458

[6] Chen, Y., Bose, A. and Bothun, G.D. (2010) Controlled Release from Bilayer-Decorated Magnetoloposomes via Electromagnetic Heating. *ACS Nano*, **4**, 3215-3221. https://doi.org/10.1021/nn100274v

[7] Al-Jamal, W.T., Al-Jamal, K.T., Tian, B., Lacerda, L., Bomans, P.H., Frederik. P.M. and Kostarelos, K. (2008) Lipid-Quantum Dot bilayer Vesicles Enhance Tumor Cell Uptake and Retention *in Vitro* and *in Vivo*. *ACS Nano*, **2**, 408-418. https://doi.org/10.1021/nn700176a

[8] Binder, W.H., Sachsenhofer, R., Farnik, D. and Blaas, D. (2007) Guiding the Location of Nanoparticles into Vesicular Structures: A Morphological Study. *Physical Chemistry Chemical Physics*, **9**, 6435-6441. https://doi.org/10.1039/b711470m

[9] Kim, S.J., Wi, H.S., Km, K., Lee, K., Kim, S.M., Yang, H.S. and Pak, H.K. (2006) Encapsulation of CdSe Nanoparticles inside Liposome Suspended in Aqueous Solution. *Journal of Korean Physical Society*, **49**, S684-S687.

[10] Zheng, W.W., Liu, Y., West, A., Schuler, E.E., Yehl, K., Dyer, R.B., Kindt, J.T. and Salaita, K. (2014) Quantum Dots Encapsulated within Phospholipid Membrane: Phase-Dependent Structure, Photostability, and Site-Selective Functionalization. *Journal of the American Chemical Society*, **136**, 1992-1999. https://doi.org/10.1021/ja411339f

[11] Nandi, S., Malishev, R., Bhunia, S.K., Kolusheva, S., Jopp, J. and Jelinek, R. (2016) Lipid-Bilayer Dynamics Probed by a Carbon Dot-Phospholipid Conjugate. *Biophysical Journal*, **110**, 2016-2025. https://doi.org/10.1016/j.bpj.2016.04.005

[12] Gopalakrishnan, G., Danelon, C., Izewska, P., Prummer, M., Bolinger, P.Y., Geissbuhler, I., Demurtas, D., Dubochet, J. and Vogel, H. (2006) Multifunctional Lipid/Quantum Dot Hybrid Nanocontainers for Controlled Targeting of Live Cells. *Angewandte Chemie International Edition*, **45**, 5478-5483.

[13] Wi, H.S., Lee, K. and Pak, H.K. (2008) Interfacial Energy Consideration in the Organization of a Quantum Dot-Lipid Mixed System. *Journal of Physics*: *Condensed Matter*, **20**, Article ID: 494211. https://doi.org/10.1088/0953-8984/20/49/494211

[14] Daniel, M. and Reznickova, J. (2014) Energy of Quantum Dots Encapsulated in Biological Membrane. *Procedia Engineering*, **79**, 137-142. https://doi.org/10.1016/j.proeng.2014.06.322

[15] Wi, H.S., Kim, S.J., Lee, K., Kim, S.M., Yang, H.S. and Pak, H.K. (2012) Incorporation of Quantum Dots into the Lipid Bilayer of Giant Unilamellar Vesicles and Its Stability. *Colloids and Surfaces B*: *Biointerfaces*, **97**, 37-42. https://doi.org/10.1016/j.colsurfb.2012.04.025

[16] Kloepfer, J.A., Cohen, N. and Nadeau, J.L. (2004) FRET between CdSe Quantum Dots in Lipid Vesicle and Water- and Lipid-Soluble Dyes. *The Journal of Physical Chemistry B*, **108**, 17042-17049. https://doi.org/10.1021/jp048094c

[17] Israelachvili, J. (1998) Intermolecular and Surface Forces. Harcourt Brace & Company, New York.

[18] Segota, S. and Tezak, D. (2006) Spontaneous Formation of Vesicles. *Advances in Colloid and Interface Science*, **121**, 51-75. https://doi.org/10.1016/j.cis.2006.01.002

[19] Tanford, C. (1972) Micelle Shape and Size. *The Journal of Physical Chemistry*, **76**, 3020-3024. https://doi.org/10.1021/j100665a018

[20] Holmberg, K., Joensson, B., Kronberg, B. and Lindman, B. (2002) Surfactants and Polymers in Aqueous Solution. John Wiley & Sons, New York.

[21] Li, X.-J. and Schick, M. (2008) Theory of Lipid Polymorphism: Application to Phosphatidylethanolamine and Phosphatidylserine. *Biophysical Journal*, **78**, 34-46. https://doi.org/10.1016/S0006-3495(00)76570-2

[22] Angelova, M.I. and Dimitrov, D.S. (1986) Liposome Electroformation. *Faraday Discussions of the Chemical Society*, **81**, 303-311. https://doi.org/10.1039/dc9868100303

[23] Estes, D.J. and Mayer, M. (2005) Electroformation of Giant Liposomes from Spin-Coated Films of Lipids. *Colloids and Surfaces B*: *Biointerfaces*, **42**, 115-123. https://doi.org/10.1016/j.colsurfb.2005.01.016

[24] Ninham, B.W. and Evans, D.F. (1986) The Rideal Lecture. Vesicles and Molecular Forces. *Faraday Discussions of the Chemical Society*, **81**, 1-17. https://doi.org/10.1039/dc9868100001

Scientific Research Publishing

Open Journal of Biophysics, 2018, 8, 176-183
http://www.scirp.org/journal/ojbiphy
ISSN Online: 2164-5396
ISSN Print: 2164-5388

A Comparison of Gamma Irradiation Response Models of Bovine Blood, Liver and Kidney Tissues at Radiofrequency

T. Sombo[1*], E. H. Agba[2], T. A. Ige[3], T. Igbawua[1], T. S. Azande[1], E. R. Nyatso[1], I. S. Aondoakaa[1], T. J. Shivil[1]

[1]Department of Physics, Federal University of Agriculture, Makurdi, Nigeria
[2]Department of Physics, Benue State University, Makurdi, Nigeria
[3]Department of Physics, National Hospital, Abuja, Nigeria
Email: *jtsombo@gmail.com

How to cite this paper: Sombo, T., Agba, E.H., Ige, T.A., Igbawua, T., Azande, T.S., Nyatso, E.R., Aondoakaa, I.S. and Shivil, T.J. (2018) A Comparison of Gamma Irradiation Response Models of Bovine Blood, Liver and Kidney Tissues at Radiofrequency. *Open Journal of Biophysics*, **8**, 176-183.
https://doi.org/10.4236/ojbiphy.2018.83013

Received: December 26, 2017
Accepted: July 22, 2018
Published: July 25, 2018

Abstract

This study is aimed at identifying gamma irradiated response of bovine blood, liver and kidney tissues at radiofrequency. For this purpose, impedence meter (Booton 7200) working in conjunction with signal generators (Loadster, SG416013 and Harris G857993) and improvised parallel plate dielectric cells constructed in line with the method of Laogun *et al.*, (2005) were used to obtain the dielectric spread parameter gamma radiation α, of blood, liver and kidney tissues exposed to gamma irradiation dose range of 1.0 - 85.0 Gy. The dielectric spread parameter α gives the extent of damage induced in an irradiated tissue. Results of this work revealed that at 0 - 50 MHz frequency range, Kidney tissues displayed higher sensitive, followed Liver tissues and lasted the bovine blood between 0 - 60 Gy but reversed for blood and liver at 85 Gy. At 0 - 100 kHz frequency range liver tissue is more venerable to radiation injuries between gamma irradiation dose range of 0 - 20 Gy while between 43 - 85 Gy the Kidney's sensitivity is the highest followed by blood and liver tissues. This implies that the liver tissues are less liable to radiation injuries at radiofrequency. A comparison of the linear, exponential and polynomial models using Akaike Information Criteria (AIC) revealed that linear models were the most suitable models for describing the effect of gamma radiation on the dielectric dispersion properties of bovine tissues at low and high radiofrequencies. This implies that the response of the investigated tissues increases linearly with gamma irradiation dose.

Keywords

Gamma Irradiation, Dielectric Spread Parameter, Mathematical Models, AIC, Bovine Tissues

1. Introduction

The effect of gamma radiation on human tissues has been extensively studied and findings revealed that its beneficial effects are employed in the diagnosis and treatment of various ailments like cancers. Its non-beneficial effects include the induction of cancers, genetic disorder (mutation), and other numerous stochastic and non-stochastic effects [1]. These effects arise from the excitation, ionization and breakage of some chemical bonds in the molecules of the exposed tissue [2]. This leads to the production of complex ions (radicals) which reacts to produce toxins. These toxins are circulated throughout the body via lymphatic circulation and bloodstream causing radiation sicknesses [3].

The level of damage induced in an organ (tissue) depends on the quantity of radiation absorbed by the tissues, its composition and morphology. This implies that some tissues are more prone to radiation than others. The interaction of complex ions produced as a result of ionization event in the molecules of the irradiated tissues leads to the generation of toxins. These toxins are circulated throughout the body via lymphatic circulation and bloodstream [3]. Syndromes of Acute Radiation Sickness (ARS) are expressed depending on the type of induced toxin.

Previous studies [4] [5] [6] [7] [8] have focused attention on the dielectric characterization of tissues whereas virtually little or no information exists on development of models that explains the difference in radio sensitivity between non-lymphoid tissues (liver and kidney) and moving mammalian lymphoid tissues (blood) based on dielectric relaxation spread [9]. Hence, the need to direct efforts towards development of and comparison of response models of lymphoid and non-lymphoid tissues via mathematical models.

2. Materials and Methods

The liver and kidney tissue samples were excise from an adult white Fulani cow which was duly certified healthy by veterinary doctor attached to Gwagwalada Central Abattoir in Gwagwalada Area Council, Abuja, Nigeria. The excised tissue samples were thoroughly washed with double distilled water and preserved in laboratory oven maintained at a temperature of 37.0˚C ± 0.5˚C for six hours to remove water from their surfaces. The blood samples were collected from the certified cow by vein puncture using a 10 ml hypodermic needle attached to a disposable plastic syringe. The blood samples were immediately introduced into heparinized tubes to prevent coagulation. Percentage water content of blood, kidney and liver samples were 86.0%, 72.2% and 71.6% respectively.

Eight portions of each of the three tissue samples were irradiated at the following irradiation doses; 1.0 Gy, 4.0 Gy, 11.0 Gy, 20.0 Gy, 43.0 Gy, 60.0 Gy and 85.0 Gy respectively using the Gamma Irradiator (GS 1000) located at the Gamma Irradiation Facility (GIF) Unit of the National Nuclear Technology Centre, Abuja at a dose rate of 0.36 kGy/hr after which the various sample were introduced into their respective dielectric cells. The dielectric sample cells used in this

research were constructed and calibrated in line with the method of Laogun [6] and Agba *et al.* [7]. The dielectric constant, k and residual capacitance of the dielectric cells constructed for blood dielectric measurements was 0.0021 nF and 0.00118 nF while the dielectric cell for kidney and liver tissue measurements was 0.016 nF and 0.00912 nF respectively. Booton 7200 impedance meter in conjunction with signal generators (Loadstar, SG416013 and Harris G857993) were used to measure capacitance and dissipation factor of the samples. The dielectric spread parameters (α) of each sample were evaluated from the cole-cole plots.

3. Results and Analysis

3.1. Analysis and Results for Dielectric Spread Parameter α, at Low and High Radiofrequency Ranges for Bovine Kidney

For low Radiofrequency

1) Linear model:

$$D = 527.0\alpha - 122.0 \tag{1}$$

2) Exponential model:

$$D = 0.0016\mathrm{e}^{\frac{\alpha_1}{0.034}} + 0.0016\mathrm{e}^{\frac{\alpha_2}{0.034}} + 1.6 \tag{2}$$

3) Polynomial model:

$$D = 11226.0\alpha^2 + 5683.0\alpha + 712.0 \tag{3}$$

For high Radiofrequency

1) Linear model:

$$D = 264.0\alpha - 25.0 \tag{4}$$

2) Exponential model:

$$D = 14.0\mathrm{e}^{\frac{-\alpha}{0.184}} + 20.1 \tag{5}$$

3) Polynomial model:

$$D = 665.0\alpha^2 + 31.0\alpha - 0.2 \tag{6}$$

where D and α represents γ-irradiation dose and spread parameter α, respectively. The Akaike Information Criterion (AIC) which is a tool for comparing the performance of two or more model is found to be 56.46, 131.93 and 56.40 for the linear, exponential and polynomial model respectively at low radiofrequency while that of the high radiofrequency was 47.73, 56.93 and 56.03 for linear, exponential and polynomial models respectively. This suggest that Equations 1 and 3 (linear model and polynomial model respectively) are best for low frequency range while and Equation 4 (linear model) is the most appropriate for high radiofrequency response modeling of kidney tissues.

3.2. Analysis of Bovine Liver Tissue

For low Radiofrequency

1) Linear model:

$$D = 363.2\alpha - 42.1 \tag{7}$$

2) Exponential model:

$$D = -190.4e^{\frac{\alpha_1}{0.170}} + 92.8 \tag{8}$$

3) Polynomial model:

$$D = -1474.8\alpha^2 + 941.8\alpha - 93.8 \tag{9}$$

For high Radiofrequency

1) Linear model:

$$D = 554.5\alpha - 121.3 \tag{10}$$

2) Exponential model:

$$D = 0.202e^{\frac{-\alpha}{0.055}} + 7.0 \tag{11}$$

3) Polynomial model:

$$D = 6597.7\alpha^2 + 2964.26\alpha - 338.7 \tag{12}$$

where the D and α represent the γ-irradiation dose and dielectric spread parameter respectively. The AIC for low radiofrequency models was found to be 60.33, 69.44 and 69.37 for linear, exponential and polynomial models respectively while that of the high radiofrequency models was 60.71, 69.15 and 68.95 for linear, exponential and polynomial models respectively. Equations (7) and (8) (linear models); and Equation (10) (linear model) are preferred to other models for low and high frequency ranges.

3.3. Analysis for Bovine Blood Samples

For low Radiofrequency

1) Linear model:

$$D = 531.6\alpha - 50.3 \tag{13}$$

2) Exponential model:

$$D = -269.8e^{\frac{\alpha}{0.264}} + 126.0 \tag{14}$$

3) Polynomial model:

$$D = -1060.3\alpha^2 + 905.4\alpha - 79.3 \tag{15}$$

For high Radiofrequency

1) Linear model:

$$D = 565.0\alpha - 54.6 \tag{16}$$

2) Exponential model:

$$D = -267.9e^{\frac{-\alpha}{0.507}} + 284.9 \tag{17}$$

3) Polynomial model:

$$D = -1314.0\alpha^2 + 997.0\alpha - 86.4 \tag{18}$$

where D and α represents the γ-irradiation dose and dielectric spread parameter

respectively. The AIC was found to be 40.82, 48.15 and 48.00 respectively for the linear, exponential and polynomial models at low radiofrequency, while the AIC for linear, exponential and polynomial models was 40.80, 48.15 and 48.00 respectively for higher radiofrequency. The AIC of Equation (3) (linear model) and Equation (16) (linear model) suggest that linear model is the preferred model to exponential and polynomial models for bovine blood.

The plot of dielectric spread parameter against gamma (γ) irradiation dose shown in Figure 1 revealed that Bovine kidney was more prone to damage (sensitive) at low radiofrequencies followed by the liver tissues and lastly the blood tissue at 0 - 60 Gy; at 85 Gy, the kidney's sensitivity is higher and closely followed by that of blood (see Table 1) while at higher frequency (Figure 2), the sensitivity of liver tissues is higher than that of blood and the kidney tissues

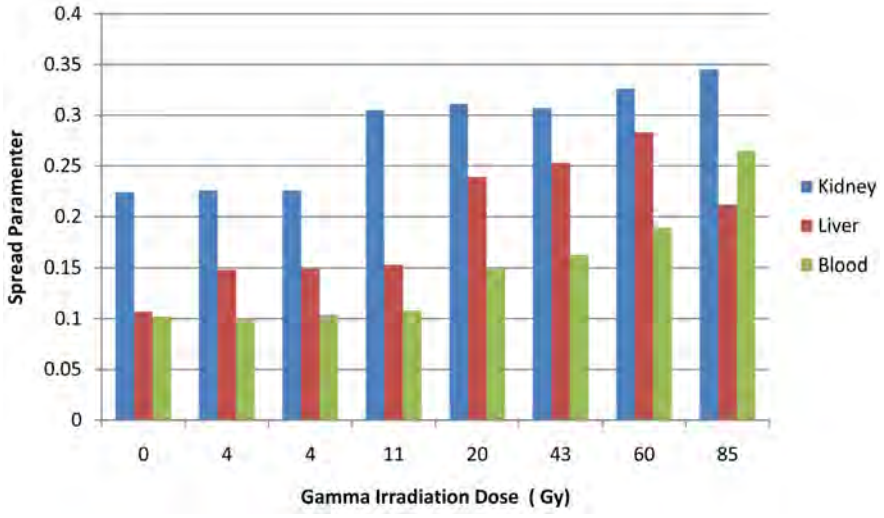

Figure 1. Variation of dielectric spread parameter with Gamma irradiation dose at 0.5 - 100.0 kHz.

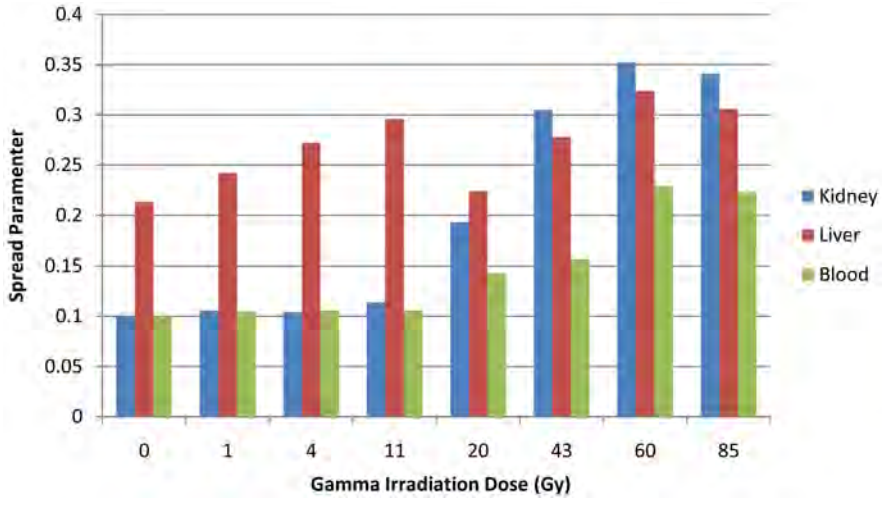

Figure 2. Variation of dielectric spread parameter with Gamma irradiation dose at 0.5 - 50.0 MHz.

Table 1. Dielectric spread parameters α, of gamma irradiation and non-irradiated bovine kidney, liver and blood at 0.5 kHz - 100.0 kHz.

Dose (Gy)	Kidney	Liver	Blood
	α	α	α
0	0.224	0.107	0.102
4	0.226	0.148	0.100
4	0.226	0.149	0.104
11	0.305	0.153	0.108
20	0.311	0.239	0.149
43	0.307	0.253	0.162
60	0.326	0.283	0.189
85	0.345	0.212	0.265

especially between the gamma irradiation dose of 0 - 20 Gy (see **Table 2**). The dose range between 45 - 85 Gy the sensitivity of kidney was observed to be more than that of the liver tissue and lastly the blood. This result at low frequencies is in good agreement to some extent with the findings of [8] which showed sequential order of the response of gamma irradiated chick embryo as follows; Heart, Kidney, Brain, Lungs, Blood and Liver tissues. The difference in the dielectric response of the bovine kidney, blood and liver tissues at the different frequency ranges may be attributed to the differences in their cellular and tissue morphology resulting in different characteristic polarization of the cell membrane and the relaxation of tissue protein [7] [10] [11]. The difference in water content and ionic conductivity of the three tissues may also account for the difference in dielectric response [12] [13].

The interchange in sensitivity of liver samples and kidney tissue at higher frequencies (**Figure 2**) may be due to changes in polarization of counter ions near charged surfaces in tissue and possibly, the polarization of the large membrane bound structures and electrolytes [5].

The information derived from this work has application in radiation oncology and dosimetry; mathematical models developed in this work can be used to generate more dielectric data for clinical applications.

4. Conclusions

We proposed mathematical response models of gamma irradiated bovine tissues at lower and higher radiofrequencies within gamma irradiation dose regime of 1 - 85 Gy. Using Akaike's Information Criterion, we show that at lower frequencies, linear mathematical models are the most preferred models for describing the response of bovine blood and liver tissues to gamma radiation; both linear and polynomial models are suitable for kidney tissues at lower radiofrequencies while linear models perform better for all the tissues at higher radiofrequencies.

Table 2. Dielectric spread parameter α, of gamma irradiated and non-irradiated bovine kidney, liver and blood at 0.5 MHz - 50.0 MHz.

Dose (Gy)	Kidney	Liver	Blood
	α	α	α
0	0.100	0.213	0.100
1	0.106	0.242	0.105
4	0.104	0.272	0.106
11	0.114	0.296	0.106
20	0.193	0.224	0.143
43	0.305	0.278	0.157
60	0.352	0.324	0.229
85	0.341	0.306	0.223

The plot of spread parameters versus gamma irradiation doses shows that at lower radiofrequencies (0 - 100 kHz) kidney is more sensitive to gamma radiation at dose regime considered, followed by liver tissue except at 85 Gy. While at higher radiofrequencies (0 - 50 MHz), liver between 0 - 20 Gy, while between 43 and 85 Gy the kidney displayed higher sensitivity followed by liver tissues and lastly the blood.

Acknowledgements

The authors of this work are grateful to Nigeria Nuclear Technology Centre (NNTC) Abuja and the Department of Physics, Benue State University Makurdifor provision of gamma irradiator and laboratory equipments used in this research. We are also grateful to Dr. Agada P.O. of Statistics Department, Federal Universiy of Agriculture Makurdifor his assistance in the analysis of our experimental data.

References

[1] Hada, M. and Georgakilas, A.G. (2008) Formation of Clustered DNA Damage after High-LET Irradiation: A Review. *Journal of Radiation Research*, **49**, 203-210. https://doi.org/10.1269/jrr.07123

[2] Janonov-Stankov, O., Demajo, M., Djuji, I. and Mandic, M. (2003) Effects of Gamma Irradiation on Magnesium Content in Rat Tissue.

[3] Maliev, V., Popov, D., Jones, J.A. and Casey, R.C. (2007) Mechanism of Action for Anti-Radiation Vaccine in Reducing the Biological Impact of High-Dose Gamma Irradiation. *Advances in Space Research*, **40**, 586-590. https://www.sciencedirect.com/ https://doi.org/10.1016/j.asr.2007.03.098

[4] Peyman, A. (1996) Dielectric Properties of Tissues as a function of Age and Their Relevance in Assessment of the Exposure of Children to Electromagnetic Field; State of Knowledge. Centre for Radiation Chemical and Environmental Hazards, Health Protection Agency.

[5] Foster, K.R. (2000) Dielectric Properties of Tissues. University of Pennsylvania,

CRC Press, Boca Raton.

[6] Laogun, A.A., Ajayi, N.O. and Agba, E.H. (2005) Influence of X-Rays on the Radio-frequency Dielectric Properties of Bovine Kidney Tissues. *Nigerian Journal of Physics*, **17**, 117-122.

[7] Agba, E.H., Laogun, A.A. and Ajayi, N.O. (2008) A Comparison of the Effect of Diagnostic X-Rays on the Radiofrequency Dielectric Properties of Bovine Liver with Bovine Kidney Tissues. *Nigerian Journal of Physics*, **20**, 11-22.

[8] Mallidi, S.M., Bhilwade, H.N., Khan, M.Z. and Chamby, R.C. (2007) Gamma Ray Induced Genetic Changes in Different Organs of Chick Embryo Using Peripheral Blood Micronucleus Test and Comet Assay. *Mutation Research/Genetic Toxicology and Environmental Mutagenesis*, **630**, 20-27. http://www.sciencedirect.com https://doi.org/10.1016/j.mrgentox.2007.02.002

[9] Suciu, D. (2005) Model for Explanation of the Difference in Radio-Sensitivity between Dividing and Resting Mammalian Non-Lymphoid Tissue Cells. *Heidelberg Journal of Radiation and Environmental Biophysics*, **29**, 203-211.

[10] Dissado, L.A. (1990) A Fractal Interpretation of the Dielectric Response of Animal Tissues. *Physics in Medicine & Biology*, **35**, 1487-1503. https://doi.org/10.1088/0031-9155/35/11/005

[11] Stoy, R.D., Foster, K.R. and Schwan, H.P. (1982) Dielectric Properties of Mammalian Tissues from 0.1 to 100.0 MHz; a Summary of Recent Data. *Physics in Medicine & Biology*, **27**, 501-513. https://doi.org/10.1088/0031-9155/27/4/002

[12] Stuchly, M.A., Athley, T.W., Samaras, G.M. and Taylor, G.E. (1982) Measurement of Radiofrequency Permittivity of Biological Tissues with an Open-Ended Coaxial line: Part II—Experimental Results. *IEEE Transactions on Microwave Theory and Techniques*, **30**, 87-91. https://doi.org/10.1109/TMTT.1982.1131022

[13] Schwan, H.P. and Foster, K.R. (1980) RF Field Interaction with Biological Systems: Electrical Properties and Biophysical Mechanisms. *Proceedings of the IEEE*, **68**, 104-113. https://doi.org/10.1109/PROC.1980.11589

Call for Papers

Open Journal of Biophysics

ISSN Print: 2164-5388 ISSN Online: 2164-5396
http://www.scirp.org/journal/ojbiphy

Open Journal of Biophysics (OJBIPHY) is an international journal dedicated to the latest advancement of biophysics. The goal of this journal is to provide a platform for scientists and academicians all over the world to promote, share, and discuss various new issues and developments in different areas of biophysics.

Subject Coverage

All manuscripts must be prepared in English, and are subject to a rigorous and fair peer-review process. Accepted papers will immediately appear online followed by printed hard copy. The journal publishes original papers including but not limited to the following fields:

- Bioelectromagnetics
- Bioenergetics
- Bioinformatics and Computational Biophysics
- Biological Imaging
- Biomedical Imaging and Bioengineering
- Biophysics of Disease
- Biophysics of Photosynthesis
- Cardiovascular Biophysics
- Cell Biophysics
- Medical Biophysics
- Membrane Biophysics
- Molecular Biophysics and Structural Biology
- Physical Methods
- Physiology and Biophysics of the Inner Ear
- Proteins and Nucleic Acids Biophysics
- Radiobiology
- Receptors and Ionic Channels Biophysics
- Sensory Biophysics and Neurophysiology
- Systems Biophysics
- Theoretical and Mathematical Biophysics

We are also interested in: 1) Short Reports—2-5 page papers where an author can either present an idea with theoretical background but has not yet completed the research needed for a complete paper or preliminary data; 2) Book Reviews—Comments and critiques.

Notes for Intending Authors

Submitted papers should not have been previously published nor be currently under consideration for publication elsewhere. Paper submission will be handled electronically through the website. All papers are refereed through a peer review process. For more details about the submissions, please access the website.

Website and E-Mail

http://www.scirp.org/journal/ojbiphy E-mail: ojbiphy@scirp.org

What is SCIRP?

Scientific Research Publishing (SCIRP) is one of the largest Open Access journal publishers. It is currently publishing more than 200 open access, online, peer-reviewed journals covering a wide range of academic disciplines. SCIRP serves the worldwide academic communities and contributes to the progress and application of science with its publication.

What is Open Access?

All original research papers published by SCIRP are made freely and permanently accessible online immediately upon publication. To be able to provide open access journals, SCIRP defrays operation costs from authors and subscription charges only for its printed version. Open access publishing allows an immediate, worldwide, barrier-free, open access to the full text of research papers, which is in the best interests of the scientific community.

- High visibility for maximum global exposure with open access publishing model
- Rigorous peer review of research papers
- Prompt faster publication with less cost
- Guaranteed targeted, multidisciplinary audience

Scientific Research Publishing

Website: http://www.scirp.org

Subscription: sub@scirp.org

Advertisement: service@scirp.org